Predicting properties of PVD and CVD coatings based on fractal quantities describing their surface

W. Kwaśny*

Division of Materials Processing Technology, Management and Computer
Techniques in Materials Science, Institute of Engineering Materials and Biomaterials,
Silesian University of Technology, ul. Konarskiego 18a, 44-100 Gliwice, Poland
* Corresponding author: E-mail address: waldemar.kwasny@polsl.pl

Methodology of research

ABSTRACT

Purpose: The goal of the presented study was to develop a methodology giving a possibility to predict functional properties of coatings obtained in the PVD and CVD processes on tool materials, based on fractal- and multi-fractal quantities describing their surface.

Design/methodology/approach: Effect of process type and deposition conditions on structure and shape of surface, as well as mechanical and service properties of the obtained coatings were determined. Methodology and detailed description of coatings topography obtained in PVD and CVD process on tool materials, including use of the fractal- and multi-fractal geometry based on images obtained on the atomic forces microscope were worked out. Relationships between fractal- and multi-fractal quantities and their mechanical and service properties were determined.

Findings: The investigation results confirmed the feasibility to predict hardness and erosion resistance of coatings obtained in the magnetron PVD process, as well as the service properties defined in the cutting ability test for coatings obtained in the arc PVD process and in the high-temperature CVD process, based on the surface fractal dimension D_s value for their surface topography.

Practical implications: Determining significant quantitative correlations between fractal quantities defining coatings' surfaces, as well as their service and/or mechanical properties provides the opportunity to predict their end-user properties.

Originality/value: Fractal analysis was applied for characterization of PVD and CVD coatings surfaces.

Keywords: Thin & Thick coatings; PVD and CVD coatings; Image analysis; Fractal and multifractal analysis; X-ray analysis; AFM microscope

1. Introduction

High - tech tool materials, because of their work nature and their wear mechanisms complexity, should meet a number of requirements like, among others: high hardness, wear resistance, high compression, tensile-, torsional- and bending strength, as well as cutting edge stability [1-3]. The "ideal" tool material of a general purpose application should merge the above-mentioned properties, and particularly the high wear resistance and hardness, including high strength and good ductility with the chemical inertness in relation to the processed material (Fig. 1).

Protection of machine elements and metal constructions from corrosion and wear, extension of life of machines and mechanisms belong to crucial materials engineering problems. Strength of the elements is ensure by using one material, and its resistance to external factors is guaranteed by development locally a coating on its surface having special properties. The mechanical strength of the elements is ensured by its core, and its resistance to the external factors (wear, corrosion, erosion) is obtained by forming thin coatings from other materials on their surface, with the differentiated chemical compositions and applications. The extended elements life results combined with other required features, along with cost reduction in many cases. Moreover, fabricating of products is possible, characteristic of the unique combination of properties, unobtainable using the traditional engineering materials. Therefore, a new approach is purposeful to materials selection both in the technical- and economic respects. However, in spite of the intensive development of materials engineering fabrication of the "ideal" material has still not succeeded because of the fundamental contradiction between such properties like hardness and ductility [2-6].

Precise definition and surface form description are important in materials engineering in consideration of the material application. Scanning electron microscopy (SEM) is one of the methods which make imaging of the geometrical surface properties possible for the investigated materials [7]. Information about topography (surface sculpture) and morphology of the test pieces is acquired mostly from a signal coming from the secondary electrons (SE). Employment of the contemporary high-resolution electron scanning microscopes makes visualisation possible of the geometrical of topographical features with the resolution ranging from 1 mm to a fraction of a nm. The digital representation of the image acquired on the scanning microscope is its discrete mapping in the form of a table of numbers specifying the grey-levels of the particular analysed image points; however, the limited capability to acquire the quantitative data characterising and describing the examined surface is its drawback. The second method commonly used for imaging the surface geometrical features with nanometric resolution is atomic forces microscopy (AFM) [8]. The measurements are made by moving a probe over the examined test piece along the parallel lines, and its swing makes it possible to work out the topographic map of the examined surface. The measurement results are logged as a table of numbers whose values may be interpreted as a probe distance from the examined surface (or as a test piece height in regards to the assumed level) at the particular, precisely defined measurement points. Although, as distinguished from scanning electron microscopy, the atomic forces microscopy makes obtaining quantitative data possible, the examination results obtained using the AFM microscope are used in a limited range only, just for the graphical presentation of the analysed surfaces. Potential offered by this investigation technique in the quantitative description on the PVD and CVD coatings remains, in the author's opinion, unexploited.
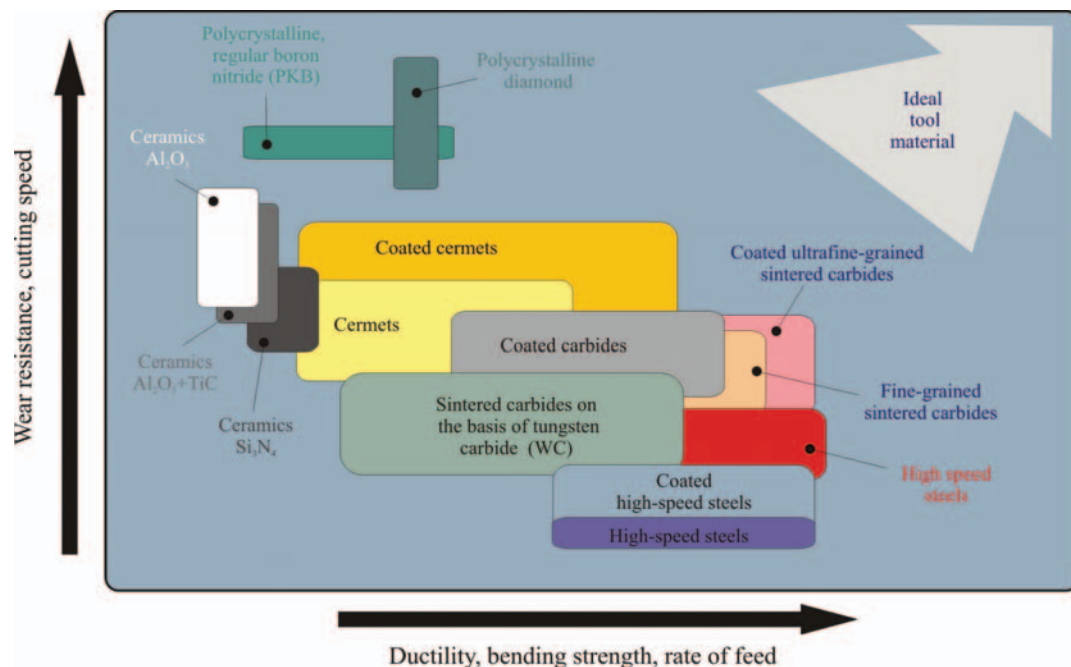
Fig. 1. Comparison of different tool materials in terms of their properties [4]

Roughness plays the especially important role among quantities describing the geometrical properties of coatings, defined as a set of the minute real surface irregularities, defined by convention as deviations from its profile, measured from the assumed reference line over the roughness sampling length at which the surface shape and waviness deviations are not taken into account [9]. There are a number of quantities that characterize surface roughness [10]; and the following are considered to be the most important ones:

- Arithmetic average of profile deviation from the roughness centerline R_a in µm,
- Roughness height R_z in µm,
- Peak-to-valley height R_{max} in µm.

Surface roughness is one of the criteria used for qualitative assessment of the PVD and CVD coatings surface. The necessity of the complementary approach is emphasized in those areas, where especially demanding requirements are imposed on the materials used, regarding the coatings description methods and using simultaneously many parameters describing them (so-called multiparametric analysis) [11-13]. Employment of fractal analysis for description and characterizing the examined objects is one of research trends in this area.

2. Theoretical premises to take up an investigative subject area

2.1. Contemporary sense of wear resistant coatings

Technology of thin coatings, resistant to wear and deposited by different methods on tool materials, has been arousing a lot of producers' interest for many years. Progress in this field is advancing in parallel with development in several areas of the material engineering, concentrating on continuous searching and implementing new materials, and also on optimisation of their chemical and phase composition as well as on technology to produce them [14, 15]. Currently, the main manners to improve service properties of tool materials are physical and chemical methods to deposit coatings. Coatings acquired in the PVD & CVD processes have already consolidated their position in many applications, allowing for explicit improvement of service properties of elements made of tool materials. The main benefits resulting from their deposition on tools are the following:

- Higher life-time of produced elements,
- Reduction of costs of production due to tools life increase,
- Reduction of inter-operational shut-downs caused by necessary exchange of tools,
- Machining capacity increase related to machine cutting speed and applied advances increase,
- Higher quality of materials' machined surfaces,
- Reduction of oxidation and corrosion processes.

These methods application does not cause environment pollution; they can be easily automated and applied in series production. Of this technology importance, among methods of surface properties improvement, the fact can testify that in a commercial offer of top manufacturers, there is a wide assortment of tools coated with crusts [16, 17].

CVD methods used for coatings deposition are that metal carbides and nitrides are formed of gas atmosphere components on surface of a machined element. In the process of formation of a layer, substrate's components take part. The process is carried out in gas atmospheres usually containing chemical compounds vapours of a metal being a basic component of a produced layer within 900-1100˚C. High temperature, necessary for a course of chemical reaction, significantly reduces a range of the applied CVD methods, particularly, in case of elements exposed to dynamic loads, being in service, or tools made of high-speed steels. It reduces a scope of CVD technologies application mainly for layers deposition on inserts made of ceramic carbide materials, for which high temperature of the process does not cause a loss of their properties. In the last years a few varieties of CVD processes were developed that generally are called as methods of chemical deposition from gas phase in the presence of a glow discharge PACVD, making utilisation of positive features for CVD high temperature processes possible (high capacity and quality of received coatings) in connection with low temperature of coating and beneficial plasma enabling to clean substrate [2, 15, 16, 18, 19].

PVD methods take advantage of physical phenomena, such as metals or alloys evaporation, or cathode sputtering in vacuum as well as gaseous ionization and metals vapours. Their common feature is vapours crystallization of metals vapours or phases from plasma. Coatings deposition is performed on a cold substrate or on a preheated one up to 200-600°C, what makes quenched and tempered substrates deposition possible, not worrying about their hardness drop. In PVD technologies, a change of process parameters has a tremendous impact on a structure of produced coatings. The basic process parameters affecting structure and topography of PVD coatings are: substrate's temperature, working gases pressure, energy of deposited ions, which together with substrate's features and properties determine their mechanical properties [2, 20-23]. Evolution of the PVD methods tends towards a direction allowing for deposition of multi-phase, multi-layer and gradient coatings being characterised by good adhesion to substrate's material [16, 17].

In the face of multitude of deposition techniques varieties of coatings there is a necessity of conscious choice for both a type of coating and a method to deposit it, as the same coatings deposited by different methods differ in terms of their service properties.
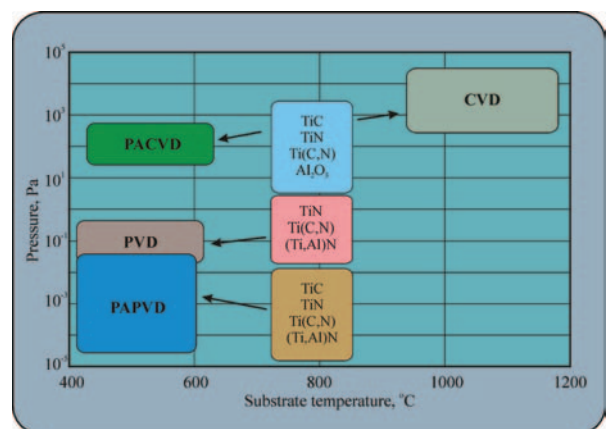
Fig. 2. Comparison of coatings' deposition techniques [29]

In the Fig. 2 a comparison of coatings' deposition techniques is shown, depending on process temperature and working pressure.

A great number of possible techniques allows to select the most adequate one for a specific application, for the sake of the required properties of coating and coated substrate. Putting high demands, for coatings resistant to wear, causes that materials used to acquire them should be characterized by, first of all, high hardness in raised temperature, high resistance to oxidation and good chemical stability. For the sake of that demands, as coatings' components resistant to wear, the most frequently compounds used for the tools are the following: titanium nitride TiN, titanium carbide TiC, titanium carbonitride TiCN, aluminium nitride TiAlN and aluminium oxide Al_2O_3 [24-29].

Currently, the most frequently used properties of single-layer coatings' are, in numerous cases, not sufficient. Far higher possibilities to form required properties in different areas of a coating make multi-layer coats happen. The multi-layer coatings, formed as a result of the subsequent layers' overlapping of different materials, predominatingly simple coatings of different properties are selected in such a way that provide gradual transition between properties of particular layers, having different assignments to make. As a result of that, a formed multi-layer coating simultaneously exhibits high adhesion to substrate's material and resistance to wear. In Fig. 3 a scheme of a multi-layer coating is presented, deposited on a cutting edge including functions of particular layers in accordance with [4].
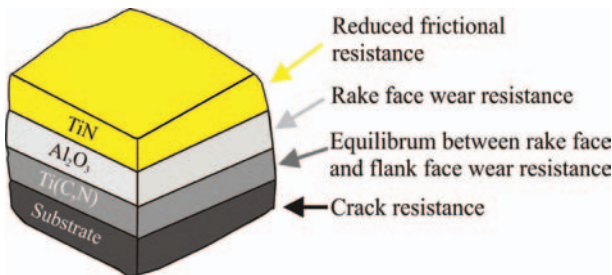
Fig. 3. Scheme of an exemplary multi-layer coating deposited on a cutting edge including functions of particular layers [4]

Coating's surface, directly exposed to a contact with foreign material, should be characterised by low chemical reactivity. From the middle part of the coating's cross-section, it is required to get high hardness and good ductility providing internal stress relaxation. Coating's contact zone with substrate's material should provide, first of all, good adhesion which can be obtained by thermal stresses minimisation and owing to approximate character of atomic bonds in substrate and material [2, 4, 16].
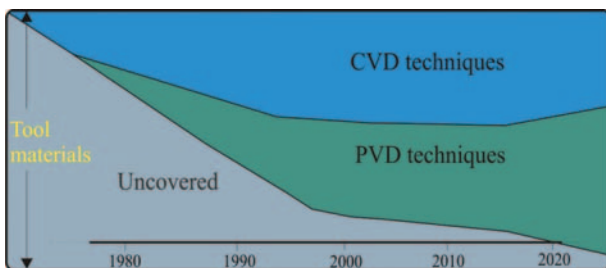
Fig. 4. Prediction of PVD & CVD techniques development [32]

For efficiency to apply coatings deposited by PVD & CVD methods, comparative findings results speak the best, performed simultaneously for coated and uncoated tools [1, 2, 6, 16, 21, 25-27]. Development of PVD & CVD processes caused usage of specific properties of coatings for commercial scale, not only to cover tool materials, but also in other area of applications: in optics and microelectronics, biomedicine, power engineering, automotive and building industry [18, 29-32].

In accordance with [32] it is planned to increase gradually tools' share covered with PVD & CVD methods in relation to uncovered tools (fig. 4). Still rising demand for coatings received with PVD & CVD methods leads to significant increase of sale of equipment used for coatings deposition, what allows to introduce new technological solutions and dynamic development of this material engineering's field. Growth of PVD & CVD technology application in commercial production and industrial processes caused a demand to apply quality system in the processes of coatings' deposition. To meet that challenge it is needed to learn precisely the process of coatings wear and also defects and failures being accompanied by it, depending on surrounding and area of considered case of coating. Considering properties of coatings, it is necessary to draw special attention to problems related to the following:

- Mechanical properties (adhesion, hardness, internal stresses),
- Physical properties (density, thermal conductivity, friction factor),
- Wear resistance (tribological properties),
- Structure, chemical and phase composition as well as texture.

Those factors influence on wear rate and tools life increase, and as a consequence, they decide about coatings' appropriation received in the PVD & CVD processes [33 - 35]. The main objective for the conducted investigations over wear mechanisms of cutting tools is to define an impact of wear conditions and parameters on tools life and reliability (fig. 5). Identification and definition of the impact's possibly the most numerous amount of factors determining tools life allow to develop more and more precise models of PVD & CVD coatings wear. Solving this problem makes machining capacity and quality increase possible at simultaneous reduction of energy-consumption and material-consumption [2, 5].
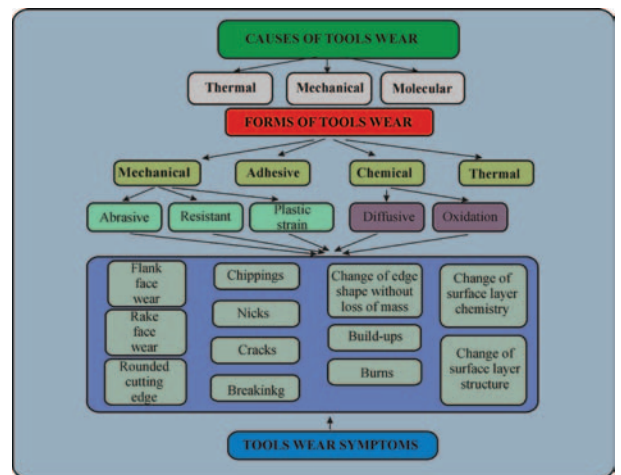
Fig. 5. Causes, forms and symptoms of tools wear [21]

Practically, the end of technological tool's life period usually occurs when it stops acquiring an object of required dimensions and surface quality. Numerous tests performed in scientific laboratories let PVD & CVD coatings' life define, among which the most frequently used are cutting ability tests and erosion test.

Many papers [2, 3, 33-39] are dedicated to process' quantities influence of coatings' deposition, substrates' polarisation and temperature, reactive gases pressure and flow on their properties expressed through adhesion, hardness, internal stress status, phase composition and crystallographic orientation, and also a type of structure. Knowledge status on dependencies among structure, physical properties and conditions to acquire coatings in the PVD & CVD processes is still unsatisfactory and it requires laboratory investigations, supported by computer technology. Applying the computer technology significantly increases analysing possibilities of received experimental results and reduces necessity to run costly and time-consuming technological tests in favour of mechanical and service properties prediction of coatings obtained in the PVD & CVD processes on tool materials [40, 41].

2.2. Fractal analysis as a tool to assess surface topography

The fractal analysis is a mathematical method created in 1960's of last century by B.B. Mandelbrot used to describe the abstract mathematical constructions and then, forms commonly appearing in nature, having self-similarity features [42, 43]. From examples of self-similar objects, we can enumerate such different structures as: decompositions of galaxies in outer space, exchange rates fluctuations on the Stock Exchange and surfaces of mountain massifs, what makes the fractal methods become a useful tool in theoretical and experimental studies in many disciplines, among other things: astrophysical, geological, biological, medical, physical, economic and IT [44-48].

Topography of surface of many actual engineering materials, including CVD and PVD coatings, draws a self-similar feature [49-53], what allows to be applied to their description of the fractal analysis method. As surfaces of actual materials are never

perfectly "smooth", so once adequately large enlargement of their fragments is applied, irregularities in the form of valleys and convexities appear. It can be noticed that for some materials, a degree of those irregularities is constant regardless of scale. It means that if analysed surface is smooth and regular, their fragments maintain this feature after being enlarged. When surface is irregular and rough, also its enlarged fragments look the same. It occurs like this, because additional details are disclosed which were not apparent earlier. Fractal geometry is a tool which allows characterizing degree of surface irregularities in qualitative and quantitative way when this value does not depend on scale. The basic fractal quantity that characterizes efficiency of space filling by surface and describes its shape is the surface fractal dimension - D_s. The fractal dimension D_s, being a real number in interval [2, 3) is a measure of irregularities and a degree of complexity of surface shape. Low value of fractal measure is characteristic for smooth surfaces, whereas high value describes surfaces of complex and complicated shape.

Methods of fractal geometry make not only fractal measure determining for analyzed objects possible, but also surface modelling of optionally selected, set value of that parameter [54]. In thesis [55] the author of the presented study displayed three algorithms enabling to get data modelling surfaces of fractional value for fractal dimension: two versions of randomized algorithm for a midpoint displacement method [56, 57] and Falconer algorithm [54]. On fig. 6 examples graphs of fractal surfaces of different values for fractal dimension are presented ($D_s = 2.25$ and $D_s = 2.75$), generated using a randomized algorithm for a midpoint displacement method. Comparing these two sets, whose dimensions (width and length) are identical, one may notice that surface of lower value of fractal dimension (Fig. 6a) is less developed (smaller area of surface) than surface of its higher value (Fig. 6b). The comparison of both graphs of surface allows interpreting the meaning of D_s. Surfaces, characterized by a low D_s value, demonstrate simultaneously relatively low amplitude and frequency, however, frequency and amplitude of unevennesses appearing on surfaces with higher D_s value are greater. The surfaces of low D_s value are homogenous and smooth, and objects shapes, whose surface dimension is higher, are more irregular and complex.

a)   b)
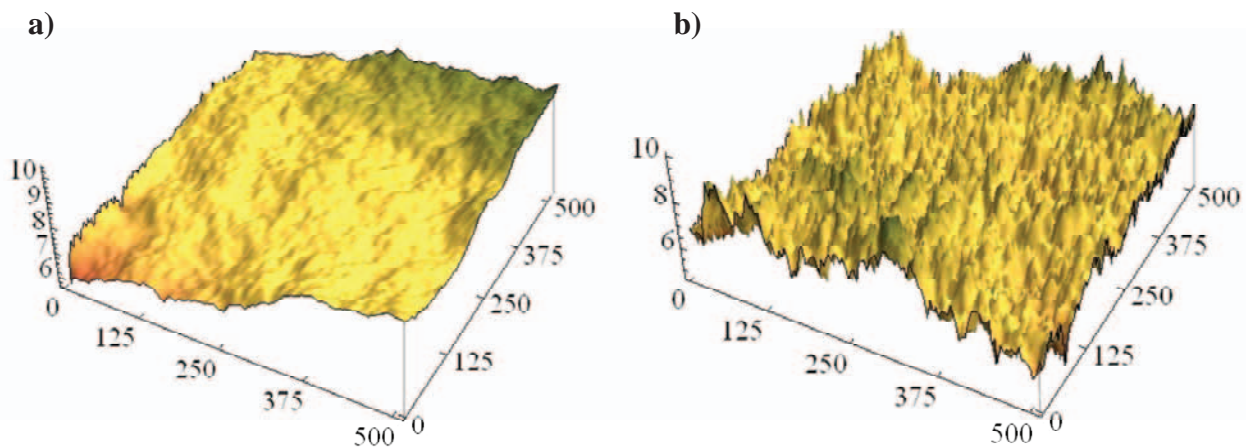
Fig. 6. Examples of fractal surfaces graphs, of different fractal dimension values a) $D_s = 2.25$ and b) $D_s = 2.75$ (generated using randomized algorithm for midpoint displacement method) [55]

For Euclidean surfaces ("classical"), D_s fractal dimension adopts an integral number, equalled 2, being compatible with intuitive value of dimension. In case of objects with more irregular shapes, composed of tiny fragments, which become "visible", not before application of appropriate "enlargement", a value of that quantity increases. A set of data modelling surfaces of fractal dimension set values can also be used to check correctness of methods to determine the fractal dimension. Conducted analyses let associate the fractal dimension value with roughness, i.e. with one of quantities commonly used in material engineering for description of surface topography of analyzed materials. Usually, surfaces of low roughness are characterized by low fractal dimension value; however, roughness increase is accompanied by increase of its value. If an analyzed object is a fractal, application of the fractal dimension for characteristics of coatings topography has principal advantage over traditional quantities determining roughness, as in contradiction to them; it does not depend on selection of measuring range. Roughness is determined for one measuring range and it does not allow inferring on features of the sample surface in other measuring ranges. Surface of higher roughness, e.g. determined by high R_a value, can contain great grains, whose walls being observed at significant enlargement, turn out to be smooth, and in such selected, lower measuring range, adopt low value of R_a quantity. Surface of lower roughness, determined by low value of R_a that should be smooth, once adequate enlargement is applied, it can contain a great number of tiny grains and in lower measuring range, it can adopt a high value of R_a. It is worth emphasising that in contrast to abstract, ideal, mathematical constructions, the self-similarity feature for actual surfaces appears purely in statistical sense as well as in a specified quantity range. Particularly, one should not assume that coatings' surfaces obtained in the CVD & PVD processes point out this feature in all measuring ranges. For that reason determining the fractal dimension value should be preceded by specifying a range, in which a degree of irregularities of investigated surfaces is independent on scale. If the above condition is fulfilled, the fractal geometry becomes a tool that makes quantitative characteristics of actual surfaces possible, including coatings obtained in the PVD & CVD processes.

Practically, as early as the theory of fractals was established, B.B. Mandelbrot [58] indicated that, for description of the majority of actual objects (he chose distribution of copper deposits for example), application of the fractal formalism is insufficient. It results from a fact that actual objects are not homogenous, and because of that, it is impossible to describe geometrical features of objects of irregular shapes (except for the abstract mathematical constructions) with the help of one number – the fractal dimension. Surfaces of investigated engineering materials usually are not ideal self-similar objects, because that feature occurs only locally. Irregularities distribution changes depending on analysed fragment selection of a sample area. In some fragments, surfaces can be characterized by high irregularity, whereas they may reveal a more regular shape in the others. Mandelbrot has proposed to generalize a concept of the fractal set and replace it by a multi-fractal measure. The multi-fractal measure enables to characterize complex shapes, including surface, for which determined dimension adopts different values in different areas. Therefore, a multi-fractal analysis is an extension of the fractal method, enabling to characterize the

geometrical features of actual surfaces in more complete and accurate way [59, 60].

In contemporary science, the fractal and multi-fractal geometry found application, among other things, to investigate surface irregularities and to describe its shape. So far, fractal and multi-fractal features of surface have been determined for a number of materials, among which it is necessary to enumerate: metal materials [61, 62] and their alloys [63-66], ceramic, polymeric and amorphous materials [67-72]. Besides, the fractals' concept was used for description fractures surface morphology in 2D & 3D dimension for the sake of stereology [73]. As a result of amorphous samples tests, made of FeNiVSiB alloys, shown in [74], it is indicated that their resistance to fracture toughness proportional to a value of the fractal dimension of fracture topography. In the thesis [75], test results over TiO_2 semiconductor layers are presented showing correlation between the fractal dimension describing and characterizing the investigated surfaces and their absorbing capacity of light. Application of electron microscopy enables to investigate polymer-composite materials strengthens by mineral particles. The fractal analysis that has been conducted on the basis of obtained results facilitates a quantity description of quality scattering of mineral particles, thanks to application of numerical indicator connected with multi-fractal spectrum [76]. Serving the multi-fractal analysis, an attempt to describe the Portevin - Le Chatelier effect was undertaken (PLC) [77]. From a deformation curve, probability of plastic instability occurrence inside the investigated structure is determined, and a measure of a degree of material surface heterogeneity, in which plastic strain is found, was the fractal dimension. In the thesis [78], surface tests results are presented for materials remelted by laser. It is shown that materials remelted by a laser beam of higher energy are characterized by higher heterogeneity of surface, and over a specific character of multi-fractal spectrum describing it, energy of the laser beam has an impact. The multi-fractal analysis for complex coatings Si/TiN/Pd deposited on a substrate, made of NiCuP alloy by electroless plating method depending on duration of this process, is presented in the thesis [79]. Received results show correlation between quantities describing a multi-fractal spectrum and changes about heterogeneity of coating in case of increase of the process time needed to deposit it.

Fractal and multi-fractal geometry also finds broad application in terms of characterizing and describing surface morphology of biomedical materials (biomaterials). Preparation of implants and coats for materials surface implantation in human organism's interior or used for prolonged contact with it (e.g. pacemakers and artificial heart valves, catheters, drains, surgical sutures) is for the present very intensively developing course of scientific research. Biomaterials, the most frequently used, include polymers, ceramic materials and some metals and their alloys. For their imaging, depending on the size of investigated areas, optical, confocal, atomic force, scanning or transmission microscopy is applied, and in order to assess the obtained results we mainly use methods for automatic image analysis, including the fractal analysis [80-82]. In case of biomedical materials, used as implants, topography of their surface plays extraordinary important part in it. The fractal analysis application enables in this area to determine quantity parameters describing amplitude of irregularities on surface and a degree of their arrangement.
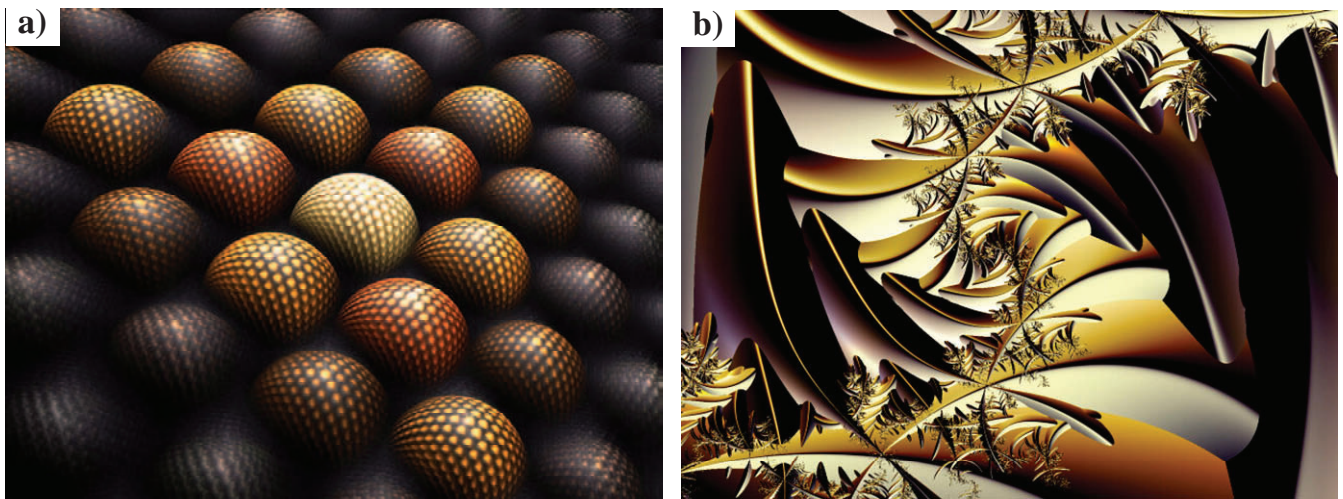
Fig. 7. a), b). Fractal objects generated by computer [90]

A complementary approach, considering, except for roughness measurement, also the fractal dimension determining, has been practically used to optimize a process to obtain materials of demanded surface properties [83, 84]. In the field of ceramic materials investigation, used in medicine, researchers' efforts are focused upon elaboration of methods making a quantity assessment for applied materials porosity possible. The tests results [85] determine that the fractal is proportional to the ceramic materials porosity, and there is correlation between its value and water amount which can be absorbed by the material. It is determined that in case of the ceramic materials applied in dentistry, there is a dependence between hardness and the fractal dimension [86], moreover, the fractal geometry was used to monitor morphological changes of dental implants characterizing, including its application, the analyzed biomaterials consumption [87]. Besides, the fractal and multi-fractal geometry is commonly used for analysis of medical images (ECG, EEG, USG, X-raying, mammographic examinations, and the like) [88]. The fractal geometry is also applied commercially, e.g. for production of film special effects, for images coding and compression as well as to make complicated images of fractals (Fig. 7a & 7b) [89, 90].

2.3. Thesis, goal, and scope of the work

Own research and literature study indicate that both process type and conditions, substrate material type, and also chemical composition of the deposited coatings decide the structure, and consequently surface topography of coatings obtained in the PVD and CVD processes, which – in turn – decide their mechanical properties and wear resistance. This is confirmed especially by works of Thornton [36], Messner [37], as well as Mowczan and Demcziszyn [38], presenting the models of coatings structural zones and being the most often cited literature works in numerous publications pertaining to layers obtained in the PVD and CVD processes. Confirming, and further explaining the relationships mentioned above is not only important from the cognitive point of view, but also may find practical applications shortly, yielding the possibility to predict coatings properties based on their surfaces topography assessment. Therefore, te following work thesis was formulated: Surface topography analysis of coatings obtained in the PVD and CVD processes makes prediction possible of their mechanical and service properties.

Precise surface description of coatings obtained in the PVD and CVD processes is of a significant importance in materials engineering; however, this issue was not addressed with the due attention so far, as the relevant tool was missing, giving the possibility to characterize quantitatively the complex shapes of the examined surfaces. Fractal geometry, in author's opinion, may feature the valuable complement to methods used till now. For example, using the fractal dimension for characterizing the topography of coatings has the essential advantage in respect to the traditional quantities defining roughness, as – other than they – does not depend on selection of the roughness sampling length, whereas, the multi-fractal analysis is an extension of the fractal method, making precise characterizing possible of the geometrical properties of the real surfaces for which the dimensions determined in various areas assume different values.

Therefore, working out a method was assumed as the goal of the work, rendering it possible to predict properties of coatings obtained in the PVD and CVD processes on tool materials based on fractal quantities describing their surface.

Investigation and analyses were carried out within the framework of the completed study, including:

- determining the effect of process type and deposition conditions on structure and surface topography and mechanical- and service properties of the obtained coatings,
- development of the method for characterizing and precise description of coatings obtained in the PVD and CVD processes on tool materials, using fractal- and multi-fractal geometry based on images acquired using the atomic force microscope,
- determining correlation between the fractal quantities characterizing the analysed surfaces of the PVD and CVD coatings and their mechanical- and service properties.

3. Material for studies and study methodology

3.1. Material for studies

Studies are performed on:
- Multi-edge inserts made of oxide ceramics Si_3N_4,
- Multi-edge inserts made of oxide tool cermets $Al_2O_3+ZrO_2$,
- Multi-edge inserts made of oxide tool cermets Al_2O_3+TiC,
- Multi-edge inserts made of oxide tool cermets Al_2O_3+SiC,
- Multi-edge inserts made of tool cermets TiCN+TiC+TaC+Co+Ni (T130A),
- Multi-edge inserts of tool cermets TiCN+TiC+WC+TaC+Co+Ni (CM),
- Samples made of sintered high-speed steel PM HS6-5-3-8, thermally treated

uncovered and covered in PVD & CVD processes with single and multi-layer coatings resistant to abrasion. Investigated ceramic tool materials are covered with single and multi-layer coatings in a process of cathodic arc evaporation - PVD (Fig. 8) and in a high temperature process - CVD.

Investigated sintered high-speed steel were treated thermally in a salt bath furnace with austenitizing at 1180° C and threefold tempering at 540° C. Once heat treatment is finished, steel obtains hardness 67-68 HRC. On the surface of steel samples in a magnetron PVD process (Fig. 9) the following coatings are generated Ti+(Ti,Al)N, Ti+(Ti,Al) (C_xN_{1-x}), received at different N_2 & CH_4 concentrations in a chamber of a vacuum furnace as well as Ti+(Ti,Al)C at 460, 500 and 540° C. Characteristics of investigated materials is presented on drawing 10 and compiled in table 1.

3.2. Study methodology

Structure of generated coatings was observed at lateral fractures on a High Resolution Scanning Electron Microscope SUPRA 35, ZEISS Company, equipped with a system of chemical composition analysis EDS. For imaging SEM, a lateral (SE) and in-lens detector using secondary electrons detection at accelerating voltage in a range of 1-20 kV were applied and maximum zoom of 35 000 x was obtained.

Ceramic samples are prepared by chasing the notches with a diamond blade with a machine made by Struers Co., whereas, steel samples are chased with a spark erosion cutter, and then, they are quenched in liquid nitrogen and afterwards, broken. Besides, chemical composition, for coatings acquired in PVD magnetron process, was determined in a glow discharge spectrometer - GDS-750 QDP made by Leco Instruments Co.

Investigations for material surface topography of substrates and generated coatings are carried out in an exchanged scanning electron microscope and using a method of atomic force microscopy (AFM) on a unit of Nanoscope E made by Digital Instruments company (Fig. 11). For each of analyzed surface, six measurements are made at scanning range of 5 µm.

X-rays studies for the analyzed materials are carried out on X´Pert PRO system made by Panalytical Company using filter radiation of a cobalt anode lamp. A phase analysis of the analysed materials is carried out in Bragg-Brentano geometry (XRD) using a Xcelerator strip detector, and in grazing incidence geometry (GIXRD) of primary beam using a collimator of parallel beam before a proportional detector.

Fig. 8. Scheme of a work-stand for coatings deposition by CAE (Cathodic Arc Evaporation) method
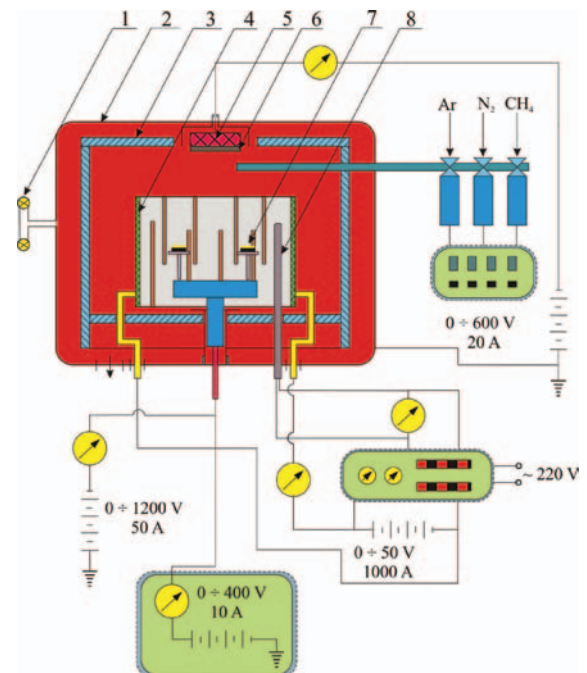
Fig. 9. Scheme of a work-stand to deposit coatings by a magnet method (1 – vacuum measuring system, 2 – vacuum chamber, 3 – furnace chamber, 4 – vacuum furnace, 5 – magnetron, 6 – magnetron shield, 7 – sample, 8 – thermocouple)

Table 1.

Characteristics of the investigated coatings obtained in PVD & CVD process

Item	Material of substrate	Type of coating	Type of process	Process temperature, °C
1	Si_3N_4	$TiN+Al_2O_3$	High temperature CVD	1000
2	Si_3N_4	$TiN+Al_2O_3+TiN$	High temperature CVD	1000
3	Si_3N_4	$TiN+Al_2O_3+TiN+Al_2O_3+TiN$	High temperature CVD	1000
4	Si_3N_4	Al_2O_3+TiN	High temperature CVD	1000
5	Si_3N_4	$TiC+TiN$	High temperature CVD	1000
6	Si_3N_4	$Ti(C,N)+TiN$	High temperature CVD	1000
7	Si_3N_4	$Ti(C,N)+Al_2O_3+TiN$	High temperature CVD	1000
8	Si_3N_4	$Ti(C,N)+Al_2O_3$	High temperature CVD	1000
9	$Al_2O_3+ZrO_2$	$TiN+Al_2O_3$	High temperature CVD	1000
10	$Al_2O_3+ TiC$	$TiN+Al_2O_3$	High temperature CVD	1000
11	$Al_2O_3+ SiC_{(w)}$	$TiN+Al_2O_3$	High temperature CVD	1000
12	PM HS6-5-3-8	$Ti+(Ti,Al)N$	magnetron PVD (100%N_2)	460
13	PM HS6-5-3-8	$Ti+(Ti,Al)N$	magnetron PVD (100%N_2)	500
14	PM HS6-5-3-8	$Ti+(Ti,Al)N$	magnetron PVD (100%N_2)	540
15	PM HS6-5-3-8	$Ti+(Ti,Al)(C,N)$	magnetron PVD (75%N_2:25%CH_4)	460
16	PM HS6-5-3-8	$Ti+(Ti,Al)(C,N)$	magnetron PVD (75%N_2:25%CH_4)	500
17	PM HS6-5-3-8	$Ti+(Ti,Al)(C,N)$	magnetron PVD (75%N_2:25%CH_4)	540
18	PM HS6-5-3-8	$Ti+(Ti,Al)(C,N)$	magnetron PVD (50%N_2:50%CH_4)	460
19	PM HS6-5-3-8	$Ti+(Ti,Al)(C,N)$	magnetron PVD (50%N_2:50%CH_4)	500
20	PM HS6-5-3-8	$Ti+(Ti,Al)(C,N)$	magnetron PVD (50%N_2:50%CH_4)	540
21	PM HS6-5-3-8	$Ti+(Ti,Al)(C,N)$	magnetron PVD (25%N_2:75%CH_4)	460
22	PM HS6-5-3-8	$Ti+(Ti,Al)(C,N)$	magnetron PVD (25%N_2:75%CH_4)	500
23	PM HS6-5-3-8	$Ti+(Ti,Al)(C,N)$	magnetron PVD (25%N_2:75%CH_4)	540
24	PM HS6-5-3-8	$Ti+(Ti,Al)C$	magnetron PVD (100%CH_4)	460
25	PM HS6-5-3-8	$Ti+(Ti,Al)C$	magnetron PVD (100%CH_4)	500
26	PM HS6-5-3-8	$Ti+(Ti,Al)C$	magnetron PVD (100%CH_4)	540
27	$Al_2O_3+ZrO_2$	$TiN+(Ti,Al,Si)N$	arc PVD	550
28	$Al_2O_3+ TiC$	$TiN+(Ti,Al,Si)N$	arc PVD	550
29	$Al_2O_3+ SiC_{(w)}$	$TiN+(Ti,Al,Si)N$	arc PVD	550
30	$Al_2O_3+ZrO_2$	TiN	arc PVD	550
31	$Al_2O_3+ TiC$	TiN	arc PVD	550
32	$Al_2O_3+ SiC_{(w)}$	TiN	arc PVD	550
33	$Al_2O_3+ZrO_2$	$TiN+multi(Ti,Al,Si)N+TiN$	arc PVD	550
34	$Al_2O_3+ TiC$	$TiN+multi(Ti,Al,Si)N+TiN$	arc PVD	550
35	$Al_2O_3+ SiC_{(w)}$	$TiN+multi(Ti,Al,Si)N+TiN$	arc PVD	550
36	$Al_2O_3+ZrO_2$	$(Ti,Al)N$	arc PVD	550
37	$Al_2O_3+ TiC$	$(Ti,Al)N$	arc PVD	550
38	$Al_2O_3+ SiC_{(w)}$	$(Ti,Al)N$	arc PVD	550
39	$Al_2O_3+ZrO_2$	$TiN+(Ti,Al,Si)N+(Al,Si,Ti)N$	arc PVD	550
40	$Al_2O_3+ TiC$	$TiN+(Ti,Al,Si)N+(Al,Si,Ti)N$	arc PVD	550
41	$Al_2O_3+ SiC_{(w)}$	$TiN+(Ti,Al,Si)N+(Al,Si,Ti)N$	arc PVD	550
43	Cermet T130A	$TiN+(Ti,Al,Si)N$	arc PVD	550
44	Cermet CM	$TiN+(Ti,Al,Si)N$	arc PVD	550
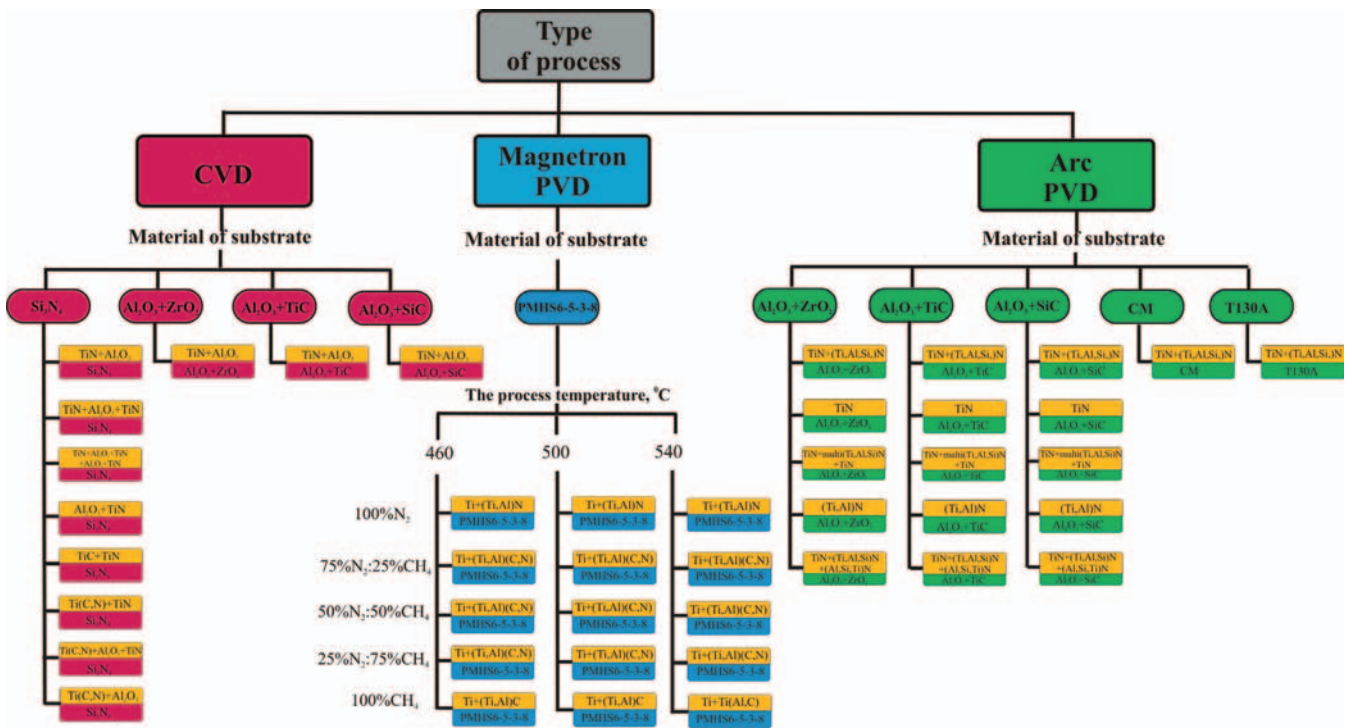
Fig. 10. The investigated materials classification

In order to specify distribution of normal coatings towards a selected plane and to determine FRO (orientation distribution function of crystallites) acquired in PVD and high-temperature CVD processes, not less than three pole figures were measured for each analysed sample made by a reflection method employing Euler's circle of diameter 187 mm in a range of samples inclination angle from zero to 75°. The FRO analysis of the analyzed materials was conducted with the help of procedures available in LaboTex 3.0 software using a discreet ADC method employing an iterative operator. The method allows to calculate FRO from measured pole figures including disturbances correction (so called ghosts correction) [39].

Measurements of stresses for the analyzed coatings were made by $\sin^2\psi$ and/or $g-\sin^2\psi$ technique depending on the investigated samples properties on the basis of X'Pert Stress Plus company's

programme, which contains, in a form of a database indispensable to calculate, values of material constants [92].

Fig. 12. Linear dependence in a classical method of $\sin^2\psi$ valid for assumptions of homogenous and flat state of stresses; points 1, 2, 3 correspond to measurements of values for interplanar distance at suitably - oriented grains of microstructure in different directions at ψ angle [91]

Fig. 11. Schematic diagram of an atomic force microscope (AFM) [8]
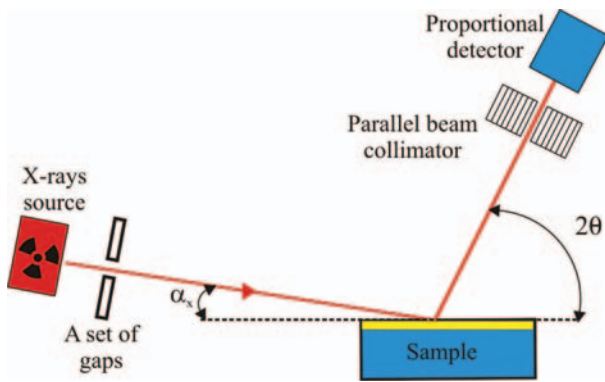
Fig. 13. Goniometer arrangement for diffraction image recording in grazing incidence geometry (GIXRD) [33]

Fig. 14. Schematic diagram for a work-stand to measure adhesion of hard coatings (1 – pressure generating drive, 2 – acoustic emissions detector, 3 – penetrator, 4 – sample, 5 – sample advance drive, 6 – pressure lever) [35]

In the method of $\sin^2\psi$ (fig. 12), based on diffraction lines displacement effect for different ψ angles, appearing in the conditions of stress of materials with crystalline structure, a silicon strip detector was used at the side of diffracted beam. Samples inclination angle ψ towards the primary beam was changed in the range of $0° \div 75°$. Moreover, measurements of stresses are made by a diffraction technique in grazing incidence geometry (Fig. 13) using a collimator of a parallel beam in front of the proportional detector [33, 93].

Selection of incident angle of the primary beam ($\alpha_x = 0,5°$; $1°$; $2°$; $3°$; $5°$; $7°$) was mainly dependant on linear absorptivity and combination of the applied layers, but the effective X-rays penetration depth g is estimated on the basis of the following dependence:

$$g = \left(\frac{\mu}{\sin\mu} + \frac{\mu}{\sin(2\theta_{\{hkl\}} - \alpha_x)}\right)^{-1} \qquad (1)$$

where:
μ – Linear absorption of the X-rays,
α_x – Incident angle of the primary beam.

Microhardness investigations for produced coatings and substrates hardness are conducted by means of an ultramicrohardness tester - DUH 202 manufactured by Shimadzu Co. using Vickers method at load of 0.05 N for coatings acquired in PVD arc process and 0.07 N for coatings acquired in magnet process – PVD, and in high-temperature CVD process too. Precise meter circuit allows to record depth of generated impression while loading, also during indenter load, and applied load was chosen so that the impression depth was less than 1/10 thick of generated coatings, what eliminates in large extent the substrate influence over obtained measurements results [34].

Assessments for coatings adhesion to the substrate's material were made by a drawing method [35] on Revetest device manufactured by CSEM Co (Fig. 14). In this method, a diamond indenter moves over investigated surface at fixed speed while continuously increasing load. The lowest load, at which coating failure follows, so called critical load L_c, was determined based on a value of increase of acoustic emission recorded when
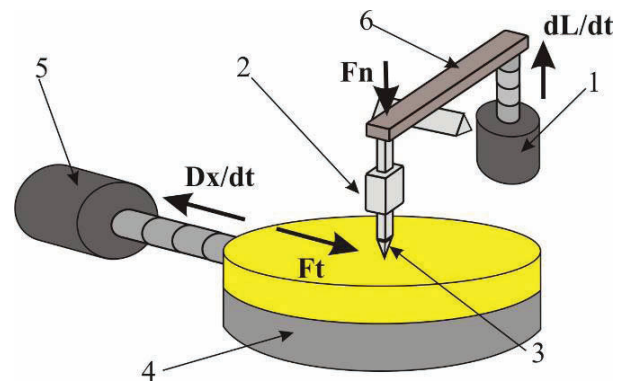
measurement was taken, being formed where the indenter and the investigated sample meet. The investigations were made at the following parameters:

- Impression force range 0-200 N,
- Speed for increasing impression force (dL/dt) – 100 N/min,
- Penetrator travelling speed (dx/dt) – 10 mm/min,
- Acoustic emission detector sensitivity – 1, 2.

Roughness investigations for the generated coatings and substrates surface were carried out on Stronic3 profile measurement gauge + Taylor-Hobson companies. R_a quantity is adopted as a value, which determined the surface roughness in accordance with PN-EN ISO 4287.

Plates life without coatings and with deposited coatings in a high-temperature CVD process & an arc PVD process are determined on the basis of technological cutting test in room temperature. Cutting ability test for investigated materials is made as a continuous turning method at PDF D180 loathe without cutting fluids. The material subjected to machining was grey cast iron EN-GJL-250 of hardness approx. 215 HBW. In cutting ability research the following parameters are taken:

- Feed - f = 0.2 mm/rev.,
- Turning depth a_p = 2 mm,
- Machining speed v_c = 400 m/min.

Life of plates is determined based on wear bandwidth measurements upon flank face, measuring a mean bandwidth wear VB after machine cutting in specified period of time (Fig. 15). Cutting tests were stopped, when VB value exceeded an assumed criterion (VB = 0.3 mm), both for uncovered tools and deposited coatings tools.

VB measurements with an accuracy of up to 0, 01 mm were made employing a Carl Zeiss Jena light microscope.

Classification of operational properties for PVD coatings, deposited on a substrate made of sintered high-speed steel PM HS6-5-3-8, is specified in erosion test with a unit of Falex Air Jet Eroder type made by Falex Corporation Co., in which powdery erodent coming out of a nozzle at set pressure strikes against tested sample surface, set at a located angle towards the nozzle. Microscopic observations of the obtained failures are conducted in an Axiovert 405 light microscope, employing differentiation
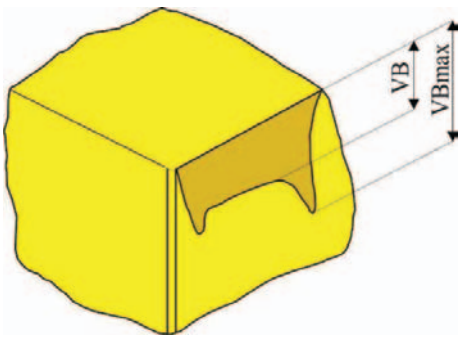
Fig. 15. VB criterion for a main cutting edge applied to assess life period of plates

of colour of substrate's material and coating, and additionally in a scanning microscope, where x-rays microanalysis is performed. Considering that analyzed coatings point out different thickness dependent on evaporation parameters, in this thesis time is presented, after which a layer 1 μm thick is removed.

Indication of the fractal dimension and the multi-fractal analysis for investigated materials is carried out on the basis of optical measurements in atomic force microscope AFM, being grounded on projective covering method [60]. In the course of this analysis, N_s=512x512 measurements of a sample height h_i are made, where the first number determines an amount of lines to be scanned, whereas the second one is a number of measuring points in each of them. A distance between the lines and the measuring points is constant and the same.

The measurements, which are carried out, using an atomic force microscope AFM enabled furthermore, indication of a quantity determined by the author as R_{2D} and characterizing roughness for analysed sample surface. R_{2D} roughness is determined in two stages. In the first one, each set of measurements results for the h_i sample height is approximated by the regression plane of H(x, y), for which a sum of squares of the distance from experimental data is minimal, and then, a roughness quantity value R_{2D} is determined for the analyzed sample surface on the ground of a dependency:

$$R_{2D} = \left[\frac{\sum_i (h_i - H_i)^2}{N_s} \right]^{\frac{1}{2}} \qquad (2)$$

where:
N_s – Number of measuring points,
h_i – Sample height at i point,
H_i – Value of H(x, y) at i point.

Application of the above procedure eliminated influence of sample inclination (levelling error) over an acquired value of calculated quantity.

To verify significance of the product-moment correlation coefficients of the obtained results in mechanical, applicable and fractal studies, t statistics is used being subject to Student's distribution with a number of independent variables equals n – 2, where n is a number of measurements taken in calculations into account. Analyses were performed at the level of significance α_{stat}=0, 05. Empirical value for the test statistics t was determined in accordance with a formula:

$$t = \frac{r}{\sqrt{1-r^2}} \sqrt{n-2} \qquad (3)$$

where, r is an empirical Pearson product-moment correlation coefficient, based on a random sample. The symbol t_{kryt} standing for a critical value, read out of tables for the test statistics distribution. Decision about a possible null hypothesis rejection (lack of correlations), was taken on the ground of the result for empirical value comparison of the test statistics with a critical value, read out from distribution tables of the test statistics. If $|t| > t_{kryt}$, the null hypothesis on lack of correlations was rejected as statistically less probable and the alternative hypothesis on correlations significance was accepted [94].

4. Investigations results and discussion

4.1. Structure, chemical and phase composition for investigated coatings

The performed metallographic studies allow to state that the tested oxide ceramic tool materials on the basis of Al_2O_3, nitride tool ceramics Si_3N_4, and tool cermets are characterized by compact structure. As a result of factographic investigations performed on a scanning electron microscope for the analysed CVD & PVD coatings, it was found that the deposited coatings determine single, double, or multilayer structure depending on applied system of layers, and particular layers are uniformly deposited and tightly adhere to each other as well as to the substrate's material. Structure of particular layers depends on substrate's material and a type as well as conditions of process. In case of coatings: Ti+(Ti,Al)N, Ti+(Ti,Al)(C_xN_{1-x}), acquired at different N_2 & CH_4 fraction in a vacuum furnace chamber, and Ti+(Ti,Al)C deposited in a magnetron PVD process, phases columnar structure when carbon concentration increase in coatings it becomes more compact and it is more difficult to observe distinct distribution between columns, whereas coatings of high carbon concentration (>20% atomic) are characterized by structure with glassy character (Fig. 24, 25). In coatings acquired in a high-temperature CVD process or in an arc PVD one, it is also columnar structure of particular layers that is distinctly visible, when a coating is formed by such phases as: TiN, Ti(C,N) and (Ti,Al)N.

Coatings roughness (defined by R_a quantity) for PM HS6-5-3-8 deposited sintered high-speed steel in the PVD magnetron process is decidedly lower than coatings obtained by the CVD technique and in the arc PVD process (Table 6, 7). That low value of roughness quantity, defined by R_a should be bound with topography of coatings surface, and it results from the applied deposition method. Upon coatings extracted in the magnetron PVD process, merely single elementary particles in a form of drops appeared, from several decimals to 0.5 μm in size (Fig. 24, 25), whereas there are more of them in the other two processes (Fig. 20, 23), when the surface layer is not Al_2O_3 – in those cases, elementary particles occurrence was found in the surface of coatings in a shape of polyhedrons, characteristic for that type of layer (Fig. 16, 22).
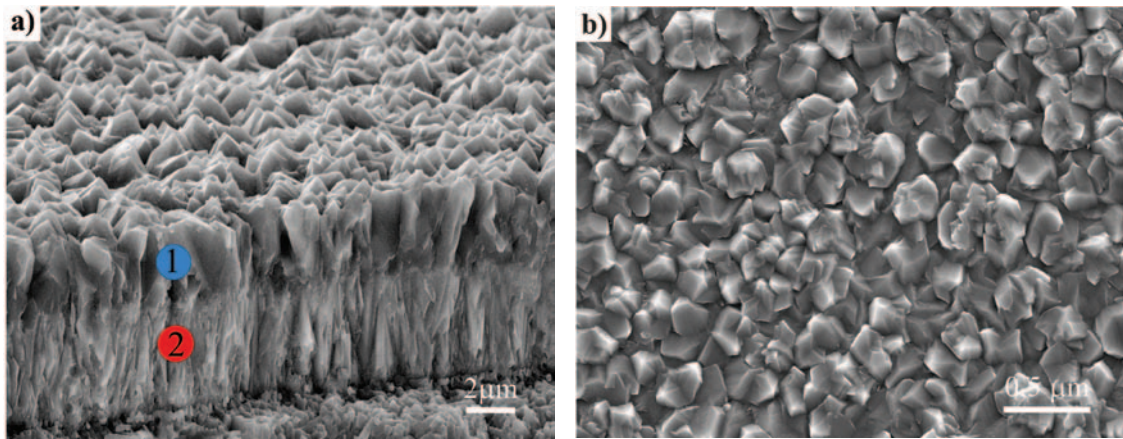
Fig. 16.a) Brittle fracture surface of a coating TiN+Al_2O_3 obtained on a substrate made of nitride ceramics Si_3N_4 in high-temperature CVD process b) its picture corresponding to surface topography (SE detector)
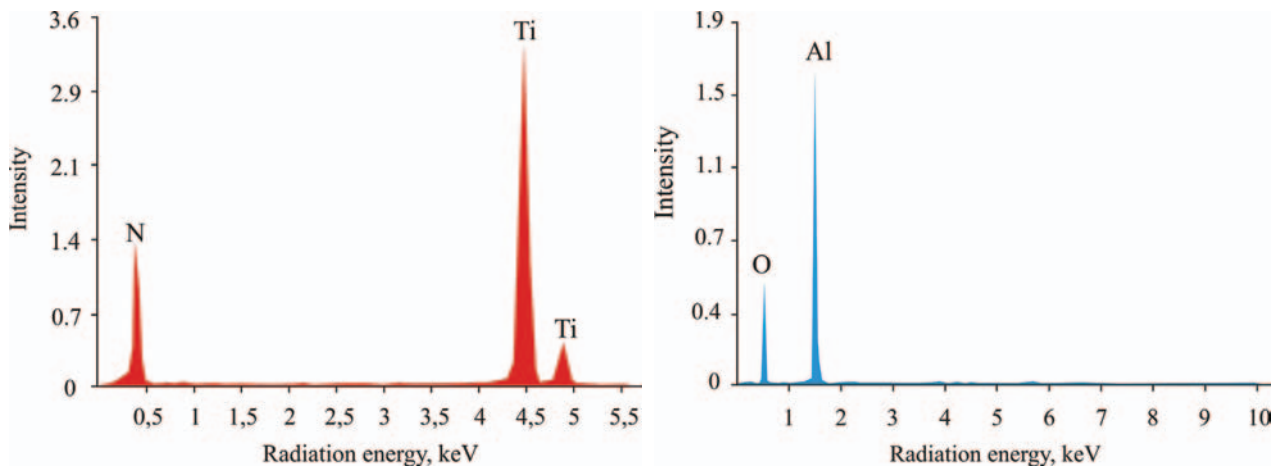
Fig. 17. A graph for scattered X-rays radiation energy from micro-area 1 and 2 respectively in accordance with Fig. 16a
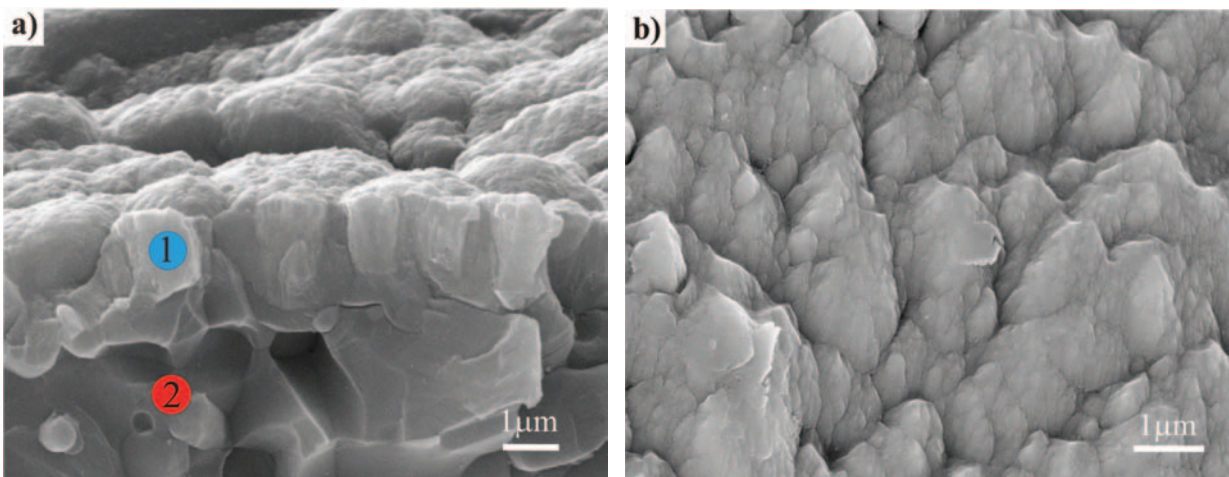
Fig.18. a) Brittle fracture surface of a coating (Ti,Al)N obtained on a substrate made of tool ceramics Al_2O_3+SiC in the arc PVD process and b) Its picture corresponding to surface topography(SE detector)
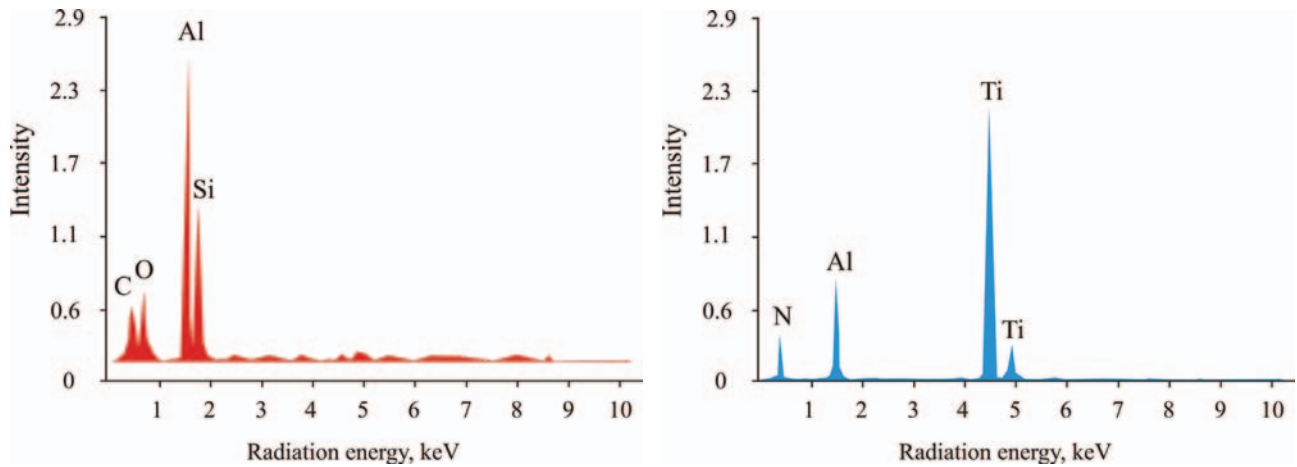
Fig. 19. A graph for scattered X-rays radiation energy from micro-area 1 and 2 respectively in accordance with Fig. 18a
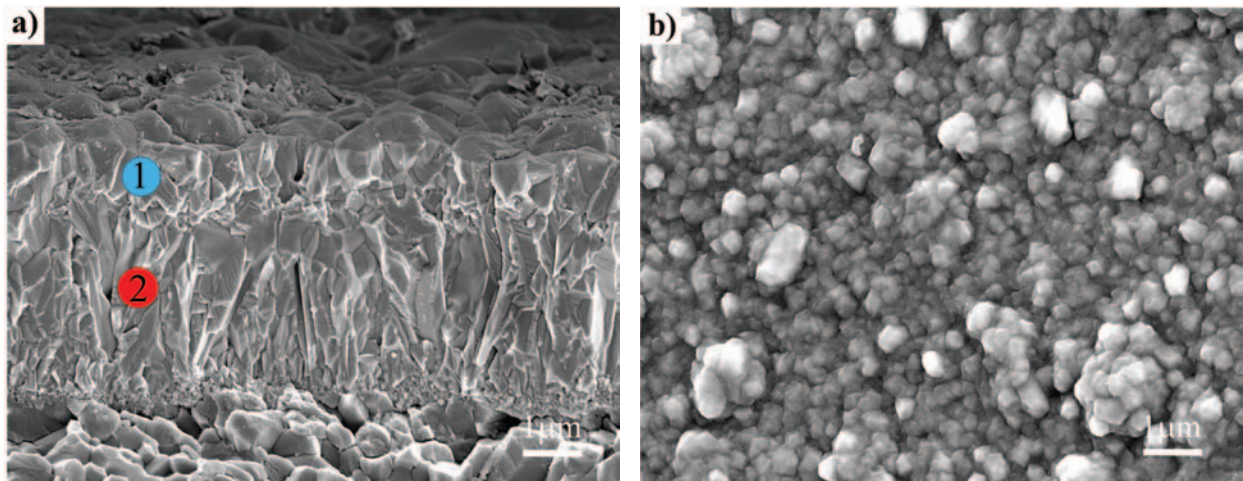
Fig. 20. a) Brittle fracture surface of a coating Ti(C,N) +TiN obtained on a substrate made of nitride ceramics Si_3N_4 in high-temperature CVD process (InLens detector) and b) its picture corresponding to surface topography (SE detector)
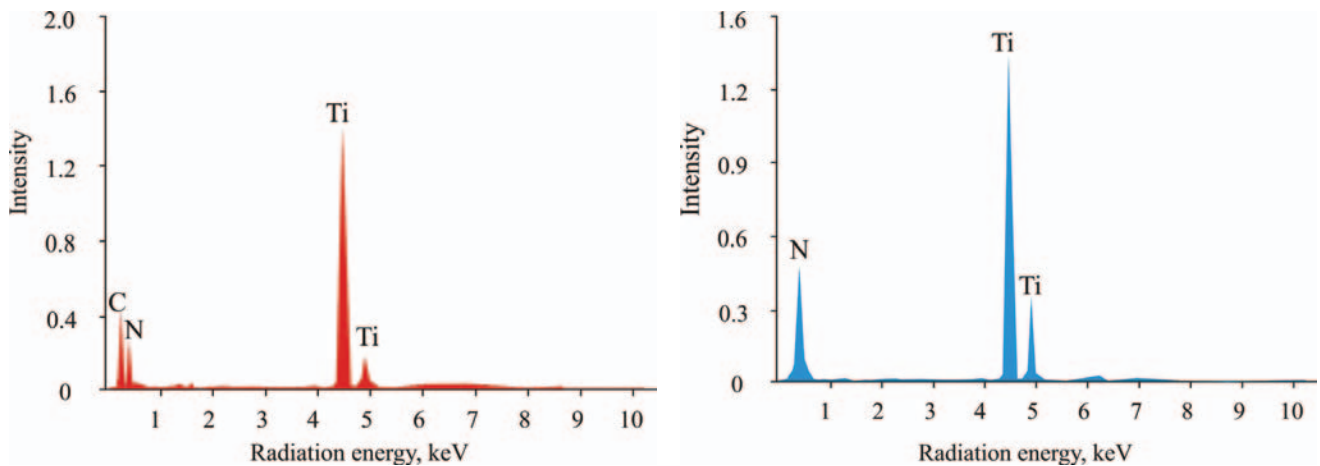
Fig. 21. A graph for scattered X-rays radiation energy from micro-area 1 and 2 respectively in accordance with Fig. 20a
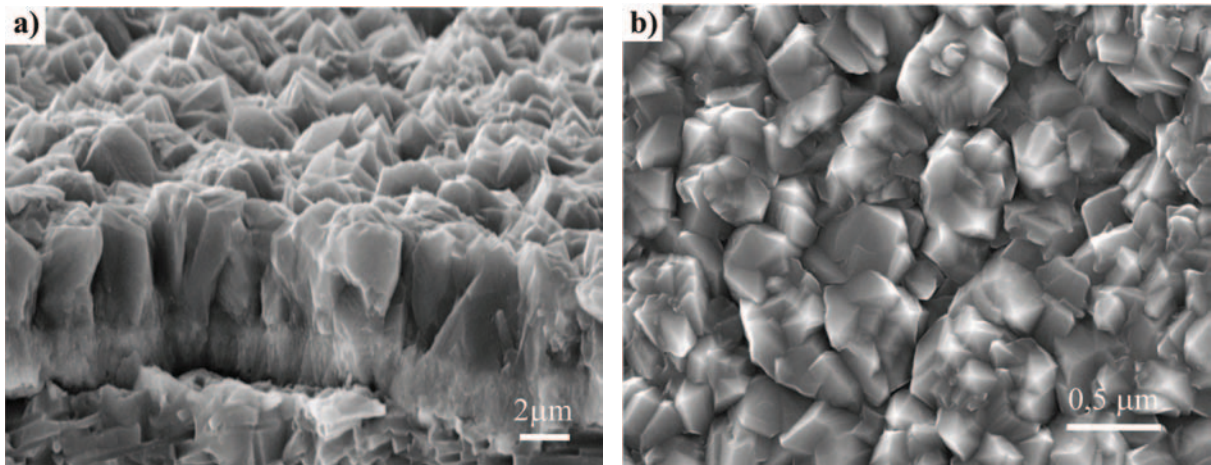
Fig. 22. a) Brittle fracture of a coating TiN+Al$_2$O$_3$ received on a substrate made of tool ceramics Al$_2$O$_3$+SiC in high-temperature CVD process and b) its picture corresponding to surface topography (SE detector)
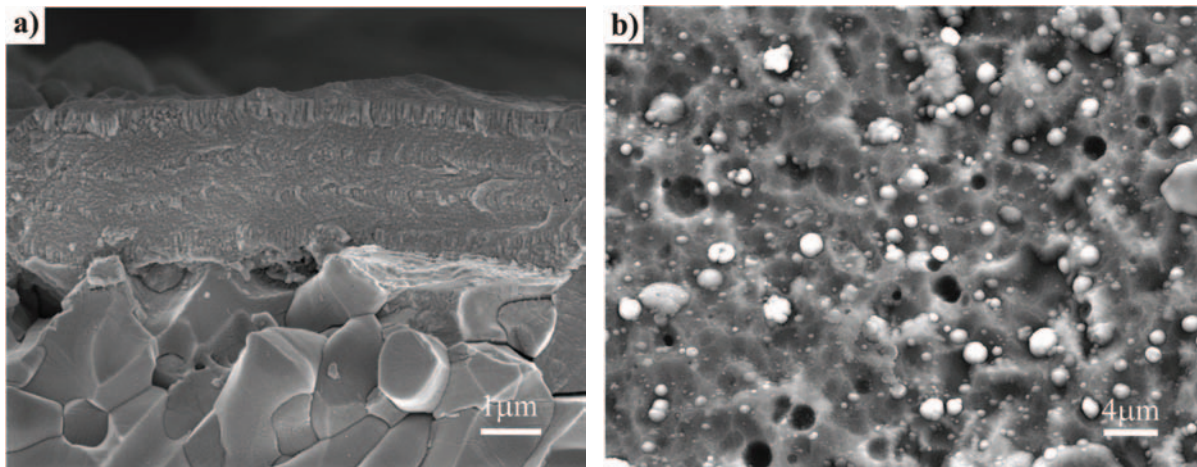
Fig. 23. a) Brittle fracture of a coating TiN+multi(Ti,Al,Si)N+TiN acquired on a substrate made of tool ceramics Al$_2$O$_3$+ SiC in the arc PVD process and b) its image corresponding to topography of surface (SE detector)
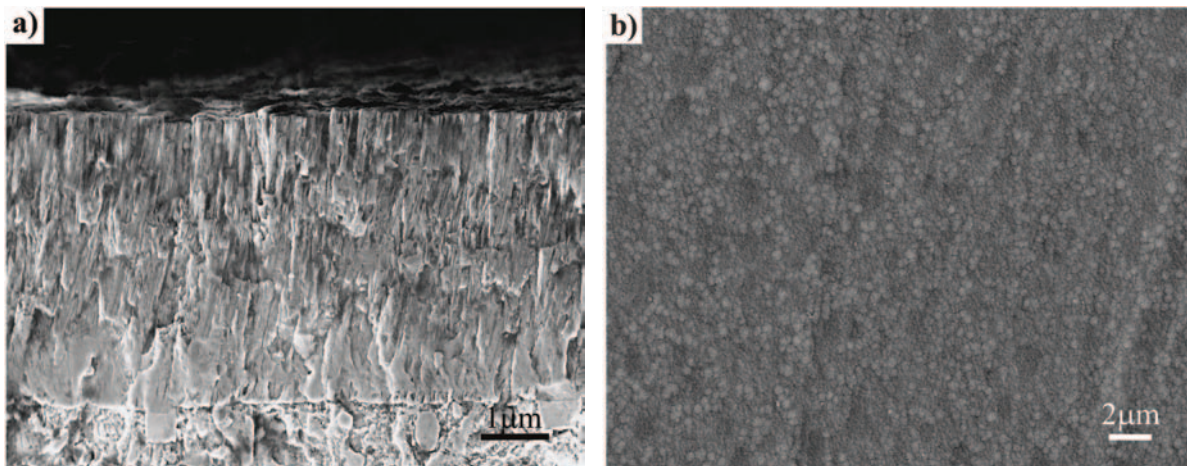
Fig. 24. a) Brittle fracture of a coating (Ti,Al)N obtained in the magnetron PVD process (InLens detector) and b) its image corresponding to topography of surface (SE detector) – the process temperature is 500ºC
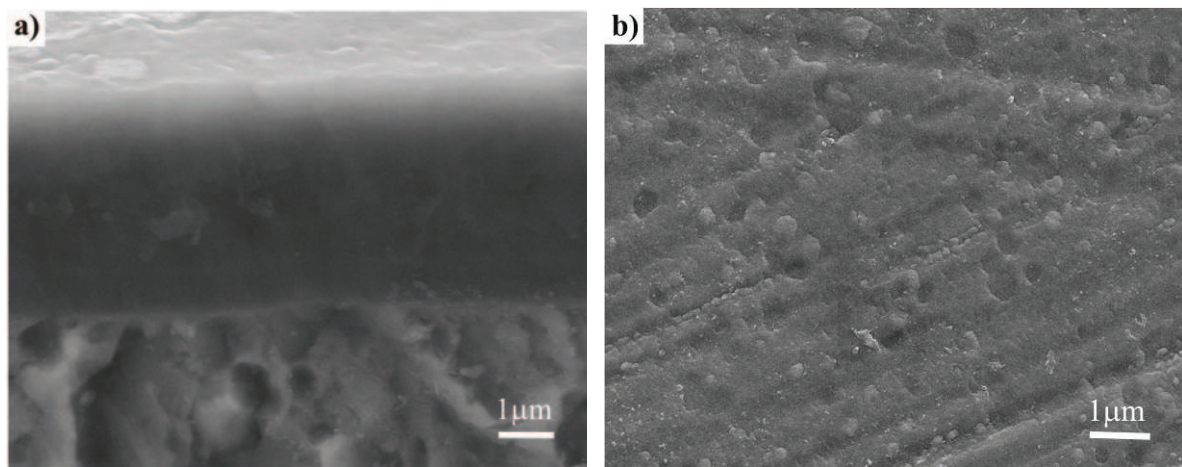
Fig. 25 a) Brittle fracture of a coating (Ti,Al)C obtained in the magnetron PVD process and b) its image corresponding to topography of surface (the process temperature is 500°C, SE detector)

Chemical composition investigations for elementary particles of energy, in a shape of drops were made by use of a spectrometer, for EDS scattered X-rays radiation point out that inside the elementary particles Titanium predominates; what suggests that liquid metal drops are solidifying on the substrate surface. Observations of surface topography for the analysed coatings using scanning microscopy demonstrate that the observed characteristic columns endings located on surface, forming appropriate coatings, have a shape of reversed pyramids, cones, polyhedrons or craters. However, it is difficult unequivocally to indicate differences among particular coatings in terms of quality and quantity on the basis of observations of the received topography images for the analysed surfaces (Fig. 16-24).

The chemical composition investigations for coatings acquired in the magnetron PVD process, made by a glow-discharge optical emission spectroscopy method, confirm Titanium, Nitrogen, Carbon and Aluminium occurrence in the investigated coatings, and the qualitative content of chemical elements (Table 2) making up a coating defined at 1 μm deep on the basis of profiles intersection of the investigated coatings (Fig. 26), drawn up while investigating. The chemical composition studies of coatings obtained in an arch PVD and high-temperature CVD processes made, using EDS system (Fig.17, 19, 21) confirm proper elements appearance in any analyzed layers, whereas for the sake of low thickness of the deposited layers and characteristics of incident beam, in some cases the applied method allows for a mean measurement of scattered X-rays radiation energy for two or more layers of the investigated coating.

The applied method of X-ray qualitative phase analysis carried out in Bragg-Brentano geometry confirms occurrence of appropriate phases in the investigated substrates and coating materials. Some of identified reflexes on analysed diffraction patterns are moved towards lower or higher angles of reflection as well as their intensity differ from values given in JCPDS card files, what may indicate on occurrence of texture as well as of compressive or tensile, internal stresses in the investigated coatings – a fact one can come across frequently in coatings deposited by the PVD and CVD [20, 95] technique.
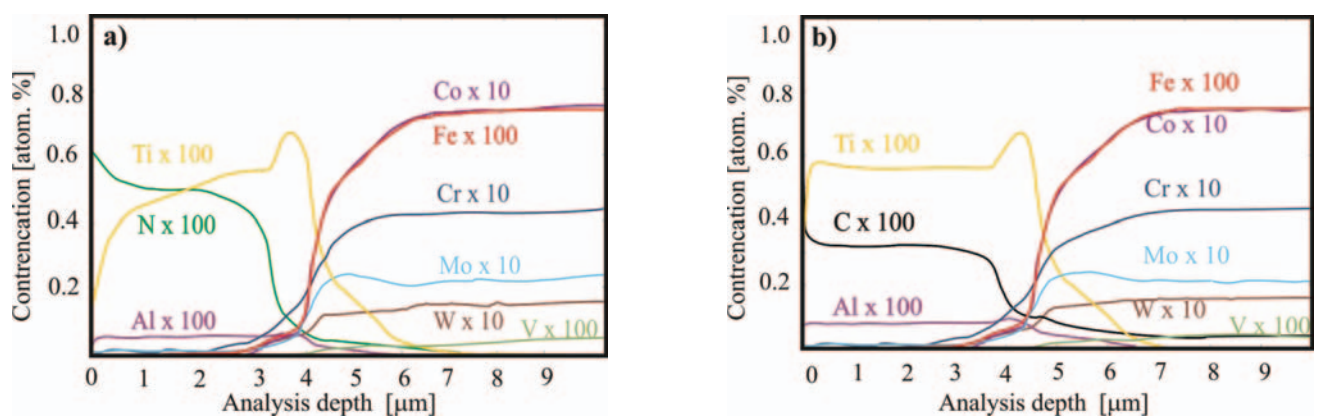
Fig. 26. Changes for coatings components concentration: a)Ti+(Ti,Al)N and b)Ti+(Ti,Al)C obtained in 500°C, and for the material substrate (magnetron PVD process)

Table 2.
The analyses of chemical composition of coatings acquired in the magnetron PVD process at sintered high-speed steel PM HS6-5-3

Type of coating (furnace atmosphere)	Process temperature, [°C]	Atomic concentration of the elements, [%]			
		Ti	N	C	Al
Ti+(Ti,Al)N (100%N_2)	460	48	42	-	9
	500	44	51	-	5
	540	43	51	-	3
Ti+(Ti,Al)(C,N) (75%N_2:25%CH_4)	460	59	28	4	8
	500	60	28	4	7
	540	58	31	4	4
Ti+(Ti,Al)(C,N) (50%N_2:50%CH_4)	460	58	24	11	6
	500	67	15	10	7
	540	63	19	11	6
Ti+(Ti,Al)(C,N) (25%N_2:75%CH_4)	460	62	10	21	6
	500	60	10	23	6
	540	59	11	25	6
Ti+(Ti,Al)C (100%CH_4)	460	58	-	32	8
	500	57	-	34	8
	540	55	-	36	8

For the sake of reflexes overlapping of material substrate and coating/coatings, as well as their intensity, making sometimes the analysis of obtained results more difficult; and in order to acquire more accurate information from subsequent layers of the analyzed materials, additional technique of diffraction is applied at grazing incidence geometry (GIXRD), for the primary X-rays beam using a parallel beam collimator in front of proportional detector. Thanks to the possibility to register the diffraction patterns at low incidence angles of the primary beam onto the test piece surface, one can obtain the diffraction lines from thin layers due to volume growth of the material participating in diffraction and acquiring information on the changing phase composition at different depths of the examined material – which do not exceed the rays beam penetration depth
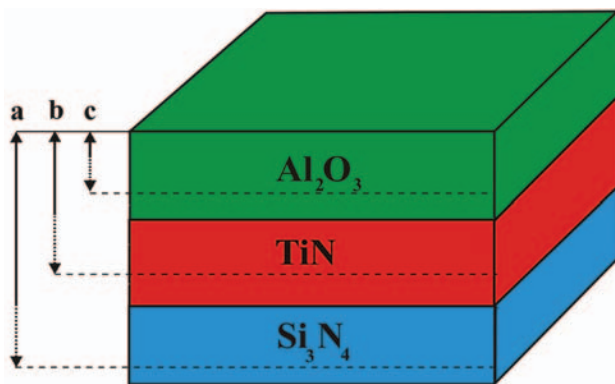
Fig. 27. Scheme for layers on-lapping/packing on a TiN+Al_2O_3 coating received in high-temperature CVD process made of nitride ceramics Si_3N_4 and areas covered by diffraction depending on applied geometry measurement: a) Bragg-Brentano geometry, b) in grazing incidence geometry, $\alpha_x = 3°$, c) in grazing incidence geometry, $\alpha_x=1°$

when their incident angle is perpendicular to the test piece [96]. Carried out investigations at such assumptions conform the right sequence of layers (Fig. 27-29) in analyzed coatings.

Texture analysis for investigated coatings is carried out by a reflexion method. Concentric distribution of pole figures intensity changing along with a beam of those figures indicates occurrence of axial component texture of coatings acquired in the arc and magnetron PVD process. Areas of intensity increase on recorded figures, independently on conditions to obtain coatings in the magnetron PVD process correspond to fibres presence <110> with direction close to a perpendicular direction in respect of sample plane. Depending on parameters needed to obtain a sample, fibres direction <110> is deviated from normal one against sample surface from 1 to 4˚, thus, the distinguished axis deviation is dependent on vacuum furnace atmosphere and process temperature, and it is decreased when increasing supply current voltage in the course of a process of their depositing. Texture image of an exemplary coating acquired in the magnetron PVD process is presented in the form of experimental pole figures determined as CPF, complete pole figures calculated from FRO determined as RPF, pole figures determined from FRO after transformation, determined as APF (Fig. 30), and FRO before and after transformation (Fig. 31). Calculations of volume fractions for texture components were carried out using integration of those components in FRO space subjected to transformation. In calculations of volume fractions, in identified texture components, angle broadening is taken into account ($\Delta\Phi$, $\Delta\phi_1$, $\Delta\phi_2$), which is situated in the range of 10-15°. Obtained calculations results of identified component fractions, depending on conditions to acquire coatings, are shown in table 3. Judging by analyzed coatings, the preferred orientation should be <111>, because this is a plane of the densest atoms packing and it should be perpendicular to a plasma beam. Introducing additional source of energy, which in the analyzed case was a vacuum furnace causes

inclination of orientation <111> to magnetron axis, in effect it is the observed texture <110> of the analyzed coatings, and its intensification, is mostly dependant on the process atmosphere composition and conditions to obtain coatings. In order to define, whether distinguished orientation in the analyzed coatings acquired in the magnetron PVD is not inherent, pole figures of substrate's material and titanic interlayer are measured. On the ground of analysis of the pole figures and FRO, it is stated that orientation distribution of crystallites in substrate's material and in the interlayer is very close to equi-probable distribution, what indicates that fibres occurrence <110> ‖ KW in external coatings it is related neither to substrate texture, nor to interlayer texture.

In case of coatings obtained in the arc PVD process, for the sake of overlapping reflexes, in most cases, of substrate and coating/coatings material, the full FRO analysis was not succeeded for the applied symmetrical Bragg-Brentano geometry of pole figures measurement, except for TiN coating obtained on substrate made of tool ceramics - Al_2O_3+SiC, in which volume fraction of the distinguished component <111> is approx. 46% (Fig. 32, 33). The pole figures measurement in grazing incidence geometry ($\alpha_x = 1°$) determine that application of additional angle in relation to the symmetrical geometry cause that coordinates of a pole figure in a sample arrangement cannot be directly expressed by vector's coordinates of diffraction in this arrangement. A figure, received in that way, depending on its recording angle 2Θ, may be internally contradictory; therefore, it is not an appropriate set of data to reproduce a reliable, three-dimensional function of orientation distribution.
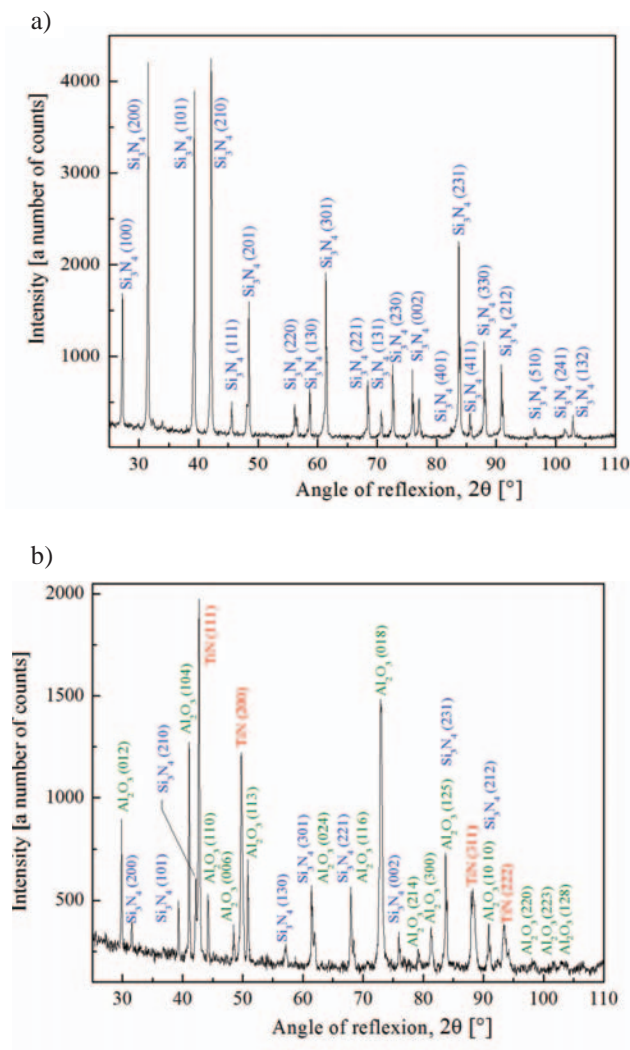
Fig. 28. X-rays diffraction patterns acquired in Bragg-Brentano geometry a) nitride ceramics and b) TiN+Al_2O_3 coatings obtained in high-temperature CVD process on a substrate made of Si_3N_4
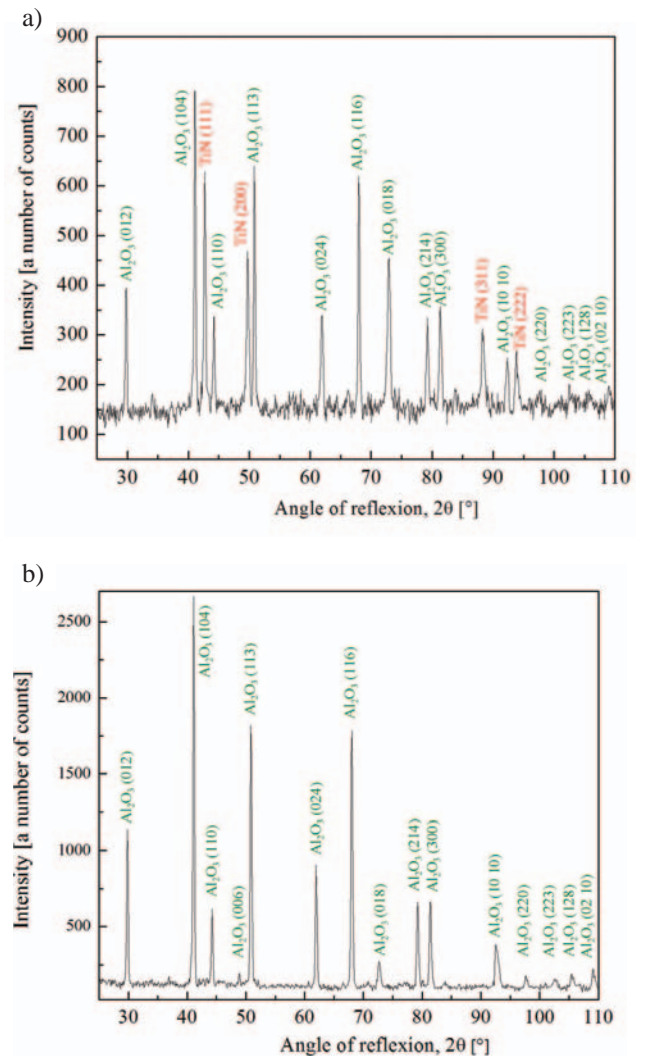
Fig. 29. X-rays diffraction patterns of TiN+Al_2O_3 coating obtained in high-temperature CVD process on a substrate made of nitride ceramics Si_3N_4 received in geometry of constant angle of incidence: a) GIXRD method, $\alpha_x = 3°$, b) GIXRD method, $\alpha_x = 1°$
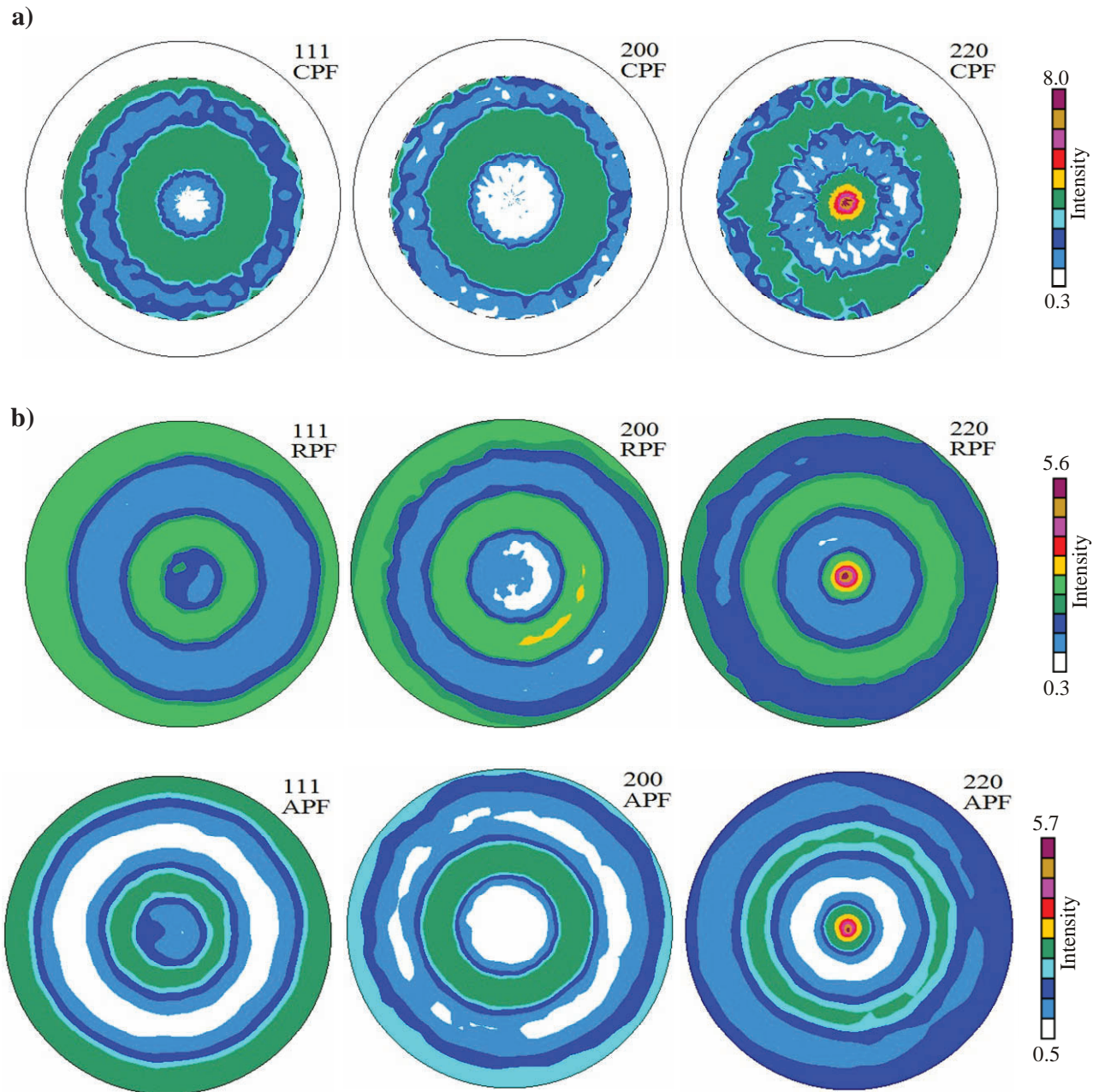
Fig. 30. Pole figures (111), (200) and (220) of (Ti,Al)N coating obtained in the magnetron PVD process on a substrate made of sintered high-speed steel PM HS6-5-3-8 in 540ºC a) experimental, b) calculation based on FRO, c) calculation based on FRO after transformation

Detailed issues related to X-rays texture tomography were presented by Bonarski [97], describing proper measuring procedures for different geometries of pole figures measurement. In accordance with [97], the obtained pole figure in grazing incidence geometry must be transformed into normal figures, and then, subjected to interpolation, because it is "incomplete" on the edges as well as in the middle part to carry out a full FRO analysis. The analysis of texture made for coatings obtained in the arc PVD process allows stating, based on qualitative analysis of recorded single pole figures, that independently on substrate's material, in the following coatings TiN, TiN+(Ti,Al,Si)N+(Al,Si,Ti)N, TiN+(Ti,Al,Si)N,

a)

b)

c)
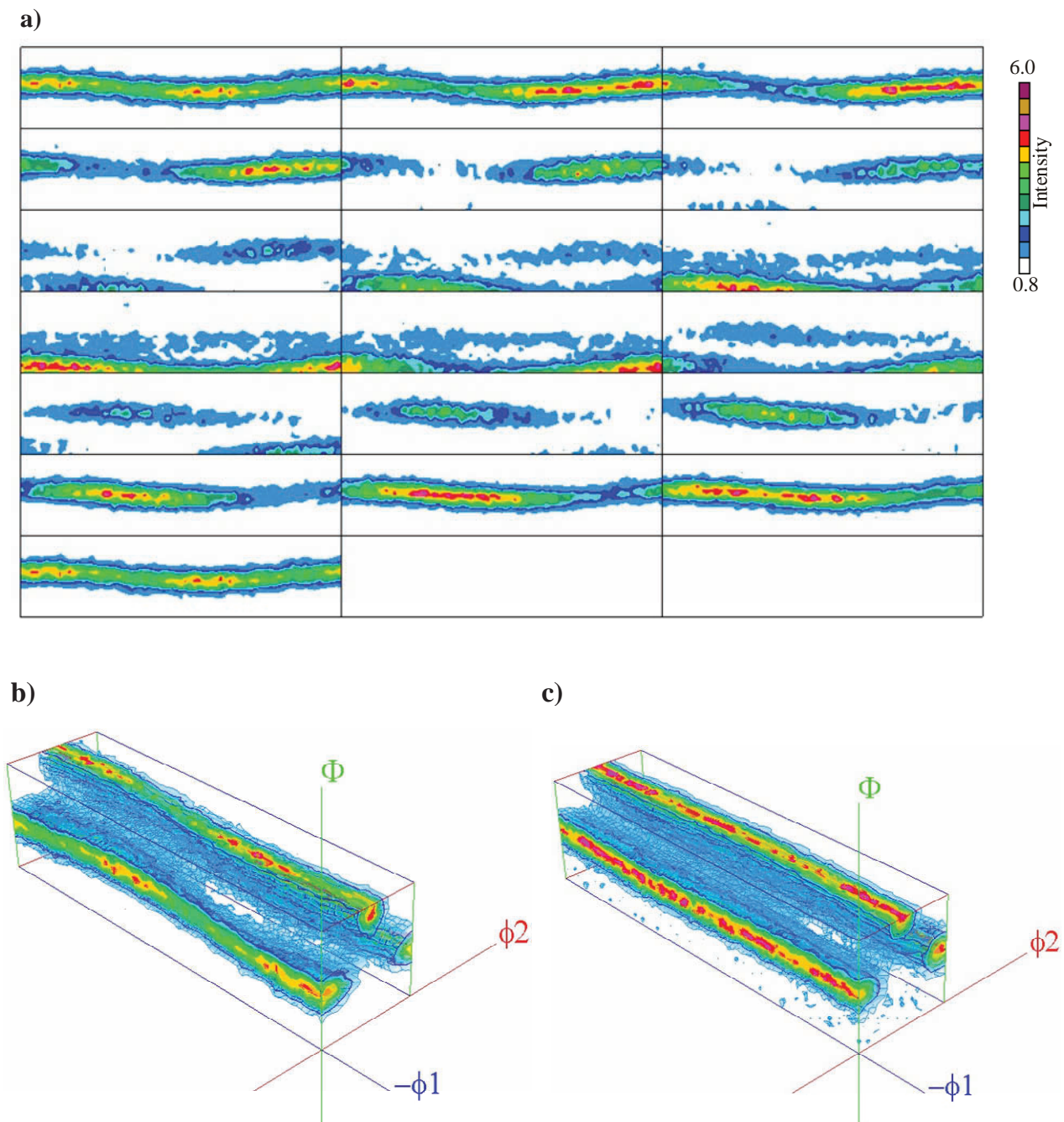
Fig. 31. A distribution function of coating orientation (Ti, Al)N obtained in the magnetron PVD process on a substrate made of sintered high-speed steel PM HS6-5-3-8 in 540°C: a) section acc. to φ_2 (for the following values φ_2: 0, 5, 10...90°), b) 3D FRO, c) 3D FRO view after transformation

TiN+multi(Ti,Al,Si)N+TiN the distinguished plane of increase is a plane of {111} family, whereas, in case of (Ti,Al)N coatings the texture of deposited layers is very weak. The analysis of pole figures of coatings acquired in the high-temperature CVD process proves that their texture is very weak, and density of poles projections hesitates within 0.9 to 1.1 of density corresponding to equi-probable distribution.
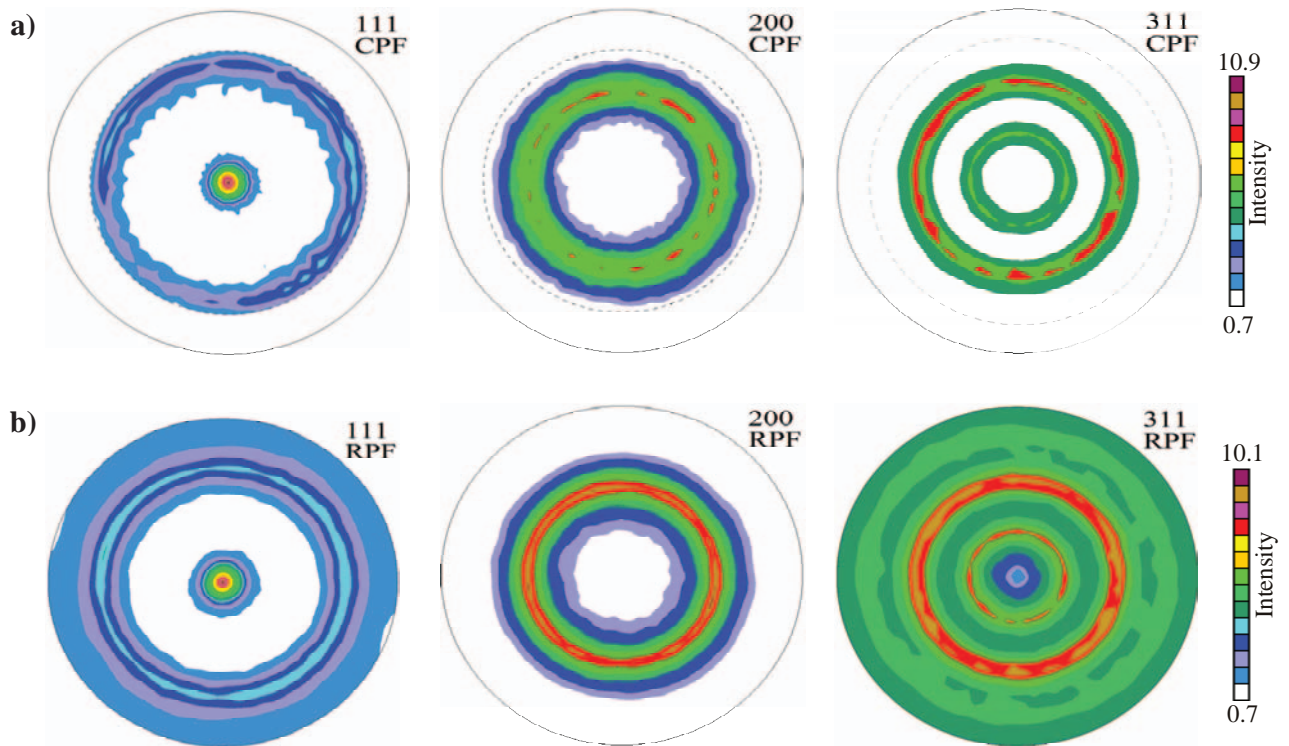
Fig. 32. Pole figures (111), (200) and (311) TiN coatings obtained in the arc PVD process on a substrate made of tool ceramics Al_2O_3+SiC
a) experimental, b) calculation based on FRO

Table 3.
Texture volume fractions, deviation of distinguished axis and conditions to acquire coatings in the magnetron PVD process on a substrate made of sintered high-speed steel

Type of coating	Process temperature [°C]	Vacuum furnace atmosphere	U for magnetron [V]	I for magnetron [A]	Volume fraction for <110> component in areas covered by diffraction [%]	Deviation of distinguished axis from normal one to surface [°]
Ti+(Ti,Al)N	460	100%N_2	380	7	59	2
Ti+(Ti,Al)N	500	100%N_2	390	8	53	1
Ti+(Ti,Al)N	540	100%N_2	360	8	46	4
Ti+(Ti,Al)(C,N)	460	75%N_2:25%CH_4	385	6	75	3
Ti+(Ti,Al)(C,N)	500	75%N_2:25%CH_4	390	6	67	2
Ti+(Ti,Al)(C,N)	540	75%N_2:25%CH_4	400	6	55	1
Ti+(Ti,Al)(C,N)	460	50%N_2:50%CH_4	380	6	53	4
Ti+(Ti,Al)(C,N)	500	50%N_2:50%CH_4	420	6	35	-
Ti+(Ti,Al)(C,N)	540	50%N_2:50%CH_4	395	6	55	3
Ti+(Ti,Al)(C,N)	460	25%N_2:75%CH_4	420	6	34	-
Ti+(Ti,Al)(C,N)	500	25%N_2:75%CH_4	400	6	37	1
Ti+(Ti,Al)(C,N)	540	25%N_2:75%CH_4	400	5	42	1
Ti+(Ti,Al)C	460	100%CH_4	395	5	35	1
Ti+(Ti,Al)C	500	100%CH_4	400	5	48	-
Ti+(Ti,Al)C	540	100%CH_4	410	5	61	-

a)

b)

c)
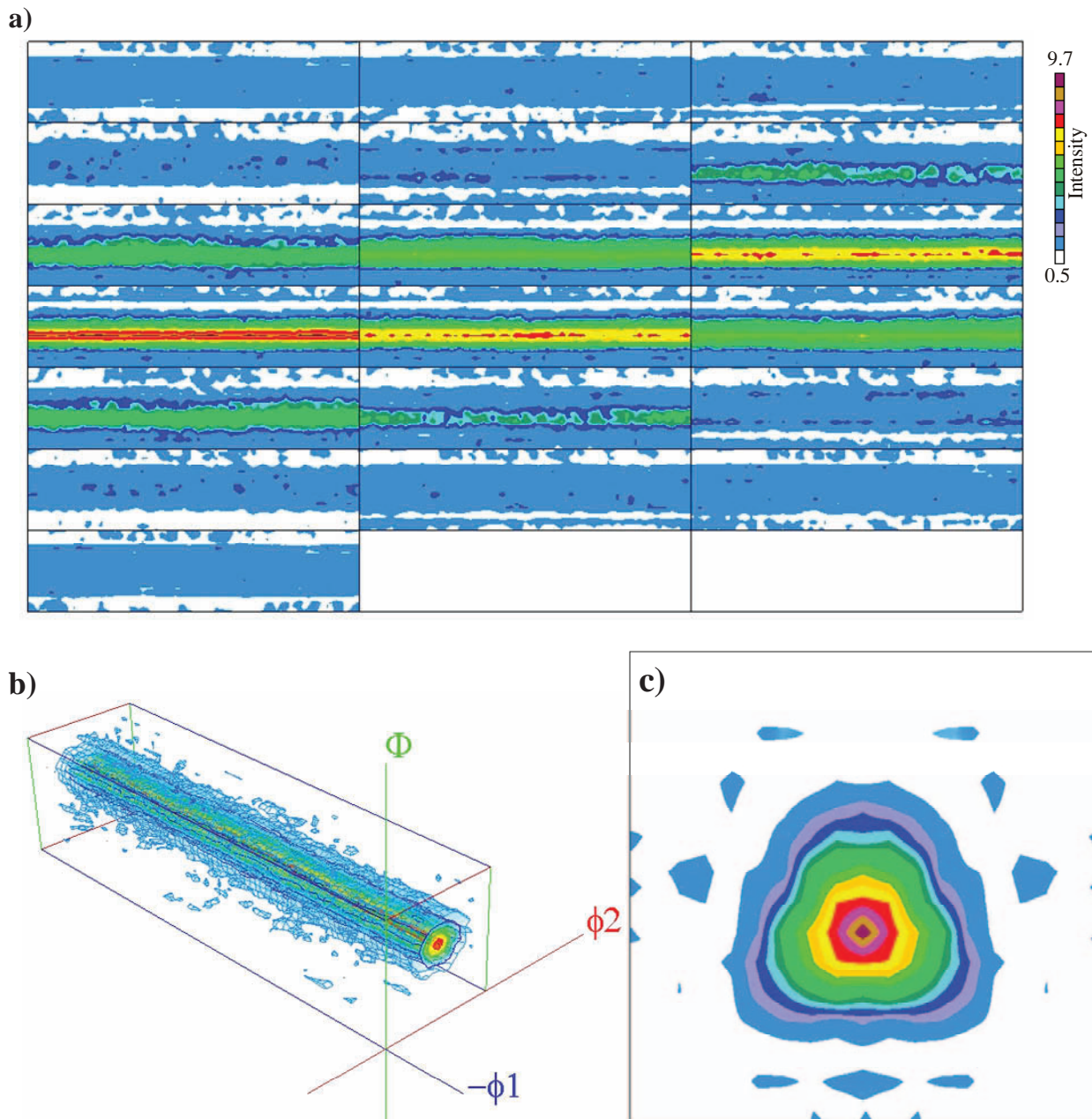
Fig. 33. Distribution function of coating orientation TiN obtained in the arc PVD process on the basis made of tool ceramics Al_2O_3+SiC a) section acc. to φ_2 (for the following values φ_2: 0, 5, 10…90°), b) 3D view FRO, c) FRO determined on the basis of pole figures subjected to symmetrisation (section acc. to φ_1)

4.2. Mechanical and operational properties of investigated coatings

So that deposited coating on a tool could properly fulfil its task, it has to be characterized by suitable usable properties determined by numerous factors, among which the following should be specified: appropriate structure, chemical and phase composition, proper hardness and thickness, and above all, high adhesion to substrate's material [21, 22]. Adhesion dependence of the analysed coatings for substrates material on conditions of a process needed to obtain them is evaluated by a "scratch test" method at changing load, establishing a value of critical load L_c, allowing to determine a force value inducing the coating damage (table 6 and 7). The critical value L_c is settled as adequate to growth of acoustic emission intensity (Fig. 34), signalling fraction

imitation of coating. The highest values of the critical load $L_c > 100$ N are found for (Ti,Al)N & (Ti,Al)C coatings obtained in the magnetron PVD process, deposited with vapour in 460 and 540° C on a substrate made of sintered high-speed steel, as well as TiN+(Ti,Al,Si)N & (Ti,Al)N acquired in the arc PVD process, on a substrate from tool cermets and tool ceramics made of Al_2O_3+SiC, respectively. In case of coatings got in high-temperature CVD process, a value of critical load is contained within 25.8 to 85.2 N, if a substrate is nitride ceramics Si_3N_4, and a coating is formed of layers' combination TiC+TiN and TiN+Al_2O_3, respectively.

Specific nature of damages being responsible for fractions initiation, observed by means of a scanning microscope at the edge of scratch-coating depends on a type of process and a combination of the applied layers, and the following might be mainly enumerated: spallings formation on the edges in the shape of tiny craters, that in some cases are related to local delamination of a coating's fragment (the magnetron PVD process), conformal cracks induced by tension, undergoing single scaling (the arc PVD process), periodical delamination and one and
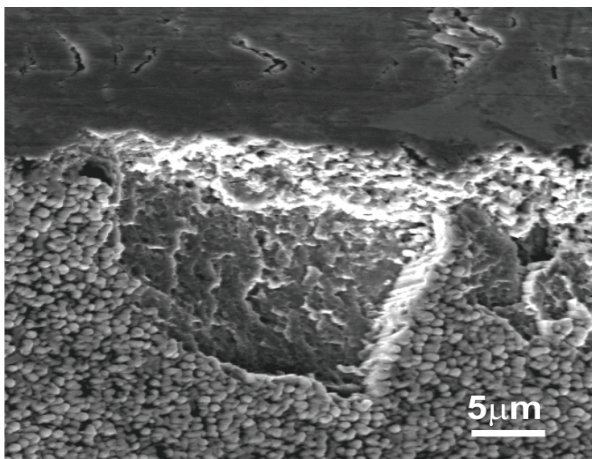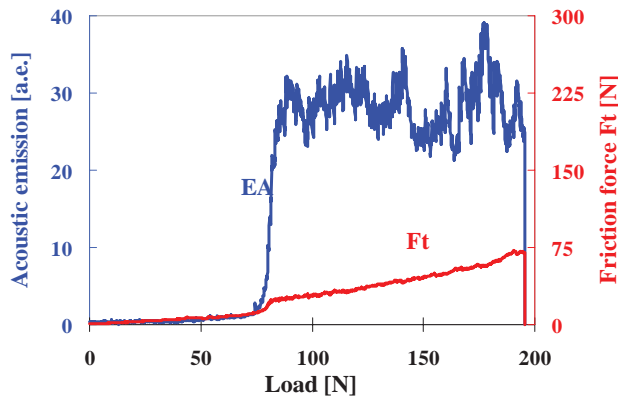
two-sided spallings, as well as local stratification, and the following, as a consequence, displacement of torn fragments of the coating (high-temperature CVD process) [17, 35]. Obtained outcomes of adhesion assessment depend on a type of process and applied layers, their thickness, chemical and chase composition, and also on material, upon which they were produced, what consequently has an impact on stresses value in the analysed coatings (results of stresses measurement and its influence on the adhesion to substrate's material are presented further in this paper).

Stresses' measurements of the analyzed materials are performed by two methods, and obtained results are presented in tables 4 & 5. Stresses' measurements by $\sin^2\psi$ method are made for three φ angles of samples arrangement towards an initial configuration, in which goniometer axis was in two opposite directions continuously ($\varphi = 90$ & $270°$, $\varphi = 150$ & $330°$, $\varphi = 210$ & $30°$). Applying this geometry of measurement enables to observe changes of state of stress for chosen directions of investigated material and to determine its highest value [98-100]. In case of coatings obtained in the magnetron PVD process, the stresses' assessment by $\sin^2\psi$ method is made based on analysis of reflexes (311) (Fig. 35) for the sake of the privileged <110> direction of their increase. For coatings acquired in the arc PVD and high-temperature CVD process, stresses are defined on the ground of analysis of reflex displacement recorded at the highest value of 2Θ angle, free from influencing on its shape and location of the other components of the investigated material (substrate's material, possible other layers included in the coating). Locations of the recorded reflexes were determined by a Gaussian curves matching method. In the method of $\sin^2\psi$, to assess stresses, the reflexes recorded at higher values of the angle 2θ are preferred considering higher deformations sensitivity and lower error of obtained results, however, it is not always possible to achieve that in experimental studies, when too low peaks intensity, resulting from texture of analyzed coatings, extensive or irregular shape and relatively small depth of penetration of X-rays radiation at high angles of reflexion make impossible correct and proper assessment.

Fig. 34. Dependence of acoustic emission EA and friction force Ft on loading force quantity and its corresponding image of damage observed on a scanning microscope for a Ti+(Ti,Al)N coating obtained at 540° C
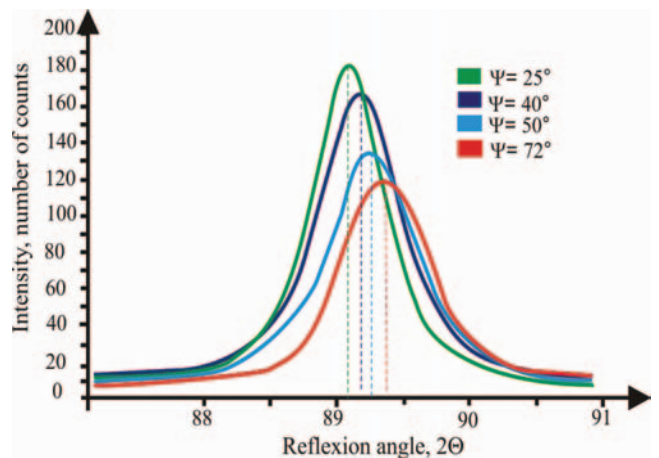
Fig. 35. A graph for reflex location changes (311) of a Ti+(Ti,Al)N coating obtained in 540° C for a selected angle value ψ
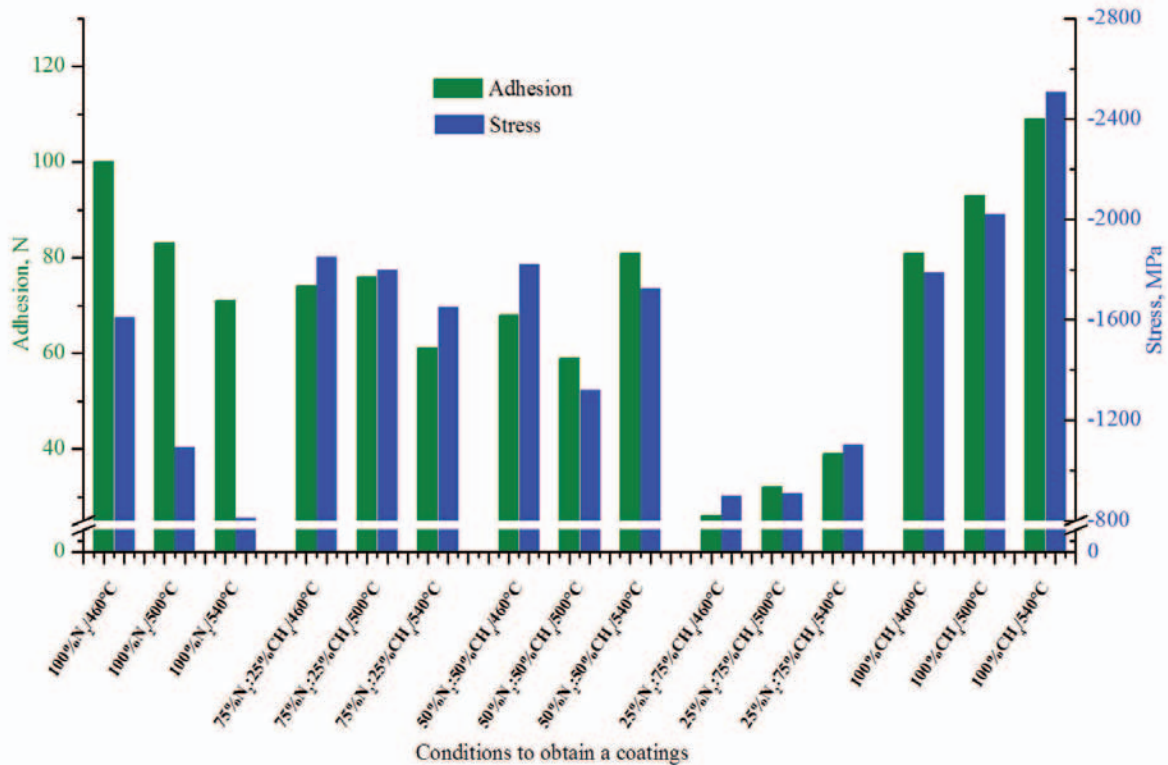
Fig. 36. Adhesion and stresses dependence on conditions allowing to get coatings in the magnetron PVD process

In case of studying multi-layer coatings and/or coatings of phase composition close to the substrate's material, applying this geometry of measurement not always guarantees reception of correct results of measurements as a result of particular components reflexes overlapping of the investigated materials. Because of this, measurements of the analyzed coatings stresses are conducted additionally by a method of g-$\sin^2\psi$. The method g-$\sin^2\psi$ defining stresses based on geometry of a constant incidence angle was proposed by Van Hacker [101], Quaeyhaegens and Knuyt [102], and then, it was expanded by Skrzypek. Finally, algorithm for calculations of stresses was applied by Skrzypek and Baczmański [33, 91, 103]. The method of g-$\sin^2\psi$ is characterized by the use of many diffraction lines from planes {hkl} in contradiction to a classical method of $\sin^2\psi$, using one diffraction line [104]. The main advantage of the method g-$\sin^2\psi$ in reference to the classical method $\sin^2\psi$ measuring stresses, where we are engaged in variable, effective depth of penetration of X-rays radiation into the investigated material, it is almost a constant value for a fixed value α_x, which can be changed by incidence angle or selection of different type of radiation. Moreover, in this method, changing reflexes {hkl} for a crystallographic plane are simultaneously used in a measuring procedure to determine stresses and the method can be easily applied for changing geometries of measurement [33, 91, 99, 103, 104].

Each time measurements of stresses were carried out upon external coating, and as far as it was possible, depending on a type of substrate's material, properties and configurations of the applied layers, in a coating adhering to it, using one or two non-destructive methods to measure this size. Results of the performed studies for internal macro-stresses of the analyzed coatings (determined for the magnetron PVD process by a method $\sin^2\psi$
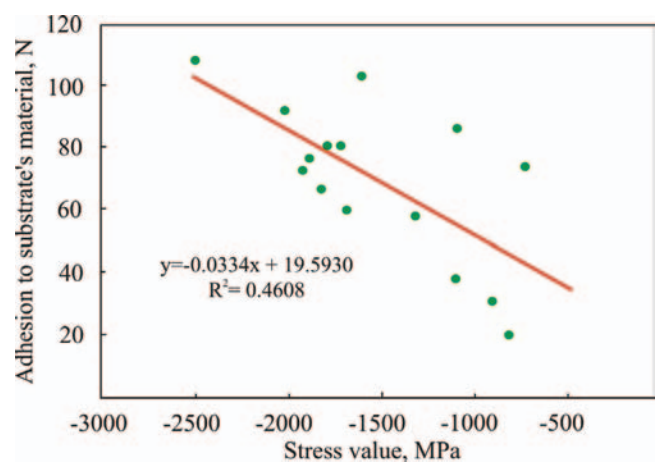
Fig. 37. Adhesion dependence on stresses' values determined by the g-$\sin\sin^2\psi$ method for coatings received in the magnetron PVD process
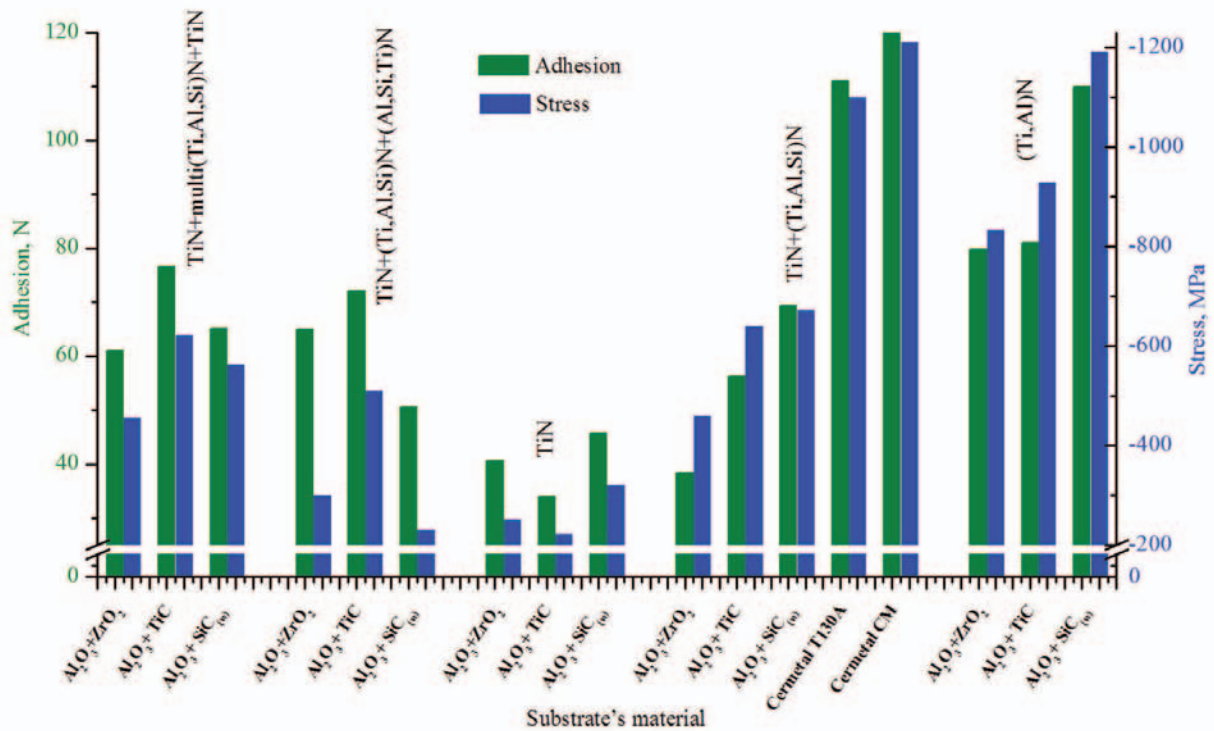
Fig. 38. Adhesion and stresses dependence on substrate's material for coatings obtained in the arc PVD process

and g-sin $\sin^2\psi$ for the arc PVD process) indicate a correlation between a size of stresses and hardness as well as adhesion to substrates of the investigated coatings (Fig. 36-39). A value of adhesion to substrate's material from stresses occurring in coatings can be defined by the following analytical dependence y=-0.0334x+19.5930 (Fig. 37) for the PVD magnet process and y=-0.0691x+26.3277 for the arc process (Fig. 39). Assessing dependence between stresses and coatings' adhesion obtained in the magnetron and the arc PVD process, all correlation coefficients were found, equalling respectively r= 0.678858 and r = 0.913264. Significance of the shown correlations was confirmed by means of a test using statistics t (formula 3) subjected to student's distribution, including a number of degree of freedom equalled n – 2 at the significance level α_{stat}=0.05 (Table 11, summary of a statistical analysis result).

The carried out investigations results for internal macro-stresses (defined by the g-sin $\sin^2\psi$ method) in TiN+Al$_2$O$_3$ coatings acquired in the CVD process show dependencies between coatings' stresses size and their adhesion to substrate's material (Fig. 40). An adhesion value to the substrate's material from stresses appearing in coatings can be defined by the following analytical dependence: y=-0.1447x-0.8489 (Fig. 41). Assessing a dependence between stresses occurring in external layer made of Al$_2$O$_3$ and its adhesion to the substrate's material, the following high correlation (table 11) was found (correlation coefficient r=0.960) and essential one (t=4.871 towards t$_{kryt}$=4.303).

Depending on their value, internal stresses can affect the substrate – coating arrangement unfavourably or positively, and by

extension, they can decide about application of produced tools afterwards. Compressive stresses (Fig. 42 & 44 – "negative" slope of a line acquired while stresses measuring) increase crack resistance and to some degree, dependent on thickness, phase and chemical composition as well as material, at which they have been reached, minimize a coating chipping increasing their adhesion to substrate [91].
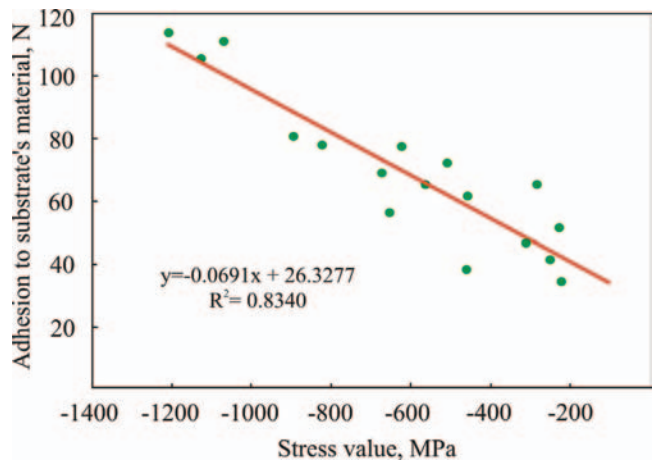
Fig. 39. Adhesion and stresses dependence on substrate's material for coatings obtained in the arc PVD process

The opposite type of stresses (Fig. 43 & 45 – "positive" slope of a line acquired while stresses measuring), compressive stresses can accelerate destruction of a coating while imposing an external load. A very important factor having an impact on state of internal stresses in coatings is their structure, which is strictly related to a technique obtaining them, by phase and chemical composition, texture, process temperature and type of substrate, on which it was obtained [91, 103]. Besides, increase of stresses' value along with coatings' thickness was found, analyzing and comparing layers of close phase composition obtained on the same substrate; this phenomenon was described by Thornton and Hoffman in their thesis [105]. While adhesion scratch test is carried out, shearing stress in a transition zone is induced by influence of a loaded penetrator in a normal direction on a coating – substrate configuration. The stresses caused by pressure/thrust of a shifting penetrator are transferred by a coating to the transition zone. Thicker coatings, in this case, require higher load to get the same shearing stresses in the transition zone between the coating and the substrate's material.

Sheeja, while work [22] presented interdependencies of: thickness and stresses as well as thickness and adhesion to substrate's material of diamond-like carbon coatings, showing similar correlations. A deposited inter-layer Ti in case of coatings acquired in the magnetron PVD process between samples surface and coatings has an influence on relaxation of stresses on external coatings Ti+(Ti,Al)N, Ti+(Ti,Al)(C_xN_{1-x}), obtained at different concentrations of N_2 & CH_4 in a vacuum furnace chamber and Ti+(Ti,Al)C as a result of difference between coefficients of thermal expansion values for substrate and coating materials, and also for the sake of solubility limit of Fe in Ti. Similar effect was found in case of coatings obtained in the high-temperature CVD and the arc PVD process for an inter-layer being in direct position with a substrate's material, and the received results of coatings of stresses' measurements TiN+Al_2O_3 testify about that, obtained in the CVD process on a substrate made of ceramic materials (Fig. 40). Reaction influence of an intermediate inter-layer on structure and coatings properties was confirmed in theses of other authors [21, 23, 106]. Comparing both techniques of measurement of stresses, it was found that its proper selection depends, in a large degree, on structure and properties of investigated materials.
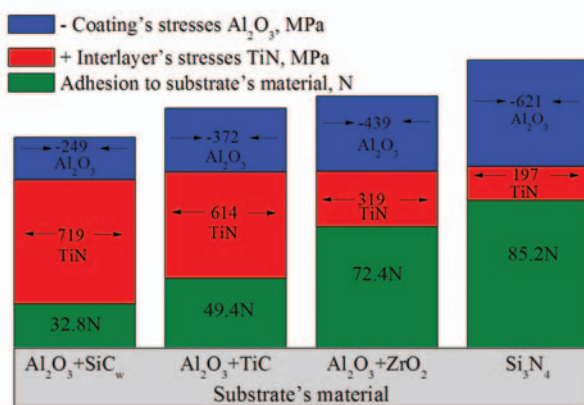
For coatings, not determined by texture, consisting of many layers giving many diffraction reflexions, it is strongly recommended to apply the method of g-$\sin^2\psi$, where measurement results of stresses are burden with a less-important mistake, whereas in some cases they are impossible to get by a classical method. The perfect example is the obtained results of stresses' measurement of coatings acquired in the high-temperature CVD process, where the analyzed coating was Al_2O_3, for the sake of lack of texture and relatively great number of diffraction reflexes from one phase in reference to the others. For coatings revealing strong texture, obtained in the magnetron PVD process, values of stresses burden with less-important mistake were obtained for measurements run by a classical method of $\sin^2\psi$. Analyzing coatings obtained in the arc PVD process, except for (Ti,Al)N coatings, where for both methods of measurement close values of mistake were reached due to substrate reflexes overlapping, analyzed layers, and low thickness of theirs; more practical in use was found in technique of stresses' measurement in grazing incidence geometry.

Phase and chemical composition, conditions and type of process as well as substrate's material and combination of the applied layers and texture influence on microhardness of the investigated coatings. In case of coatings obtained in the magnetron PVD process acquired in atmosphere containing 100% N_2, 75% N_2 and 25% CH_4 hardness value increase was found along with increasing concentration of Al in defined range (3%-9%) of concentrations of the same elements in coatings (Fig. 46 & 47). Influencing mechanism of Al on structure and coatings' properties (Ti, Al) N is described in papers [107, 108] obtaining close results to the obtained ones. For carbide and carbonitride coatings obtained in atmosphere containing 75% CH_4 & 25% N_2, hardness increase was found along with increase of carbon, carbon and nitrogen concentrations in coatings at relatively constant Al concentration. Carbon concentration increase in the analyzed coatings can be bound at facilitated dissociations CH_4 in higher temperature of depositing process. Moreover, hardness increase was noticed along with volume fraction increase of the texture component <110> in analysed coatings.

Fig. 40. A scheme for stresses influence defined by the method of g-$\sin^2\psi$ in the intermediate inter-layer and external coating on adhesion of TiN+Al_2O_3 coatings obtained in the CVD process depending on substrate's material
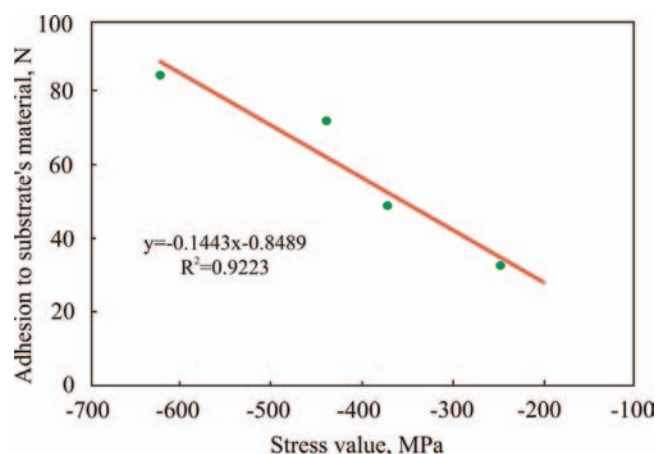
Fig. 41. Adhesion dependence on stresses' values defined by the method of g-$\sin^2\psi$ in the external coating of TiN+Al_2O_3 coatings obtained in the CVD process
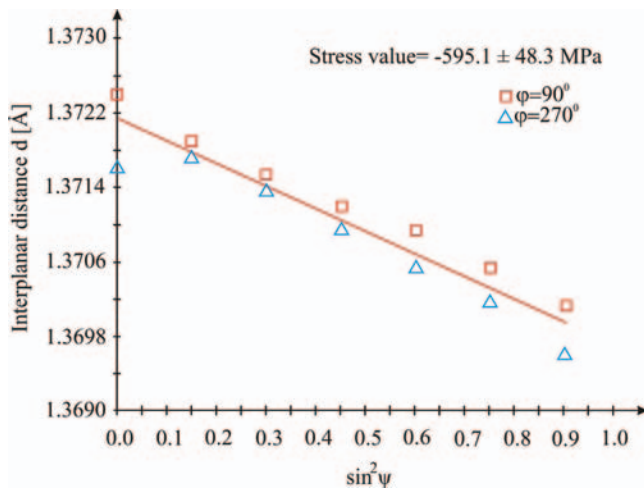
Fig. 42. Changes of interplanar distance value d of reflex (300) in the layer Al_2O_3 as a function of $\sin^2\psi$ (stresses' measurement made by $\sin^2\psi$ method for different φ values of samples setting towards goniometer axis, $TiN+Al_2O_3$ coating obtained on a substrate made of nitride ceramics - Si_3N_4)

Fig. 44. Changes of the epsilon values (ppm) specifying crystallographic lattice deformation for Al_2O_3 layer in a function of $\sin^2\psi$ (stresses' measurement by the method of g-$\sin^2\psi$, coating $TiN+ Al_2O_3$ obtained on a substrate made of nitride ceramics Si_3N_4)

As a result of conducted studies on microhardness, it was found that depositing PVD and CVD coatings on ceramic materials causes hardness increase of a surface layer, containing within 2150-3950 HV, or even by 100% in reference to substrates' hardness. In case of coatings obtained in the arc PVD process, the highest hardness is determined by TiN+multi(Ti,Al,Si)N+TiN layers, apart from a type of substrate's material. Distinct correlation among stresses, adhesion and microhardness is pointed out in case of coatings not showing any privileged orientation of increase (Ti,Al)N obtained on ceramic tool materials (Fig. 48).

In the event of CVD, coatings with external layer Al_2O_3 are characterized by higher hardness than TiN ones.

Based on performed studies for cutting ability, it was found that coatings' deposition in the PVD and CVD processes on ceramic tool materials causes increase their frictional wear resistance, what directly influences over extension of a cutting tool life. The presented results indicate that wear rate reduction of a surface cutting plates rank along with deposited coatings depends on their structure and topography of surface, phase and chemical composition, mechanical properties and substrate's material, upon which they have been obtained.

Fig. 43. Changes of interplanar distance of d reflex (222) of intermediate TiN layer as a function of $\sin^2\psi$ (stresses' measurement made by $\sin^2\psi$ method for different φ values of samples setting towards goniometer axis, $TiN+Al_2O_3$ coating obtained on a substrate made of nitride ceramics - Si_3N_4)
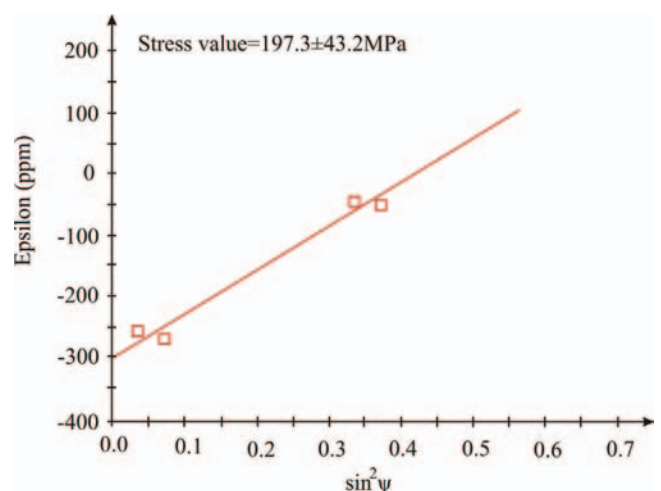
Fig. 45. Changes of the epsilon values (ppm) specifying crystallographic lattice deformation for TiN layer in a function of $\sin^2\psi$ (stresses' measurement by the method of g-$\sin^2\psi$, coating $TiN+Al_2O_3$ obtained on a substrate made of nitride ceramics Si_3N_4)

Table 4.
Results of stresses' measurements of coatings obtained in the arc and the magnetron PVD process by $\sin^2\psi$ and g-$\sin^2\psi$ methods

Type of process	Substrate's material	Type of coating	Coating thickness [μm]	Method $\sin^2\psi$ [MPa]	Method g-$\sin^2\psi$ [MPa]
PVD$_{arc}$ (550°C)	Al$_2$O$_3$+ZrO$_2$	TiN+(Ti,Al,Si)N	1.9	-	-461±45
	Al$_2$O$_3$+ TiC	TiN+(Ti,Al,Si)N	2.4	-	-651±74
	Al$_2$O$_3$+ SiC$_{(w)}$	TiN+(Ti,Al,Si)N	2.5	-	-672±62
	Al$_2$O$_3$+ZrO$_2$	TiN	1.1	-	-251±56
	Al$_2$O$_3$+ TiC	TiN	1.3	-	-221±71
	Al$_2$O$_3$+ SiC$_{(w)}$	TiN	1.1	-298±46	-311±75
	Al$_2$O$_3$+ZrO$_2$	TiN+multi(Ti,Al,Si)N+TiN	2.3	-	-455±54
	Al$_2$O$_3$+ TiC	TiN+multi(Ti,Al,Si)N+TiN	2.7	-	-621±63
	Al$_2$O$_3$+ SiC$_{(w)}$	TiN+multi(Ti,Al,Si)N+TiN	2.8	-	-551±59
	Al$_2$O$_3$+ZrO$_2$	(Ti,A)lN	2.2	-791±29	-822±34
	Al$_2$O$_3$+ TiC	(Ti,A)lN	2.2	-798±27	-893±29
	Al$_2$O$_3$+ SiC$_{(w)}$	(Ti,A)lN	2.1	-1144±24	-1128±32
	Al$_2$O$_3$+ZrO$_2$	TiN+(Ti,Al,Si)N+(Al,Si,Ti)N	2.2	-	-284±51
	Al$_2$O$_3$+ TiC	TiN+(Ti,Al,Si)N+(Al,Si,Ti)N	2.2	-	-509±63
	Al$_2$O$_3$+ SiC$_{(w)}$	TiN+(Ti,Al,Si)N+(Al,Si,Ti)N	2.5	-	-231±58
	Cermetal T130A	TiN+(Ti,Al,Si)N	4.6	-	-1070±42
	Cermetal CM	TiN+(Ti,Al,Si)N	4.5	-	-1211±39
Magnetron PVD (100%N$_2$/460°C)	PM HS6-5-3-8	Ti+(Ti,Al)N	6.9	-1611±44	-1523±98
Magnetron PVD (100%N$_2$/500°C)	PM HS6-5-3-8	Ti+(Ti,Al)N	3.9	-1093±27	-976±78
Magnetron PVD (100%N$_2$/540°C)	PM HS6-5-3-8	Ti+(Ti,Al)N	3.7	-774±32	-791±81
Magnetron PVD (75%N$_2$:25%CH$_4$/460°C)	PM HS6-5-3-8	Ti+(Ti,Al)(C,N)	6.6	-1923±37	-2023±84
Magnetron PVD (75%N$_2$:25%CH$_4$/500°C)	PM HS6-5-3-8	Ti+(Ti,Al)(C,N)	6.4	-1871±31	-1791±67
Magnetron PVD (75%N$_2$:25%CH$_4$/540°C)	PM HS6-5-3-8	Ti+(Ti,Al)(C,N)	3.8	-1689±29	-1579±77
Magnetron PVD (50%N$_2$:50%CH$_4$/460°C)	PM HS6-5-3-8	Ti+(Ti,Al)(C,N)	6.8	-1821±79	-
Magnetron PVD (50%N$_2$:50%CH$_4$/500°C)	PM HS6-5-3-8	Ti+(Ti,Al)(C,N)	7.8	-1321±74	-
Magnetron PVD (50%N$_2$:50%CH$_4$/540°C)	PM HS6-5-3-8	Ti+(Ti,Al)(C,N)	7.6	-1724±93	-
Magnetron PVD (25%N$_2$:75%CH$_4$/460°C)	PM HS6-5-3-8	Ti+(Ti,Al)(C,N)	5.8	-841±34	-723±58
Magnetron PVD (25%N$_2$:75%CH$_4$/500°C)	PM HS6-5-3-8	Ti+(Ti,Al)(C,N)	4.9	-908±27	-891±59
Magnetron PVD (25%N$_2$:75%CH$_4$/540°C)	PM HS6-5-3-8	Ti+(Ti,Al)(C,N)	5.1	-1102±29	-1012±71
Magnetron PVD (100%CH$_4$/460°C)	PM HS6-5-3-8	Ti+(Ti,Al)C	4	-1789±31	-1890±79
Magnetron PVD (100%CH$_4$/500°C)	PM HS6-5-3-8	Ti+(Ti,Al)C	4.2	-2021±32	-2108±88
Magnetron PVD (100%CH$_4$/540°C)	PM HS6-5-3-8	Ti+(Ti,Al)C	4.6	-2508±44	-2645±77

Table 5.
Results for stresses' measurement of coatings obtained the high-temperature CVD process made by method $\sin^2\psi$ & $g\text{-}\sin^2\psi$

Substrate's material	Type of coating (layers configuration)	Coating thickness [μm]	Type of coating, from which information came (external/indirect)	Method $\sin^2\psi$, [MPa]	Method $g\text{-}\sin^2\psi$, [MPa]
Si₃N₄	TiN+Al₂O₃	9.6	Al₂O₃	-595±48	-621±34
			TiN	212±34	197±43
Si₃N₄	TiN+Al₂O₃+TiN	3.8	TiN	-	-97±43
			Al₂O₃	-99±34	-151±23
Si₃N₄	TiN+Al₂O₃+TiN+ Al₂O₃+TiN	5.1	TiN	-	-120±32
			Al₂O₃	-	-191±26
Si₃N₄	Al₂O₃+TiN	2.7	TiN	69±61	-89±59
			Al₂O₃	-105±32	-123±21
Si₃N₄	TiC+TiN	5.4	TiN	-59±29	-49±43
			TiC	-142±33	-129±41
Si₃N₄	Ti(C,N)+TiN	4.2	TiN	-	-89±42
			Ti(C,N)	-	-219±52
Si₃N₄	Ti(C,N)+Al₂O₃+TiN	9.5	TiN	-	-69±34
			Al₂O₃	-	-108±27
Si₃N₄	Ti(C,N)+Al₂O₃	5.2	Al₂O₃	-452±43	-421±29
			Ti(C,N)	-86±55	-76±33
Al₂O₃+ZrO₂	TiN+Al₂O₃	6.4	Al₂O₃	-	-439±27
			TiN	-	319±56
Al₂O₃+TiC	TiN+Al₂O₃	5.3	Al₂O₃	-	-372±33
			TiN	-	614±52
Al₂O₃+SiC(w)	TiN+Al₂O₃	7.3	Al₂O₃	-	-249±29
			TiN	-	719±58
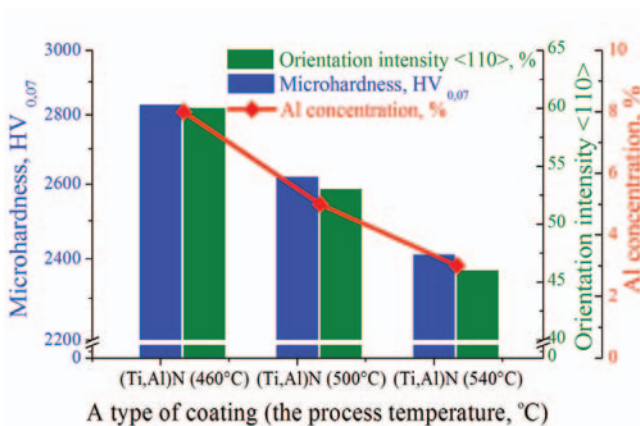
Fig. 46. Correlation of microhardness, texture and Al concentration in (Ti,Al)N coatings depending on temperature of the process to obtain them (the magnetron PVD process)
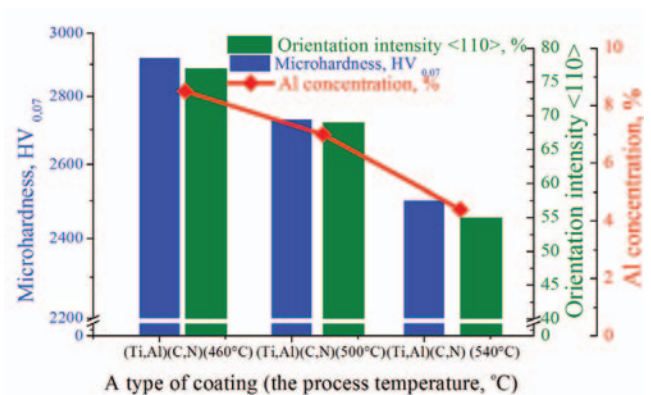
Fig. 47. Correlation of microhardness, texture and Al concentration in (Ti,Al)(C,N) coatings depending on temperature of the process to obtain them (the magnetron PVD process, atmosphere of vacuum furnace – 75%N₂: 25%CH₄)
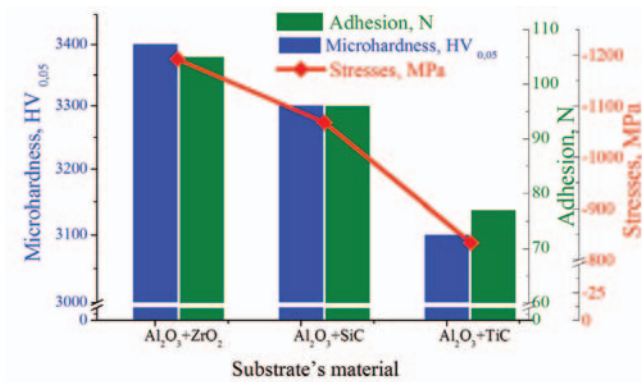
Fig. 48. Influence of substrate's material on the acquired results of microhardness, adhesion and stresses' measurement determined by the g-sin$^2\psi$ method for (Ti, Al)N coatings received in the arc PVD process

The received analyses are shown in the form of graphs depending on wear bandwidth at VB flank face in a function of test duration at specified conditions to execute the experiment, and the obtained results are of comparative character. Based on technological turning test, the most distinctive improvement tool life, comparing TiN+Al$_2$O$_3$ coatings obtained on different substrates as well as coatings obtained on substrates made of nitride ceramics Si$_3$N$_4$ (Fig. 49) acquired in the high-temperature CVD process respectively, when the substrate's material was tool ceramics Si$_3$N$_4$ and external Ti(C,N)+Al$_2$O$_3$ coating. Above-mentioned coatings are characterized by very good adhesion to substrate's material and high microhardness. High adhesion of the analyzed coatings, defined by load value L$_c$ responsible for coating's destruction is adequately 85,2 & 68,3 N, and compressive stresses value is defined by g-sin$^2\psi$ method, adequately -595 & -421 MPa. In the event of coatings received in the arc PVD process, close correlations are found, and the most distinctive improvement of the tool life was achieved for TiN+(Ti,Al,Si)N coating, obtained on a cermets' substrate T130A. In the table 6, measurements results of mechanical and operational properties are presented for coatings acquired in the arc PVD process, and in high-temperature CVD process. As a result of a metallographic analysis, conducted on a scanning electron microscope, it was found that the most frequently occurring types of tribological damages, identified on investigated
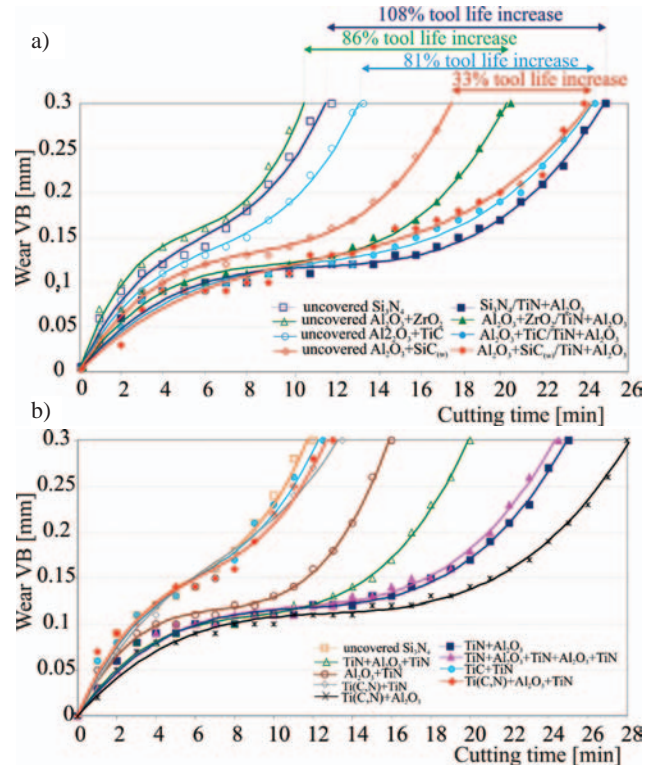
Fig. 49. Graphs of wear bandwidth dependencies on a VB flank face of cutting time for a) TiN+Al$_2$O$_3$ coatings obtained in the CVD process on a substrate made of nitride ceramics Si$_3$N$_4$ and tool ceramics Al$_2$O$_3$+ZrO$_2$, Al$_2$O$_3$+SiC, Al$_2$O$_3$+TiC, b) coatings obtained in the high-temperature CVD process on a substrate made of ceramics Si$_3$N$_4$

materials are mechanical and frictional damages, as well as thermal cracks of the surface flank, crater forming on surface of attack and a chip build-up on a cutting edge (Fig. 50 and 51) [19, 109-111].

In order to define operational properties of coatings obtained in the magnetron PVD process, erosion tests are made, whose outcomes have been presented in table 7. The carried out test showed that erosion resistance of the investigated coatings depends in a large extent on a phase and chemical composition, microhardness and adhesion to substrate's material.
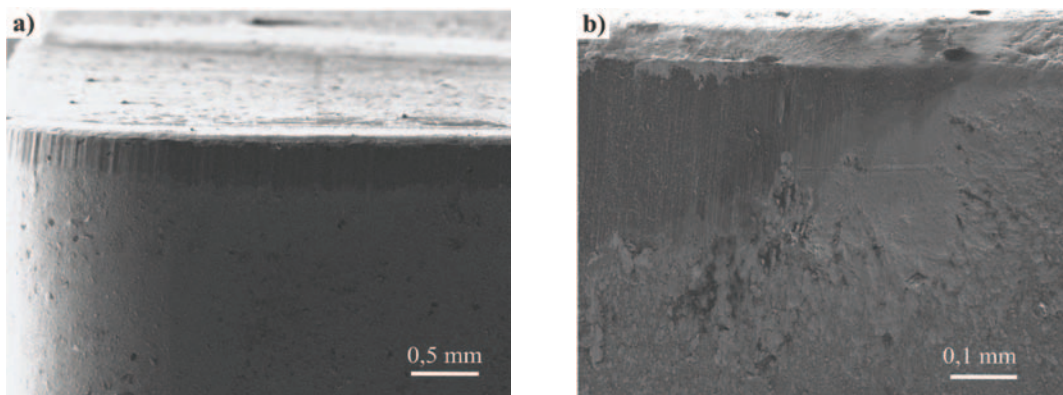
Fig. 50. a) A view of cermet flank face wear T130A with a deposited coating TiN+(Ti,Al,Si)N b) detail from a drawing a
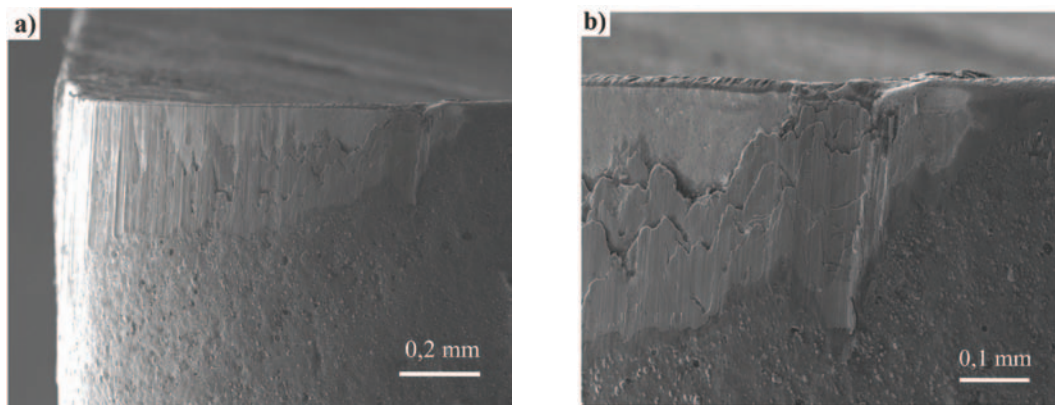
Fig. 51. a) A view of tool ceramics flank face wear made of Al_2O_3+SiC with a deposited coating $TiN+Al_2O_3$ b) detail from a drawing a

Table 6.
Results of mechanical properties measurements and erosion resistance for coatings obtained in the magnetron PVD process on a substrate made of sintered high-speed steel PM HS6-5-3-8

Process' conditions	Type of coating	Roughness R_a [μm]	Microhardness $HV_{0,07}$	Adhesion [N]	Operational properties [s/μm]
Magnetron PVD (100%N_2/460°C)	Ti+(Ti,Al)N	0.05	2790	104.2	8.9
Magnetron PVD (100%N_2/500°C)	Ti+(Ti,Al)N	0.05	2620	87.7	5.4
Magnetron PVD (100%N_2/540°C)	Ti+(Ti,Al)N	0.07	2410	72.9	4.9
Magnetron PVD (75%N_2:25%CH_4/460°C)	Ti+(Ti,Al)(C,N)	0.04	2920	74.2	9.8
Magnetron PVD (75%N_2:25%CH_4/500°C)	Ti+(Ti,Al)(C,N)	0.05	2730	77.4	8.3
Magnetron PVD (75%N_2:25%CH_4/540°C)	Ti+(Ti,Al)(C,N)	0.06	2560	61.3	5.7
Magnetron PVD (50%N_2:50%CH_4/460°C)	Ti+(Ti,Al)(C,N)	0.06	2810	68.2	8.9
Magnetron PVD (50%N_2:50%CH_4/500°C)	Ti+(Ti,Al)(C,N)	0.08	2320	59.1	2.8
Magnetron PVD (50%N_2:50%CH_4/540°C)	Ti+(Ti,Al)(C,N)	0.07	2780	81.8	7.4
Magnetron PVD (25%N_2:75%CH_4/460°C)	Ti+(Ti,Al)(C,N)	0.06	2520	24.5	2.5
Magnetron PVD (25%N_2:75%CH_4/500°C)	Ti+(Ti,Al)(C,N)	0.08	2610	32.7	4.1
Magnetron PVD (25%N_2:75%CH_4/540°C)	Ti+(Ti,Al)(C,N)	0.07	2690	39.2	4.4
Magnetron PVD (100%CH_4/460°C)	Ti+(Ti,Al)C	0.04	2640	81.4	7.6
Magnetron PVD (100%CH_4/500°C)	Ti+(Ti,Al)C	0.07	2980	93.6	7.3
Magnetron PVD (100%CH_4/540°C)	Ti+(Ti,Al)C	0.07	3290	109.6	10.8

Table 7.

Results of mechanical and operational measurements for substrates' material as well as coating obtained in the arc PVD and the high-temperature CVD process

Substrate's material	Type of coating	Roughness R_a [μm]	Microhardness $HV_{0,05}$	Adhesion N	Operational properties	
					Tool life T (min)	Increase (%)
$Al_2O_3+ZrO_2$	TiN+(Ti,Al,Si)N	0.43	2200	38.3	14	27
Al_2O_3+TiC	TiN+(Ti,Al,Si)N	0.37	2530	56.2	18.5	30
$Al_2O_3+ SiC_{(w)}$	TiN+(Ti,Al,Si)N	0.37	2300	69.4	20	11
$Al_2O_3+ZrO_2$	TiN	0.41	2300	40.6	12.5	14
Al_2O_3+TiC	TiN	0.21	2400	33.8	13.5	0
$Al_2O_3+SiC_{(w)}$	TiN	0.31	2670	45.7	25	39
$Al_2O_3+ZrO_2$	TiN+multi(Ti,Al,Si)N +TiN	0.37	3700	61.9	14.5	32
Al_2O_3+TiC	TiN+multi(Ti,Al,Si)N +TiN	0.27	3950	76.6	21.5	59
$Al_2O_3+SiC_{(w)}$	TiN+multi(Ti,Al,Si)N +TiN	0.39	3800	66.1	28	56
$Al_2O_3+ZrO_2$	(Ti,A)lN	0.23	3200	78.2	16	45
Al_2O_3+TiC	(Ti,A)lN	0.12	3100	79.6	17	26
$Al_2O_3+SiC_{(w)}$	(Ti,A)lN	0.26	3300	104.6	31	72
$Al_2O_3+ZrO_2$	TiN+(Ti,Al,Si)N+(Al,Si,Ti)N	0.39	2150	65.3	15	36
Al_2O_3+TiC	TiN+(Ti,Al,Si)N+(Al,Si,Ti)N	0.24	2950	72.2	19	41
$Al_2O_3+ SiC_{(w)}$	TiN+(Ti,Al,Si)N+(Al,Si,Ti)N	0.32	2450	50.6	24	33
Cermetal T130A	TiN+(Ti,Al,Si)N	0.36	3350	111.1	26.5	76
Cermetal CM	TiN+(Ti,Al,Si)N	0.23	3300	114.8	29.5	73
Si_3N_4	TiN+Al_2O_3	0.45	3250	85.2	25	108
Si_3N_4	TiN+Al_2O_3+TiN	0.13	2800	50.4	20	67
Si_3N_4	TiN+Al_2O_3+TiN+Al_2O_3+TiN	0.52	3050	55.7	24.5	104
Si_3N_4	Al_2O_3+TiN	0.23	2700	29.1	16	33
Si_3N_4	TiC+TiN	0.25	2050	25.8	12.5	4
Si_3N_4	Ti(C,N)+TiN	0.15	2225	34.1	13.5	13
Si_3N_4	Ti(C,N)+Al_2O_3+TiN	0.28	2030	30.8	13	8
Si_3N_4	Ti(C,N)+Al_2O_3	0.25	3250	68.3	28	133
$Al_2O_3+ZrO_2$	TiN+Al_2O_3	0.43	3400	72.4	20.5	86
Al_2O_3+TiC	TiN+Al_2O_3	0.29	3350	49.4	24.5	81
$Al_2O_3+SiC_{(w)}$	TiN+Al_2O_3	0.44	3100	32.8	24	33
Cermetal T130A	-	0.21	2490	-	15	-
Cermetal CM	-	0.37	2450	-	17	-
Si_3N_4	-	0.08	1870	-	12	-
$Al_2O_3+ZrO_2$	-	0.21	1850	-	11	-
Al_2O_3+TiC	-	0.09	1970	-	13.5	-
$Al_2O_3+SiC_{(w)}$	-	0.26	1870	-	18	-

4.3. Fractal and multi-fractal analysis of the investigated coatings

Evaluation of methodology to determine fractal dimension

In the herewith evaluation to determine the fractal dimension of coatings surface obtained in the PVD and CVD processes, a modified method for projective covering (PCM) was applied [60]. The PCM method was evaluated at the end of the last century and used for determining the fractal dimension of surface of rocks, and then, it was used many a time in studies for surface of diverse engineering materials [51-53, 112-120].

In PCM method, the surface fractal dimension of irregular shape is determined based on measurements results of a sample height in selected measuring points. It is required that a size of the analysed height of a sample fragment would be homogenous in both directions. When analysing, there are usually 512x512 measurements of height of a sample, where the first number is a scanning line, whereas the second one is a number of measuring points in each of them. Distance between points, similarly like a distance between lines is constant and identical. A number of points and measuring lines may be different than 512, however, considering the applied algorithm should be 2^n, where n is a natural number. For the sake of a scheme of made measurements, the PCM method can be directly used for measurements analysis obtained at AFM microscope.

On a figure 52a surface of an analysed sample fragment was presented schematically, marked by A symbol. Supportively, additional surface was introduced, marked by B symbol, named as a projective surface. The projective surface, in shape of a square, is divided into a great number of small squares of identical sides' length. Division goes sequentially. In the first step (the first stage of division) the whole projective surface is divided into four (2x2) smaller squares. In the next step (the second stage of division), each of the obtained squares is divided into four smaller parts. The procedure is repeated until the assumed scale of division is achieved, whereas a number of stages of division equal (n–1). When 512x512 measurements are made for the height of a sample, the number of division on steps is 9. At each projection surface division step (from the beginning one) points are determined, whose projections onto the examined surface coincide with points at which the test piece height was measured.

In a selected square, values for height of a sample are marked by an index, of abcd vertexes (fig. 50b) corresponding to points in the square's corners on the projective surface are h_{ai}, h_{bi}, h_{ci} and h_{di} respectively. Field of sample fragment, whose projection is a chosen abcd square is marked by $A_i(\delta)$ symbol, where δ is length of the square's side in a given step of division. A number of $N_K(\delta)$ squares, on which the projective plane was divided depends on a step of division and it is $N_K(\delta) = 2^{2K}$, where K is a number of a division step of the projective plane. Length of δ square's side made as a result of K-division is $\delta = L/2^K$, where L is a scanning range.

A complete field of surface $A(\delta)$ of the analysed coating fragment might be determined as a sum of surface fragments, into which it was divided:

$$A(\delta) = \sum_{i=1}^{N_K(\delta)} A_i(\delta) \tag{4}$$

Above-mentioned formula can be applied in practice only when analytical form of a function describing the analysed surface is known. In general, it is only possible to determine an approximate value.

For any fractal set (e.g. curve, surface), a number $N(\delta)$ of "boxes" with a side length δ (in case of a surface in 3D space, these are cubes of δ side) needed to cover of the considered set, fulfils the following dependence [54, 121]:

$$N(\delta) \propto \delta^{-D} \tag{5}$$
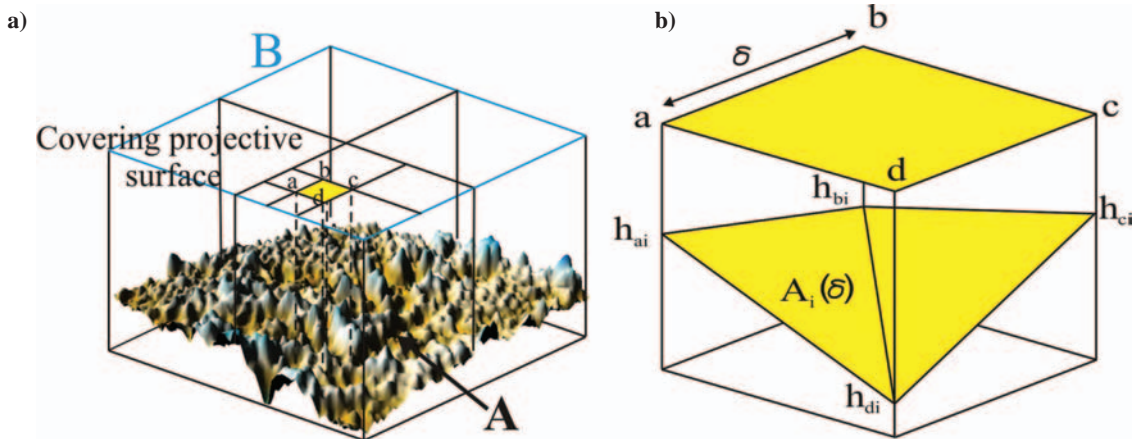
Fig. 52. Method for projective covering a) division of projective plane B by squares lattice with a projection onto analysed surface A and b) one division element enlargement covering the projective plane along with a projection onto a fragment of analysed surface

where D stands for fractal dimension of the examined set (D_s for surface in 3D space). An approximate value of fractal surface field can be determined as a product $N(\delta)$ and fields of square of set length of a side (δ^2):

$$A(\delta) = N(\delta)\delta^2 \qquad (6)$$

Dependence usage (5) in formula (6) leads to:

$$A(\delta) \propto \delta^{2-D_s} \qquad (7)$$

Out of the presented dependence, it results that:
- Only for surfaces, for which D_s=2 it is possible to determine a precise (if analytical form of a function describing its shape is known) or an approximate (if the analytical form in unknown) value of field surface. In case of determining an approximate value, divisions number increase (condensing the measuring points) cause reduction of errors determining a field value of the analysed surface, which close asymptotically to a correct value.
- In case of fractal surfaces ($D_s \neq 2$) it is impossible to determine neither precise nor approximate value of sample surface field, because the value $A(\delta)$ systematically increases in each successive step of division.
- Dependence (7) enables to determine a value of fractal dimension of the considered surface.

Dependence (7) can be written in a form of equation:

$$A(\delta) = C\delta^{2-Ds} \qquad (8)$$

where C is a factor of proportionality. After finding the logarithm double-sided, one can get:

$$\ln A(\delta) = \ln\left(C\delta^{2-Ds}\right) \qquad (9)$$

and after mathematical transformations:

$$\ln A(\delta) = (2 - D_s)\ln\delta + \ln C \qquad (10)$$
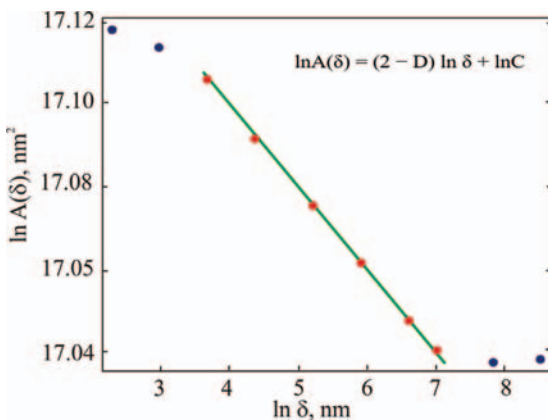
Formula (10) presents a linear dependence in double-logarithmic system, in which x-axis is determined by $\ln\delta$, whereas y-axis is defined by $\ln A(\delta)$. To define an approximate value of fractal dimension in double-logarithmic system, the points ($\ln\delta$, $\ln A(\delta)$) are determined for at least a few values of length δ (Fig. 53). Then, the obtained data are approximated by a linear function. The searched value of fractal dimension is determined based on the following dependence:

$$D_s = 2 - \beta \qquad (11)$$

where β equals a received slope of a straight line.

In case of theoretical fractal surfaces, the determined points will lie exactly along a straight line. In the event of actual surfaces, this condition usually is not met and the determined value of fractal dimension depends on selection of points, to which the line is fitted. Because of that, the author of this paper has used auxiliary diagrams that facilitate the correct choice of points, based upon which fractal dimension is determined (determining self-similarity range) (Fig. 54). The following n-points on the auxiliary graph are determined as a slope of a straight line, approximated by a method of the smallest squares of 3 points on a bilogarithmic diagrams, obtained for (n-2), (n-1) and n step for the projective plane division.

Due to obtained results, a way to determine surface field value of a sample fragment is very essential $A_i(\delta)$, occurring in a formula (4) (Fig. 52). In a paper [60] the following dependence is given, used to determine this value:

$$A_i(\delta) = \frac{1}{2}(\sqrt{\delta^2 + (h_{ai} - h_{di})^2}\sqrt{\delta^2 + (h_{di} - h_{ci})^2} + \qquad (12)$$
$$+ \sqrt{\delta^2 + (h_{ai} - h_{bi})^2}\sqrt{\delta^2 + (h_{bi} - h_{ci})^2})$$

As this formula application leads, in specific cases, to obtain incorrect results (as a result of computation made for computer-generated sets of data modelling surfaces of high roughness,

Fig. 53. A graph enabling to determine a value of fractal dimension by PCM method based on the following dependence $A(\delta) \approx \delta^{2-Ds}$ (TiN coating obtained in the arc PVD process on a substrate made of tool ceramics $Al_2O_3+ZrO_2$)
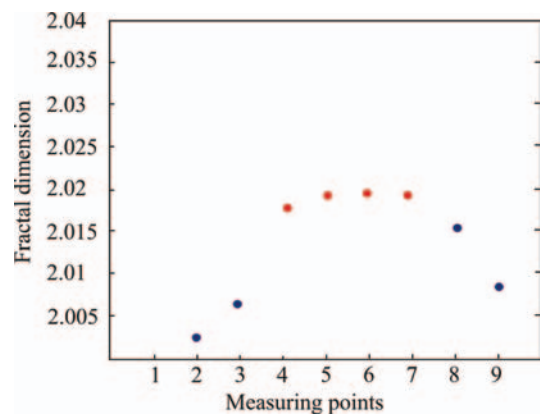
Fig. 54. A graph for values change of fractal dimension indicating a range of self-similarity; chosen points to determine a value of fractal dimension Ds (red colour) have an approximate, constant value (TiN coating in the arc PVD process on a substrate made of tool ceramics $Al_2O_3+ZrO_2$)

overstated values of fractal dimension are received D_s, equalling over 3), it was found that it is not sufficiently accurate, what inclined the author of this thesis to verify it and to formulate another dependence to determine surface field of a sample fragment $A_i(\delta)$.

Field of surface $A_i(\delta)$ determined by any function $h(x,y)$ on abcd square (curved set in space) (Fig. 55) is determined by an integral:

$$P_{abcd} = \iint\limits_{abcd} \sqrt{1 + (\frac{\partial h}{\partial x})^2 + (\frac{\partial h}{\partial y})^2}\, dxdy \qquad (13)$$

what requires knowledge of an analytical form of the function $h(x,y)$, describing a shape of analysed surface. When only values of function (x,y) are known from AFM in four corners of the considered square, it is needed to derive a dependence that will allow determining an approximate value of surface field knowing only the value of function in lattice points (the points: a, b, c and d). On fig. 56 the (A, B, C & D) points are marked of the analysed surface field $A_i(\delta)$, in which the function values $h(x,y)$ are known, or the points, in which height measurements are made. The points present the following coordinates:

$$A(x, y, h_{ai}), \quad B(x, y + \delta, h_{bi}),$$
$$C(x + \delta, y + \delta, h_{ci}), \quad D(x + \delta, y, h_{di}) \qquad (14)$$

Assuming determinations according to Fig. 56 for the considered surface, it is possible on abcd square to approximate it with two triangles: ABC and CDA. Field of the ABC triangle can be determined as field of a triangle built upon BA and BC vectors:

$$P_{ABC} = \frac{1}{2}\left|\vec{BA} \times \vec{BC}\right| = \frac{1}{2}\left|\vec{BA}\right|\left|\vec{BC}\right|\sin\varphi \qquad (15)$$

where $\times$ determinates a vector product, $\|$ stands for vector length, and φ is an angle between BA & BC vectors. Similarly, field of CDA triangle can be determined as field of a triangle built on DA & DC vectors:
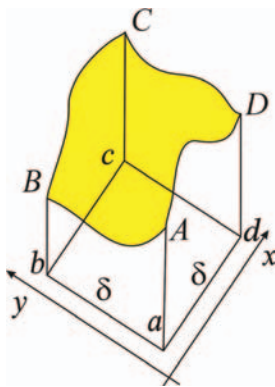
Fig. 55. Surface $A_i(\delta)$ determined by any function $h(x,y)$ on a square with a,b,c,d vertexes

$$P_{CDA} = \frac{1}{2}\left|\vec{DA} \times \vec{DC}\right| \qquad (16)$$

As for two free vectors u = (ux, uy, uz) and v = (vx, vy, vz) length of their vector product can be derived from the following formula:

$$\left|\vec{u} \times \vec{v}\right| = \sqrt{\left|\begin{matrix} u_y & u_z \\ v_y & v_z \end{matrix}\right|^2 + \left|\begin{matrix} u_z & u_x \\ v_z & v_x \end{matrix}\right|^2 + \left|\begin{matrix} u_x & u_y \\ v_x & v_y \end{matrix}\right|^2} \qquad (17)$$

so, suitable vectors adopt a form:

$$\vec{BA} = (0, -\delta, h_{ai} - h_{bi}),$$
$$\vec{BC} = (\delta, 0, h_{ci} - h_{bi}), \qquad (18)$$
$$\vec{DA} = (-\delta, 0, h_{ai} - h_{di}),$$
$$\vec{DC} = (0, \delta, h_{ci} - h_{di}).$$

Using a definition of the vector product again (dependence 16), the following is received:

$$\left|\vec{BA} \times \vec{BC}\right| = \delta\sqrt{\delta^2 + \left(h_{ai} - h_{bi}\right)^2 + (h_{ci} - h_{bi})^2} \qquad (19)$$

$$\left|\vec{DA} \times \vec{DC}\right| = \delta\sqrt{\delta^2 + \left(h_{ai} - h_{di}\right)^2 + (h_{ci} - h_{di})^2} \qquad (20)$$

Summing up the field of ABC and CDA triangles, a different formula is obtained than it was given in the point [60] for an approximate value of $A_i(\delta)$ field of the considered surface fragment:

$$A_i(\delta) = \frac{1}{2}\delta(\sqrt{\delta^2 + (h_{ai} - h_{bi})^2 + (h_{ci} - h_{bi})^2} + \\ + \sqrt{\delta^2 + (h_{ai} - h_{di})^2 + (h_{ci} - h_{di})^2}) \qquad (21),$$

this then was used in calculations and in further part of the paper.
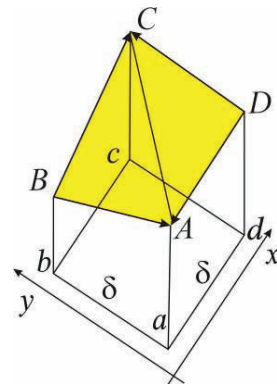
Fig. 56. A surface sketch $A_i(\delta)$ presenting points, in which a value of $h(x,y)$ function is known
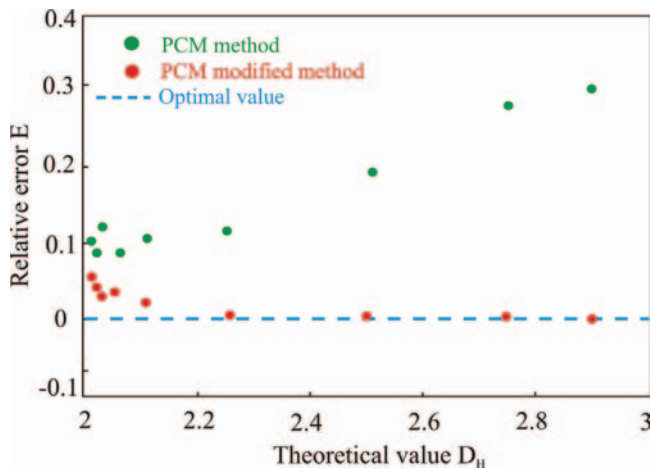
Fig. 57. Comparison for values of relative errors E to determine the fractal dimension by PCM method and modified PCM method for sets of data modelling surfaces with different values of the fractal dimension, obtained with the use of randomized centre displacement algorithm (Peitge's and Saute's version)

Correctness of the derived formula (21) specifying the field value of $A_i(\delta)$ surface of irregular shape as well as modified PCM method to determine the fractal dimension has been tested using sets of data modelling surfaces of optionally chosen, set value for the fractal dimension D_H and it is specified in this paper [55]. For that reason, it is generated after nine sets of data with fractional values of the fractal dimension, being changed within $D_H = 2.01$ to 2.9, using three different algorithms: two versions of midpoint distribution algorithm and Falconer algorithm. No significant differences are observed between obtained results using both algorithms modelling surfaces.
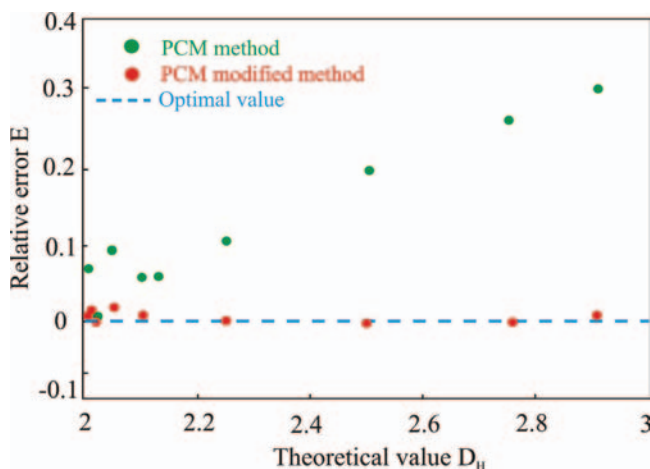
Fig. 58. Comparison for values of relative errors E to determine the fractal dimension by PCM method and modified PCM method for sets of data modelling surfaces with different values of the fractal dimension, obtained with the use of midpoint distribution algorithm (Martyn's version)
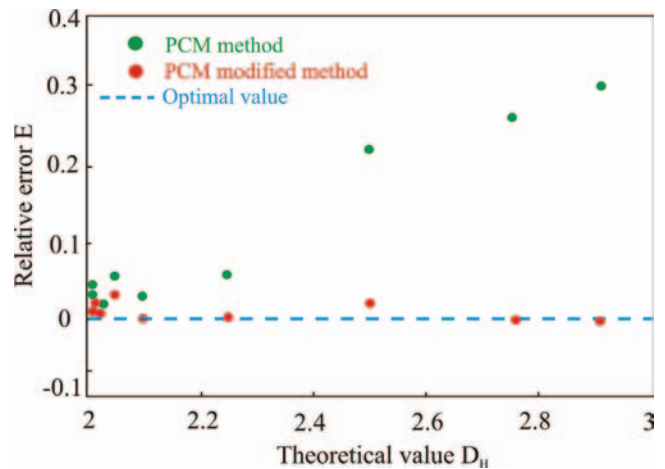
Fig. 59. Comparison for values of relative errors E to determine the fractal dimension by PCM method and modified PCM method for sets of data modelling surfaces with different values of the fractal dimension, obtained with the use of (Falconer's algorithm)

For all applied algorithms to generate surfaces with the use of the modified PCM methods, the fractal dimension values are obtained within [2, 3), whereas taking advantage of so far the used method, erroneous values often obtained Ds >3, especially in case of D_H >2,5. Based on acquired results, it was found that utilizing in PCM method, the modified formula for area field of irregular shape gives more close results to theoretical ones than calculations based on dependence (12). Differences between results got so far by the applied and new method are especially significant in the event of surface with strongly evolved, irregular surface (D_H >2,2). The above-mentioned observations also confirm extracted values of sums of relative errors acquired in calculations taking advantage of both formulae. The relative error is defined by dependence:

$$E = \frac{\left| D_s - D_H \right|}{D_H} \qquad (22)$$

where D_s denotes a calculated value of the fractal dimension, whereas D_H denotes a theoretical value of the fractal dimension, corresponding to a considered surface (Fig. 57-59).

Methodology evaluation to determine multi-fractal spectrum

In further part of the evaluation, the detailed methodology of multi-fractal surface topography description is presented in a form enabling utilization of data analysis obtained during studies using an AFM microscope. Considerations related to methodology of multi-fractal surface topography description in principal part are based upon Xie work [60]. Similarly as for determining the fractal dimension by PCM method, the author has modified the way the field $A_i(\delta)$ is determined with surface of irregular shape [55].

Results for the multi-fractal analysis usually are presented in the form of a multi-fractal spectrum. In order to determine it for a set of measuring data received for a given surface, an auxiliary

projective surface is introduced and a sequential division of the analysed surface is performed into smaller parts, whose projections upon the projective surface are squares with δ side, suitably for the PCM method to determine surface fractal dimension. Next, each surface fragment's measure (probability connected with each surface fragment) is defined:

$$P_i(\delta) = \frac{A_i(\delta)}{A(\delta)} \qquad (23)$$

With each surface fragment a singularity index also is connected α_i (it is also called a Hölder exponent of singularity):

$$P_i(\delta) \propto \delta^{\alpha_i} \qquad (24)$$

Dependence (24) is similar to dependence (7), and the principal difference is that in the formula (24) not to surface magnitude but probability related to each its fragment is scaled. Then, the analysed surface is divided into subsets, whereas, in each of them, the formed fragments, as a result of division, have a different value of the singularity index α_i. If $N_\alpha(\delta)$ denotes a number of surface fragments $A_i(\delta)$, to which the singularity index refers between α and α+dα, then a function f(α) can be defined, called a multi-fractal spectrum, as the fractal dimension of a set of surface fragments with the singularity index α. Then, the number of selected surface fragments is described by the following dependence:

$$N_\alpha(\delta) \approx \delta^{-f(\alpha)} \qquad (25)$$

Next, a new function is defined, called a partition function:

$$Z_q(\delta) = \sum_{i=1}^{N(\delta)} (P_i(\delta))^q, \quad q \in R \qquad (26)$$

Taking advantage of this dependence, one can define a generalized fractal dimension D(q) as follows:

$$D(q) = \frac{1}{q-1} \lim_{\delta \to 0} \frac{\log Z_q(\delta)}{\log \delta} = \frac{1}{q-1} \lim_{\delta \to 0} \frac{\log \sum_{i-1}^{N(\delta)} (P_i(\delta))^q}{\log \delta} \qquad (27)$$

For the division function $Z_q(\delta)$ this dependence is true:

$$Z_q(\delta) \approx \delta q^{\alpha(q) - f(\alpha(q))} \qquad (28)$$

Once the auxiliary function is introduced τ (q):

$$\tau(q) = q\alpha(q) - f(\alpha(q)) \qquad (29)$$

the former dependence can be noted as:

$$Z_q(\delta) \approx \delta^{\tau(q)} \qquad (30)$$

Differentiating the dependence (29) it is received:

$$\frac{d}{dq}\tau(q) = \alpha(q) \qquad (31)$$

Dependence (29) is called a Legendre transformation. Using dependencies (28), (29) and (30) a relation between auxiliary function τ(q) and generalized fractal dimension D(q) [122] can be determined:

$$\tau(q) = (q-1)D(q) \qquad (32)$$

A successive stage requires constructing mono-parameter family of normalized measures μ(q), where for each set value of q exponent, a measure (probability) assigned to i-fragment, whose projection is a square with δ side, and it is defined as follows [123-124]:

$$\mu_i(q,\delta) = \frac{(P_i(\delta))^2}{\sum_{i=1}^{N(\delta)}(P_i(\delta))^q} = \frac{(P_i(\delta))^q}{Z_q(\delta)} \qquad (33)$$

Taking advantage of (27) & (32), it can be noted:

$$\tau(q) = \lim_{\delta \to 0} \frac{\log Z_q(\delta)}{\log(\delta)} = \lim_{\delta \to 0} \frac{\log \sum_{i=1}^{N(\delta)}(P_i(\delta))^q}{\log \delta} \qquad (34)$$

Using a relation (31) and a defined measure above, it is received a formula for the singularity index α, in the form of:

$$\alpha(q) = \lim_{\delta \to 0} \frac{\sum_{i=1}^{N(\delta)}(\mu_i(q,\delta)\log P_i(\delta))}{\log \delta} \qquad (35)$$

Similar dependence can be derived for the multi-fractal spectrum f(α) [123]:

$$f(q) = \lim_{\delta \to 0} \frac{\sum_{i}^{N(\delta)}(\mu_i(q,\delta)\log \mu_i(q,\delta))}{\log \delta} \qquad (36)$$

Dependence (27) allows determining a general fractal dimension for the exponents' q ≠ 1. Assuming $D(1) = \lim_{q \to 1} D(q)$, an equation is received:

$$D(1) = \alpha(1) = f(\alpha(1)) \qquad (37)$$

On the basis of given dependencies, algorithms allowing to determine the multi-fractal spectrum f(α) (as a parametric dependence, in which the parameter is a q) as well as the generalized dimension D(q) can be determined. In the point [55]

method of moments algorithm [125] and Chhabry-Jensen algorithm are presented [123, 124], and it was denoted that there are no significant differences between received results when using them. The results shown in the further part of this paper are obtained using Chhabry-Jensen algorithm, whose next steps go as follows:

1. Settlement of an exponent value q_k, $k = 1, 2, \ldots, n_q$, and length of a squares' sides formed as a result of projective surface division δ_j, $j = 1, 2, \ldots, n_\delta$.
2. Formation of surface field covering (measure domain) by squares with a δ_j side for $j = 1, 2, \ldots, n_\delta$, and for each fragment determining a value of measure $P_i(\delta_j)$ (dependence 23).
3. Determining for each fragment of normalized measure value $\mu_i(q_k, \delta_j)$ for set values δ_j and set exponents q_k (dependence 33).
4. Determining a singularity index value $\alpha(q_k)$, for set values of exponents q_k, as slopes of straight lines approximating graphs of dependence

$$\sum_{i=1}^{N(\delta)} (u_i(q_k, \delta) \log(P_i(\delta))) \tag{38}$$

from log δ (it is a consequence of dependence 35).

5. Values of the multi-fractal spectrum $f(q_k)$, for set values of q_k exponents, are determined as slopes of straight lines approximating the dependence graphs:

$$\sum_{i=1}^{N(\delta)} (u_i(q_k, \delta) \log u_i(q_k, \delta)) \tag{39}$$

from log δ (it is a consequence of dependence 36).

6. Values of the generalized fractal dimension $D(q_k)$, for set values of q_k, $q_k \neq 1$ exponents, are determined as product of a slope of a straight line approximating the graph dependence

$$\log \sum_{i=1}^{N(\delta)} (P_i(\delta))^{q_k} \tag{40}$$

from log δ and binomial $q - 1$ (it is a consequence of dependence 27). However, for $q_k = 1$ we assume $D(1) = \alpha(1)$ (relation 37).

In the consequence of application of the earlier presented algorithm, one can get two equivalent graphs – the multi-fractal spectrum $f(\alpha)$ (Fig. 60) and spectrum $D(q)$ (generalized fractal dimension) (Fig. 61). Analysis of an illustrated form of a function upon those graphs allows analysing geometric features for investigated surfaces and comparing, among themselves, different surfaces in terms of shape.

Being concerned about a fact that graphs are equivalent, in further part of the paper, it is decided to apply only the first way to present the results.

At fig. 60 it is illustrated an exemplary view of the multi-fractal spectrum that is a bell-shaped curve. The most important quantities being characterized by its shape go as follows: $\Delta\alpha$ spectrum bandwidth and difference of its arms height Δf. $\Delta\alpha$ spectrum bandwidth is determined as:

$$\Delta\alpha = \alpha_{max} - \alpha_{min} \tag{41}$$

whereas height difference of its arms Δf is defined in the following way:

$$\Delta f = f(\alpha_{min}) - f(\alpha_{max}) \tag{42}$$

Dependence transformation (23) and (24) into a form of:

$$\alpha_i = \frac{\ln A_i(\delta)}{\ln(\delta)} - \frac{\ln A(\delta)}{\ln(\delta)} - \frac{\ln C}{\ln(\delta)} \tag{43}$$

where C is proportionality constant, it facilitates to understand information contained in the shape of the multi-fractal spectrum. Considering dependence (7) the component $\frac{\ln A(\delta)}{\ln(\delta)}$ can be interpreted (accurate to a constant, equal 2) as a surface fractal dimension of analysed surface D_s, whereas the component $\frac{\ln A_i(\delta)}{\ln(\delta)}$ can be interpreted as the fractal dimension in i-point (D_i). The surface fractal dimension D_s is a constant value on analysed surface, contained in the range [2, 3). A value $D_s = 2$ corresponds to e.g. a flat surface. A value $D_s = 3$ could correspond to an abstract "infinitely rough" surface; however, the fractal dimension of actual analysed objects is always lower.

Fig. 60. Exemplary multi-fractal spectrum $f(\alpha)$
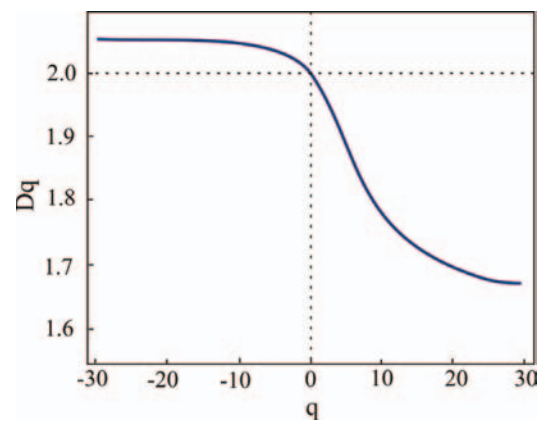
Fig. 61. Exemplary spectrum $D(q)$

The fractal dimension D_i in general case is not a constant value and it changes depending on a choice of the point, in which it is determined. The values D_i contain theoretically within [2, 3], whereas, in practice this range is narrower.

On the ground of presented considerations it can be found that:

- In case of monofractal objects, spectrum is reduced to a single point. For that surface, in each point, a value of dimension D_i is constant and equal D_s. Also, difference between them is constant (accurate to a constant) and α_i adopts only one value. An example that can be an approximation of the monofractal surface is very smooth surface, or that one, for which differences in height of particular points of surface are neglectingly small (much smaller than distance between points, in which measurements are made and/ or lower than the measuring unit resolution). The fractal dimension of this surface is 2, whereas the multi-fractal spectrum is reduced to a single point.

- The multi-fractal spectrum bandwidth certifies presence of areas of different value of the fractal dimension. For homogenous surface, dimension values in particular fragments change in a narrow range, what is visible in the form of a narrow range of variation α_i. In the event of surface, whose topography is irregular (containing fragments of both small and big difference of maximum and minimum height between points in the analysed surface), the dimension value in particular fragments is diversified, what is visible in a wide range of the variation α_i.

- Considering dependence (43) and a fact that for a given surface, D_s is a constant value and higher or equal 2, α_i adopts maximum value (α_{max}), if a local fractal dimension (D_i) adopts minimum value (or 2, what responds to flat areas). On this basis it can be assumed that the right arm of the multi-fractal spectrum corresponds to flat areas, being characteristic for large convex and concave surfaces.

- Analogically, α_i adopts minimum value (α_{min}), if the local fractal dimension (D_i) adopts maximum value. On this basis it can be assumed that the left arm of the Multi-fractal spectrum corresponds to strongly irregular areas, being characteristic for surfaces containing tiny unevenness, defined by a high dimension value.

It directly results from dependence (25) that quantities $f(\alpha_{max})$ and $f(\alpha_{min})$ reflect a number of fragments of surfaces related to maximum $(N_{Pmax}(\delta) = N_{\alpha min} \sim \delta^{-f(\alpha min)})$ and minimum $(N_{Pmin}(\delta) = N_{\alpha max} \sim \delta^{-f(\alpha max)})$ probability. Value $\Delta f = f(\alpha_{min})-f(\alpha_{max})$ is a measure of a ratio of surface fragments' number of the highest probability (big unevennesses) to a number of surface fragments of the lowest probability (tiny, densely packed unevennesses) $(N_{Pmax}(\delta)/N_{Pmin}(\delta) = \delta^{-\Delta f})$. If a value $\Delta f > 0$, an analyzed surface is dominated by areas defined by high value of probability; if $\Delta f < 0$, it is dominated by areas defined by its low value [126, 127].

Results for the fractal and multi-fractal analysis of the investigated coatings

Fractal and multi-fractal analysis of the investigated coatings obtained in the magnetron and the arc PVD process as well as high-temperature CVD process were carried out based on results acquired on atomic force microscope AFM. Initial measurements were made in measuring ranges equal 1, 2, 5 and 10 μm, however, not all analyses confirmed fractal properties of the analysed coatings. For example, in a measuring range equal 10 μm for coatings obtained in the magnetron PVD process, a determined value of the fractal dimension is 2. Similar effect occurs for a measuring range equal 2 μm, and especially 1 μm, in case of samples, in which big grains are found on surface (coatings obtained in the high-temperature CVD process), where using properly great enlargements, the analysed samples' fragments are flat surfaces (points at the bilogarithmic diagram are arranged horizontally, $D_s = 2$). Results for internal studies, which were presented by the author in points [51, 53, 128, 129], allow to find that considering possibility to compare results for coatings obtained in all three processes of deposition, the right scanning range is 5 μm.

Three dimensional images of coatings surface topography obtained based on data from measurements made by means of on AFM microscopes are precious source of information on shape of surface, however, their interpretation and comparison are difficult, subjective and often lead to false conclusions. Appearance of those graphs, in a large degree, depends on the way they are presented (applied colours and their intensity, perspective, and the like) and applied scale in z axis. Simultaneously, applying a rule that for all compared samples in z axis the same unit appears, especially a unit equal to a unit occurring in x and y axes, make the graphs more illegible. For the sake of images of coatings surface topography received based on data coming from measurements made on AFM microscopes, they can only give an idea about shape of surface, but they should not used in highly advanced analyses.

Making measurements on the AFM microscope and getting digital recording of topography of the analyzed surfaces created a possibility to determine two-dimensional quantity of roughness R_{2D}, which in comparison with classical quantities determined along one segment, enables to obtain more representative values. The roughness quantity is a commonly used value defining shape of surface, and first of all, it should be considered when comparing and assessing the shape of coatings.

R_{2D} roughness determined based on measurements made by the AFM microscope is an informing quantity on, in what degree the analyzed area differs from the flat surface, but it does not indicate what made this difference, whose source might be of two different factors:

- Surface waviness (irregularity occurrence of high amplitude),
- Appropriate roughness (densely arranged irregularity occurrence of low amplitude).

The fractal analysis enables to differentiate those factors, and additionally, thanks to determining the multi-fractal spectrum, to assess homogeneity of the analysed objects. The next stages of the fractal analysis cover:

- Bilogarithmic performance,
- Auxiliary plot performance indicating correct selection of the fractal range,
- Determining the surface fractal dimension D_s,
- Determining the multi-fractal spectrum and defining its parameters.

a)

b)

c)

d)
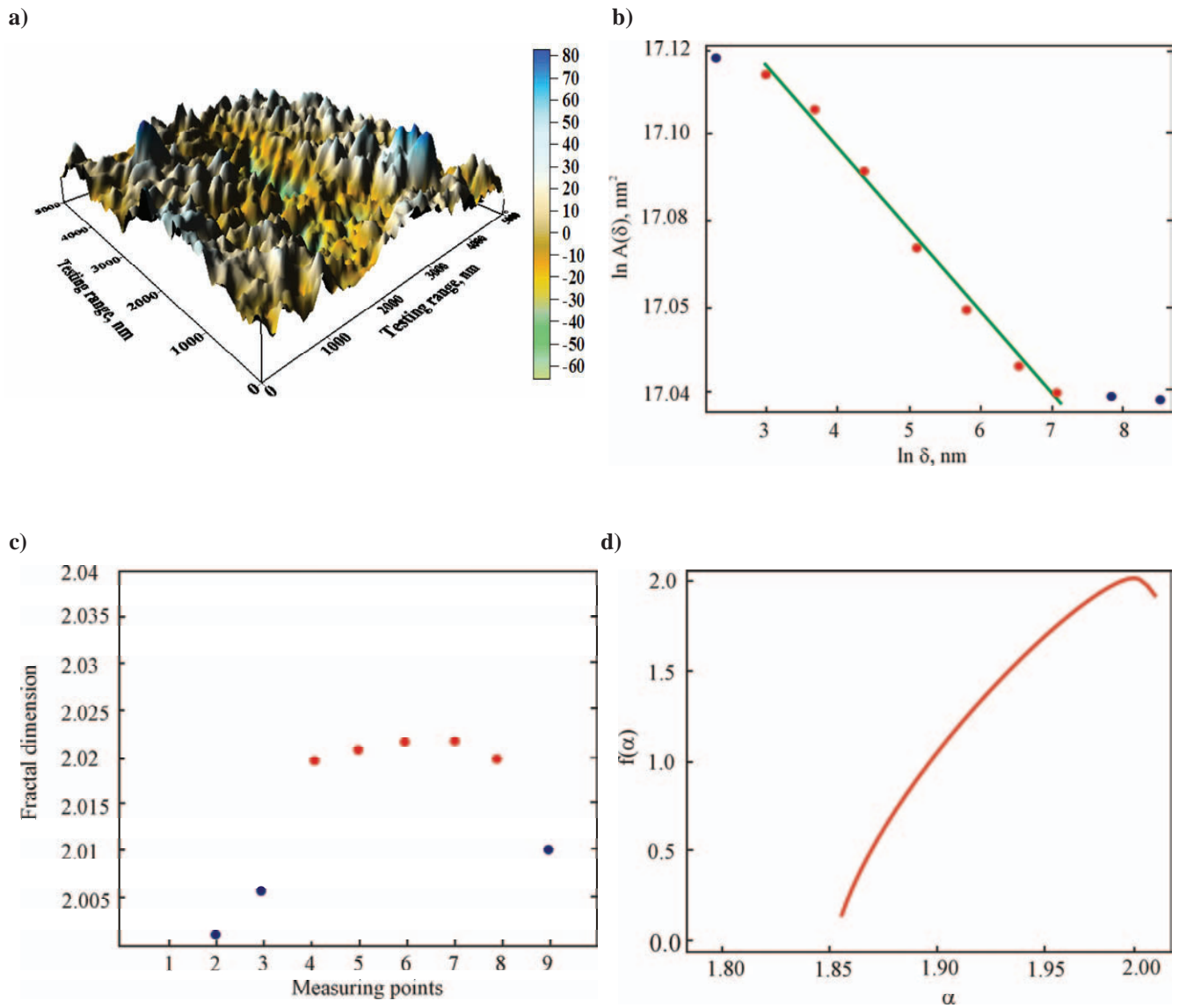
Fig. 62. a) Image of the(Ti,Al)(C,N) coating surface obtained in the PVD magnetron process at 460°C on the PM HS6-5-3-8 (50%N_2:50%CH_4) (AFM, 5 µm) sintered high-speed steel substrate b) bilogarithmic dependence of the approximated area size of the analysed surface on the mesh size used for its determination c) auxiliary diagram indicating the correct points selection on the bilogarithmic plot, and d) multi-fractal spectrum of the analysed coating surface

Points arrangement on the bilogarithmic plot is defined by a degree of an analysed surface development, and simultaneously it indicates factors which have influence on it: surface waviness or appropriate roughness. On the ground of the bilogarithmic plot also fractality of the analysed set of data is assessed. Performing an auxiliary plot facilitates the right selection of the fractality range or taking a

decision that the analysed set of data is not a fractal object.

Analysing a shape of the multi-fractal spectrum, it can be concluded on homogeneity of analysed surfaces. Homogenous surfaces, whose particular fragments do not differ among themselves, are characterized by a narrow spectrum (small difference α_{max} - α_{min}), which can be broaden, if a shape of the

a)

b)

c)

d)
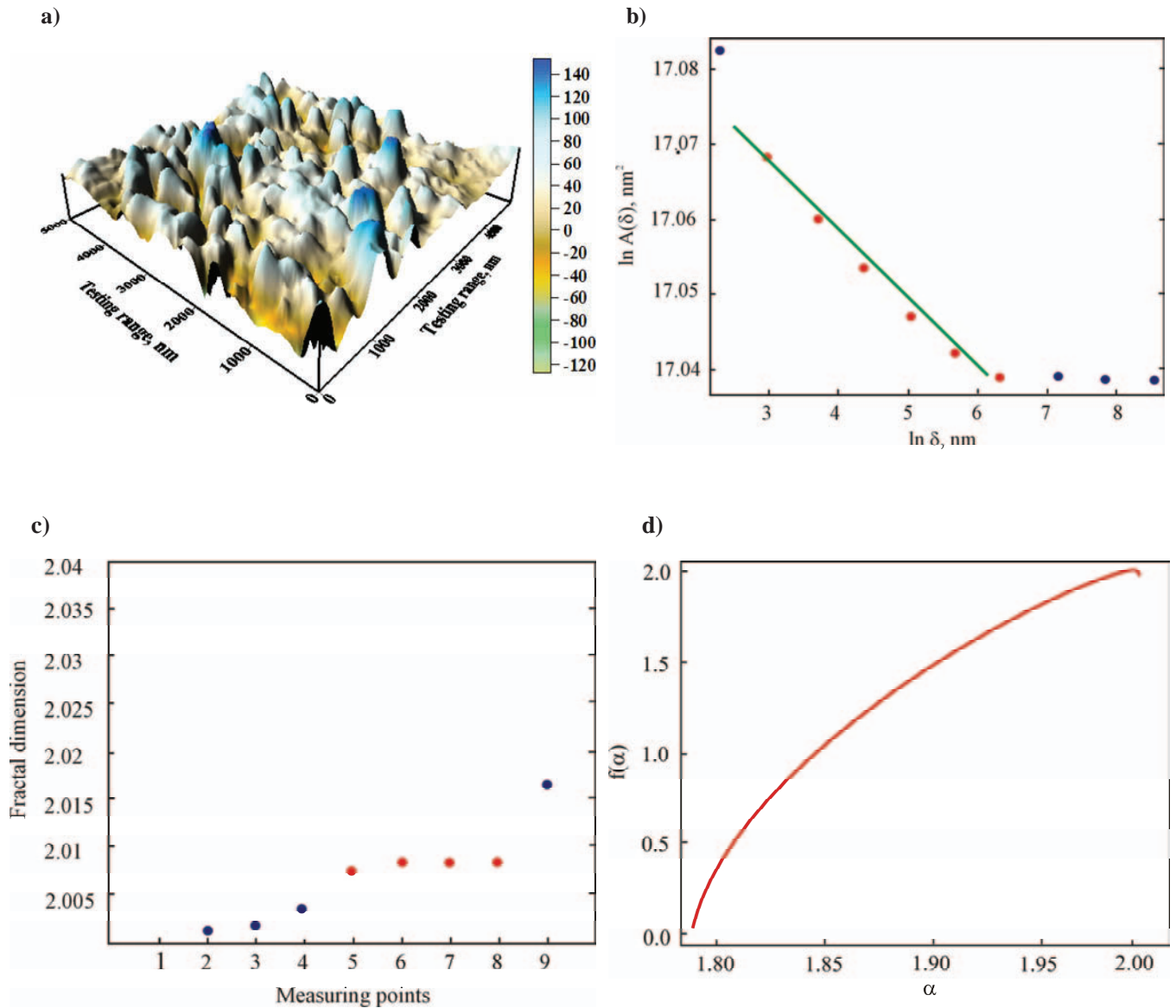
Fig. 63. a) Image of the(Ti,Al)(C,N) coating surface obtained in the PVD magnetron process at 500°C on the PM HS6-5-3-8 (50%N_2:50%CH_4) (AFM, 5 μm) sintered high-speed steel substrate b) bilogarithmic dependence of the approximated area size of the analysed surface on the mesh size used for its determination c) auxiliary diagram indicating the correct points selection on the bilogarithmic plot, and d) multi-fractal spectrum of the analysed coating surface

analysed surface will be more irregular and differentiated in various areas. For the sake of the applied methodology determining the multi-fractal spectrum in the analyzed coatings, it is assumed that its maximum appears for $\alpha = 2$. As values $\alpha < 2$ correspond to probabilities of low values and simultaneously to irregularities of low amplitude so, broadening the multi-fractal spectrum from the left side is characteristic for inhomogeneous surfaces containing tiny grains. Analogically, broadening the spectrum from the right side (for values $\alpha > 2$) it proves that big grains and/or flat areas occur. A positive difference for the spectrum arms height $\Delta f = f(\alpha_{max}) - f(\alpha_{min}) > 0$ proves that in the analysed surface, tiny grains dominate, otherwise ($\Delta f < 0$) high irregularities prevail, defined by high value of probability. Although the multi-fractal spectrum bandwidth is not commonly

a)

b)

c)

d)
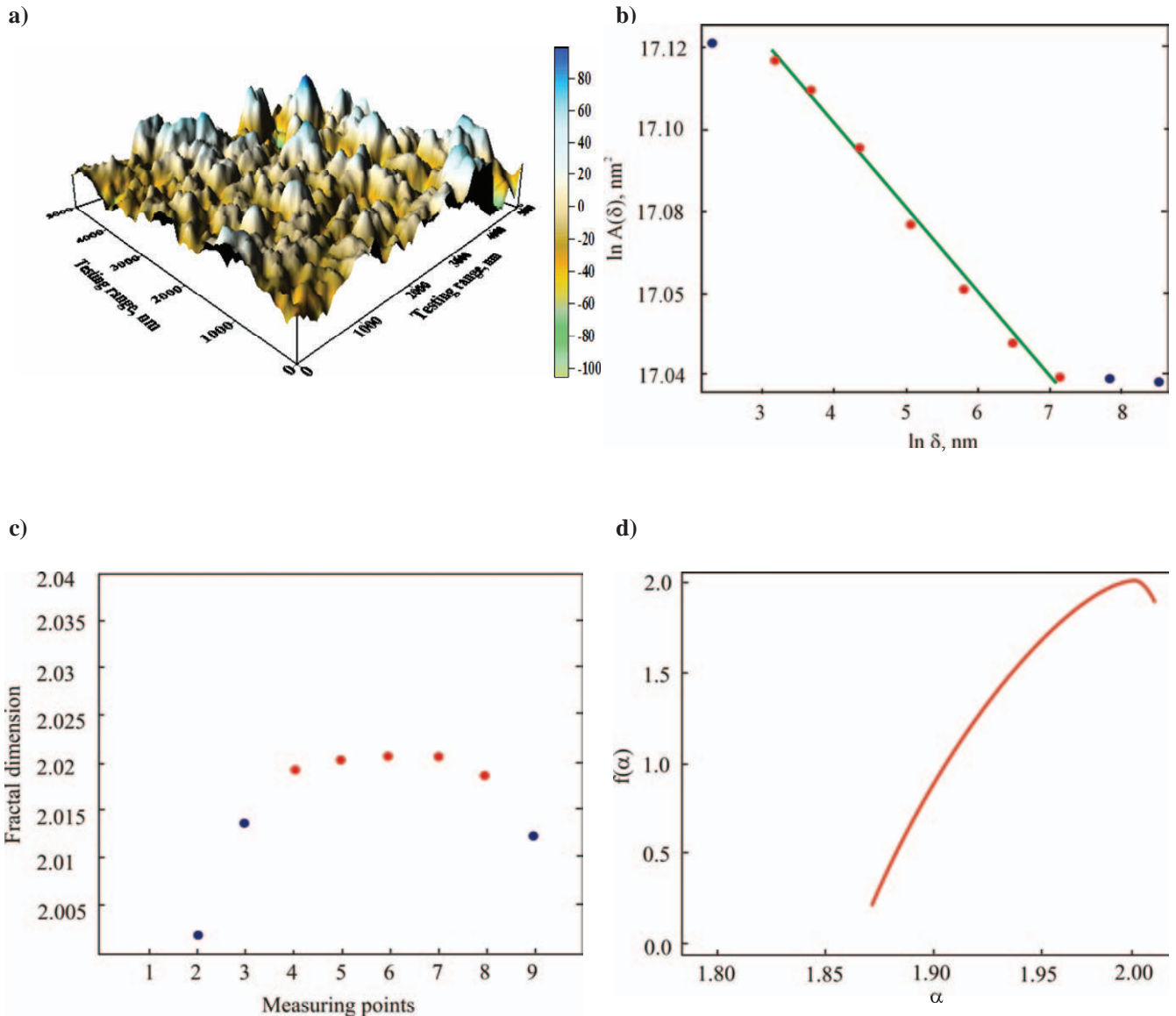
Fig. 64. a) Image of the(Ti,Al)(C,N) coating surface obtained in the PVD magnetron process at 540°C on the PM HS6-5-3-8 (50%N_2:50%CH_4) (AFM, 5 μm) sintered high-speed steel substrate b) bilogarithmic dependence of the approximated area size of the analysed surface on the mesh size used for its determination c) auxiliary diagram indicating the correct points selection on the bilogarithmic plot, and d) multi-fractal spectrum of the analysed coating surface

bound with homogeneity of analysed surface, interpretation of its shape is not unequivocal. The other factors (e.g. roughness, fractal dimension) influence additionally on values describing appearance of the multi-fractal spectrum. Therefore, values analysing that define a shape of the multi-fractal spectrum received for coatings' surface differed by simultaneously chemical and phase composition, conditions and a type of their

obtaining process and substrate's material, on which they were produced is not justified. Problems related to interpretations about shape of the multi-fractal spectrum demand further intensive investigations, nevertheless, still today one can indicate some practical applications, e.g. for quality control and repeatability of coatings' deposition process. Each $\Delta\alpha$ value increase, above or below a certain defined critical value for a given process

a)

b)

c)

d)
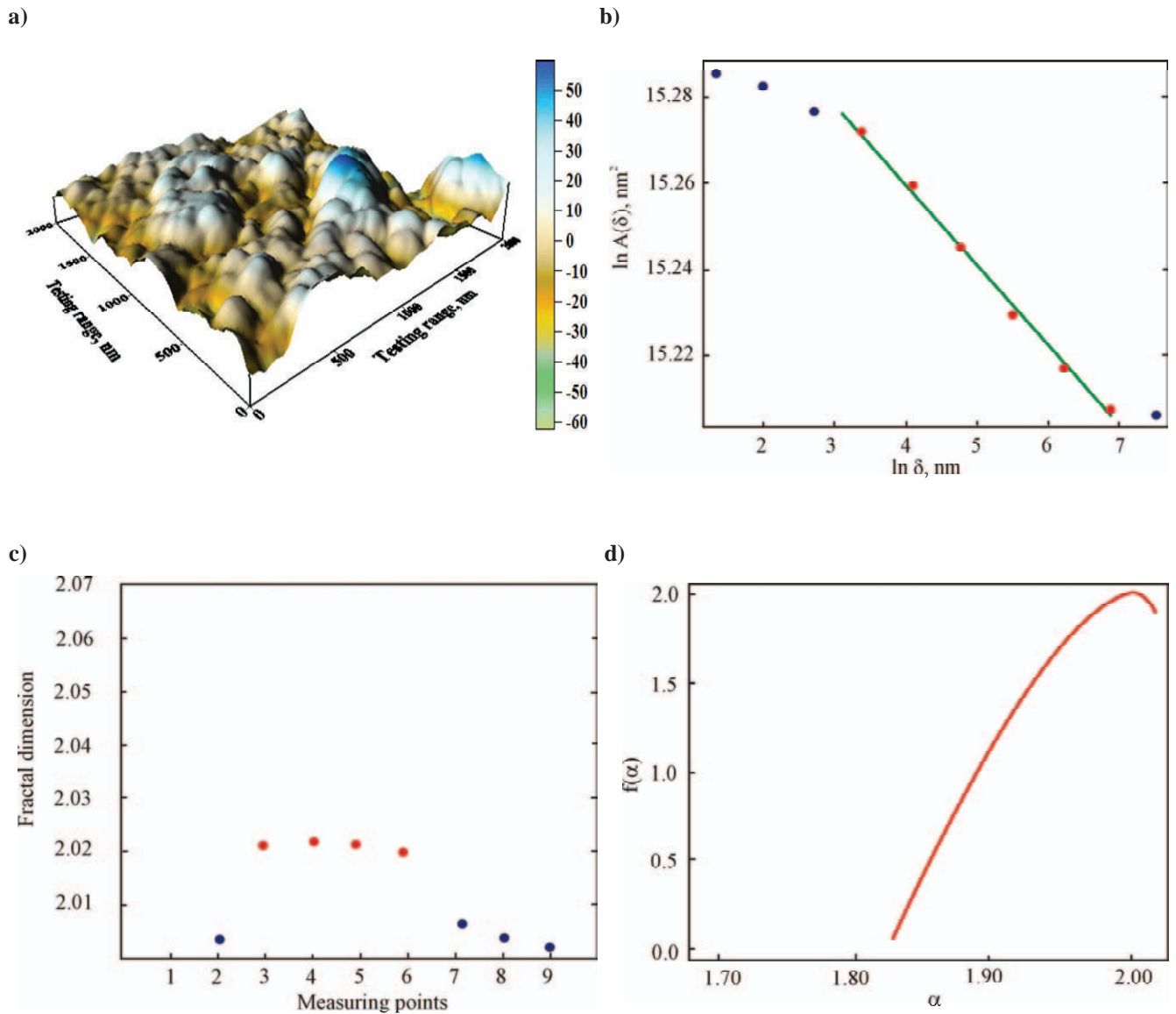
Fig. 65. a) Image of the(Ti,Al)(C,N) coating surface obtained in the PVD magnetron process at 460°C on the PM HS6-5-3-8 (50%N_2:50%CH_4) (AFM, 2 μm) sintered high-speed steel substrate b) bilogarithmic dependence of the approximated area size of the analysed surface on the mesh size used for its determination c) auxiliary diagram indicating the correct points selection on the bilogarithmic plot, and d) multi-fractal spectrum of the analysed coating surface

will be a signal informing about instability of deposition conditions. In case of surface received in conditions differing with one factor change, the multi-fractal analysis can be used to assess its influence on topography of obtained coatings. Quantities for the fractal and multi-fractal analysis and for the quantity value R_{2D} of the analysed coatings are presented in tables 8 & 9. On the basis of carried out analyses it can be found that all considered

coatings, independently on type of their manufacturing process and the applied substrate's material, show fractal character of surface, what is proved by linear, in defined ranges, the bilogarithmic graphs used for determining the fractal dimension D_s (Fig. 62b-75b).

Series factors decide on coatings topography, among which the main role is played by a type of process and conditions needed

a)

b)

c)

d)
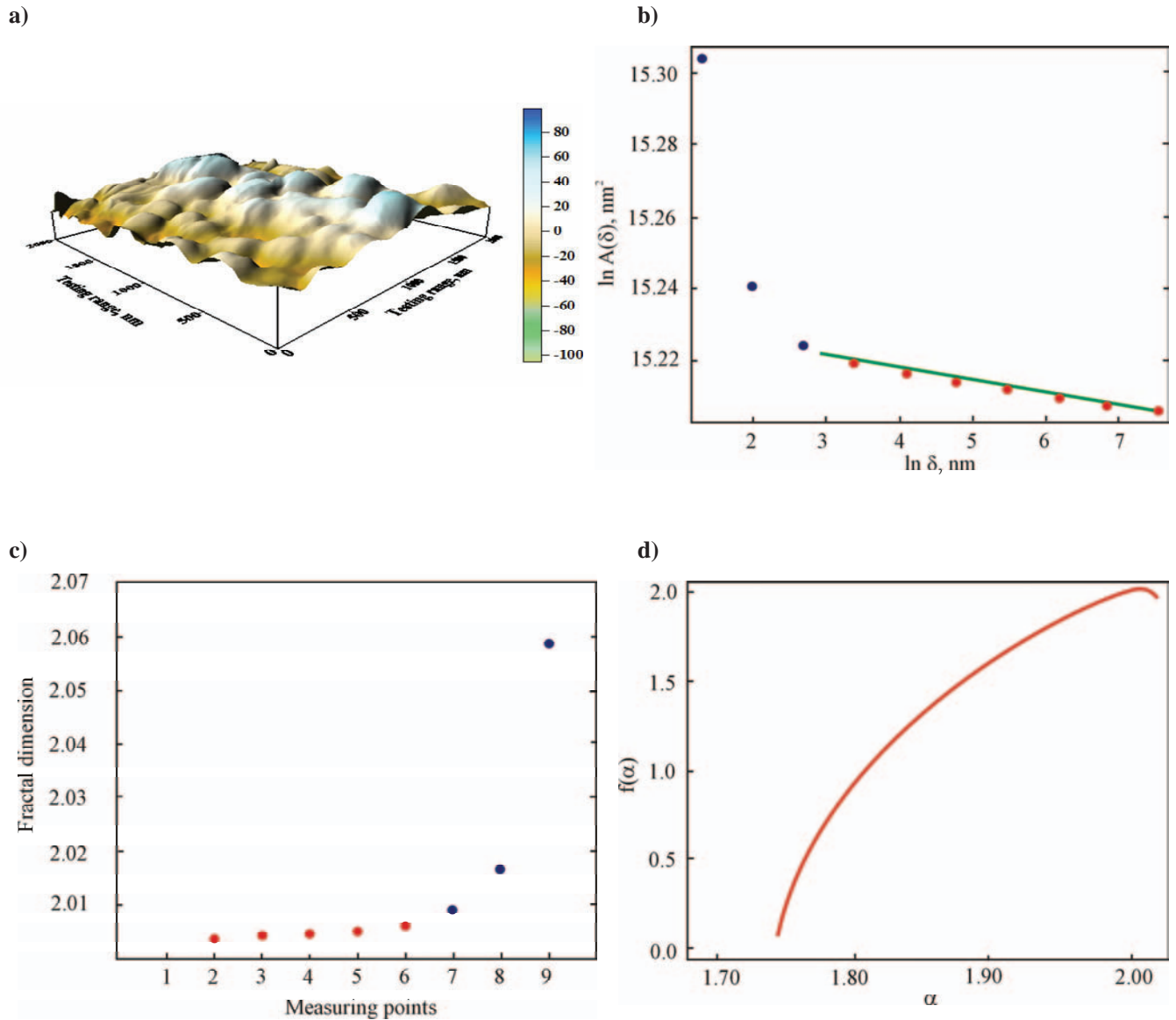
Fig. 66. a) Image of the(Ti,Al)(C,N) coating surface obtained in the PVD magnetron process at 500°C on the PM HS6-5-3-8 (50%N_2:50%CH_4) (AFM, 2 μm) sintered high-speed steel substrate b) bilogarithmic dependence of the approximated area size of the analysed surface on the mesh size used for its determination c) auxiliary diagram indicating the correct points selection on the bilogarithmic plot, and d) multi-fractal spectrum of the analysed coating surface

to acquire them, type of substrate as well as chemical and phase composition of deposited layers. In this paper, the fractal and multi-fractal analysis results of coatings are discussed, and for each type of process (the magnetron or the arc PVD process and the high-temperature CVD process) exemplary images of coatings surface topography is shown obtained as a result of investigations made by AFM microscope, auxiliary and bilogarithmic diagrams

corresponding to them, based on which, the fractal dimension is determined as well as multi-fractal spectra received by a modified PCM method (Fig. 62-75).

Analysing the obtained results for coatings acquired in the magnetron PVD process (Table 8) it was found that a value of their fractal dimension D_s is contained in the range of 2.009-2.036, whereas their roughness R_{2D} is within 0.021-0.091 μm.

a)

b)

c)

d)
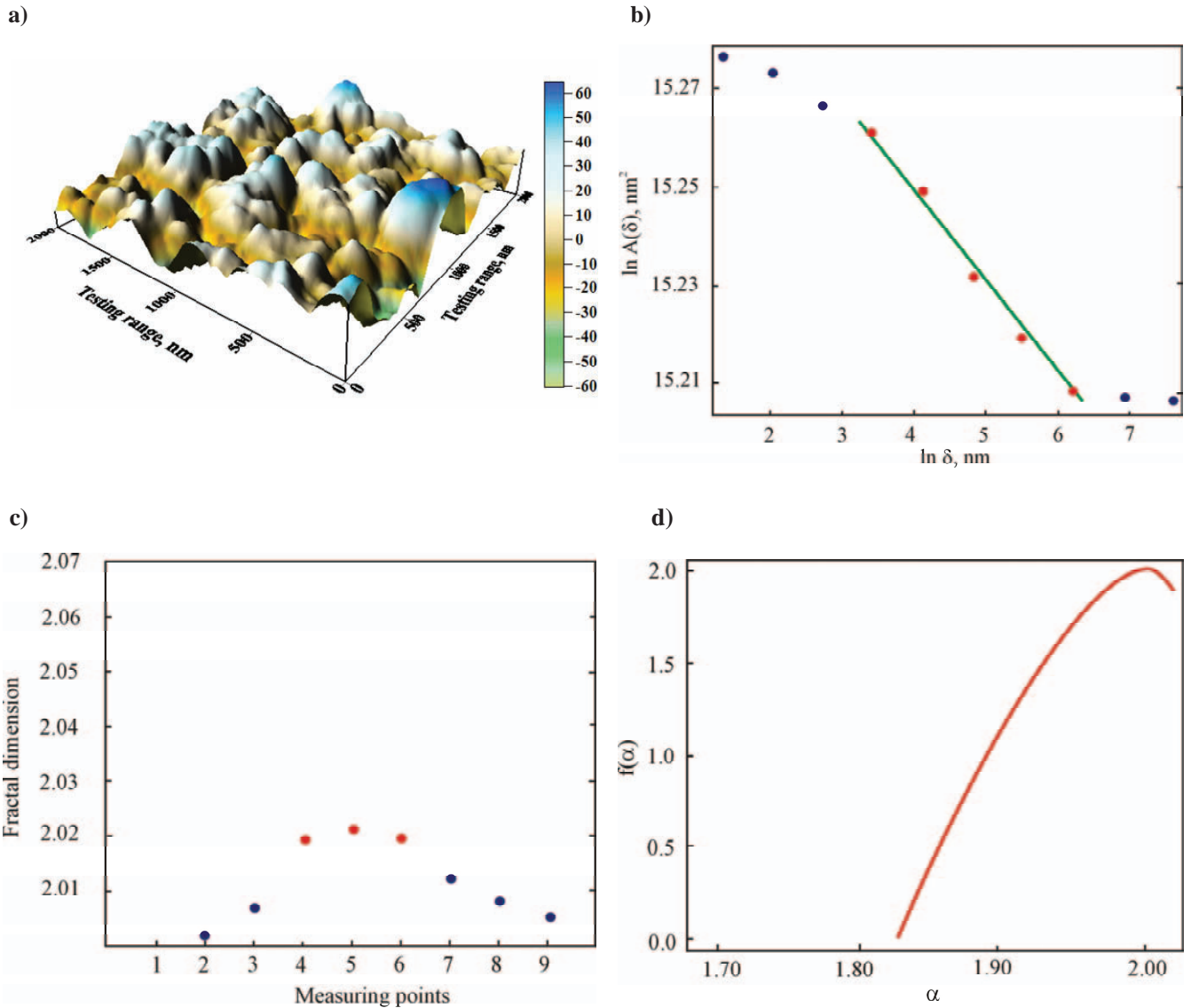
Fig. 67. a) Image of the(Ti,Al)(C,N) coating surface obtained in the PVD magnetron process at 540°C on the PM HS6-5-3-8 (50%N_2:50%CH_4) (AFM, 2 µm) sintered high-speed steel substrate b) bilogarithmic dependence of the approximated area size of the analysed surface on the mesh size used for its determination c) auxiliary diagram indicating the correct points selection on the bilogarithmic plot, and d) multi-fractal spectrum of the analysed coating surface

On figures 62-64 surface topography images and results of the fractal and multi-fractal analysis are presented (scanning range 5 µm) for (Ti,Al)(C,N) coatings obtained in the magnetron PVD process on a substrate made of sintered high-speed steel PM HS6-5-3-8 in 460°C, 500°C and 540°C in the atmosphere containing 50% CH_4 & 50% N_2. Compared surfaces are characterized by a close, low value of roughness, defined by R_{2D} (<0.05 µm)

quantity. The difference between values of the fractal dimension and R_{2D} for the obtained coatings in 460°C & 540°C ($D_s = 2.021$ & $R_{2D} = 0.037$ and $D_s = 2.023$ & $R_{2D} = 0.025$) and in 500 °C ($D_s = 2.009$ & $R_{2D} = 0.021$) is visible. Analysing bilogarithmic diagrams obtained for three different temperatures, it can be found that for a few, the first steps of division (in turns δ=5; 2.5; 1.25; 0.625 µm), ln$A$(δ) values remain on one, stable level,

a)

b)

c)

d)
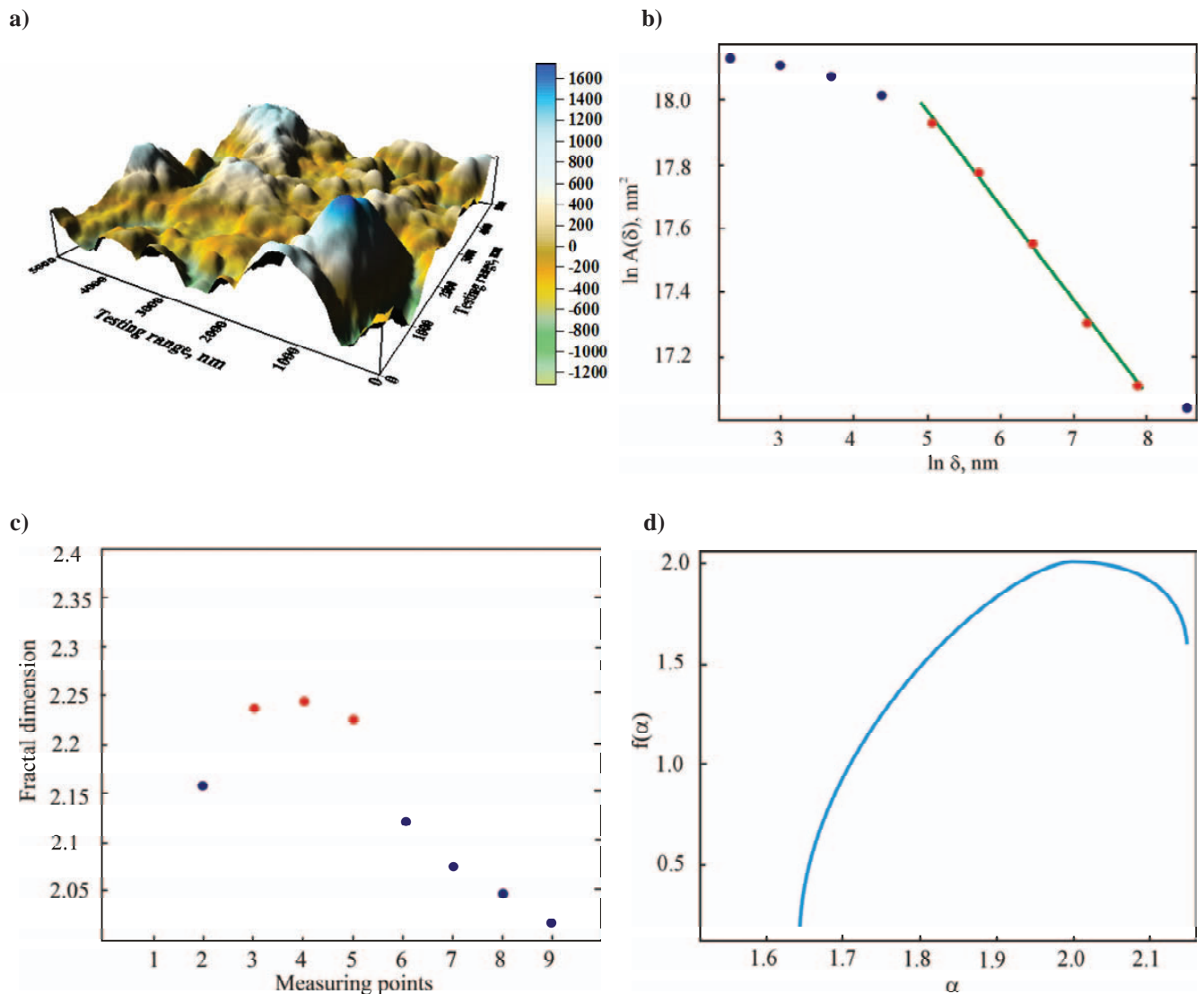
Fig. 68. a) Image of theTiN+multi(Ti,Al,Si)N+TiN coating surface obtained in the arc PVD process on the Al_2O_3+SiC (AFM, 5 μm) tool ceramics substrate b) bilogarithmic dependence of the approximated area size of the analysed surface on the mesh size used for its determination c) auxiliary diagram indicating the correct points selection on the bilogarithmic plot, and d) multi-fractal spectrum of the analysed coating surface

what proves that surface development (from lnA(δ = 5 μm value) = 17.03 nm^2 up to lnA(δ = 9.8 nm) = 17,12 nm^2 values or 17.07 nm^2 for coating obtained in 500°C) is a consequence of occurrence of densely arranged irregularities of low amplitude (grains), what is proved by images received from the AFM microscope (Fig. 62a-64a) as well as acquired data D_s (Table 8). Comparing the multi-fractal spectra it was found that

among presented surfaces, a coating received in 500°C is the most inhomogeneous (Δα = 0.217), and simultaneously it contains least unevennesses of high amplitude ($α_{max}$ = 2.004). For coatings obtained in the magnetron PVD process, it is received a positive difference in spectra arms height Δf >0, what proves that in the analysed surfaces, tiny grains predominate (surface development is related to internal roughness occurrence, and not surface waviness).

a)

b)

c)

d)
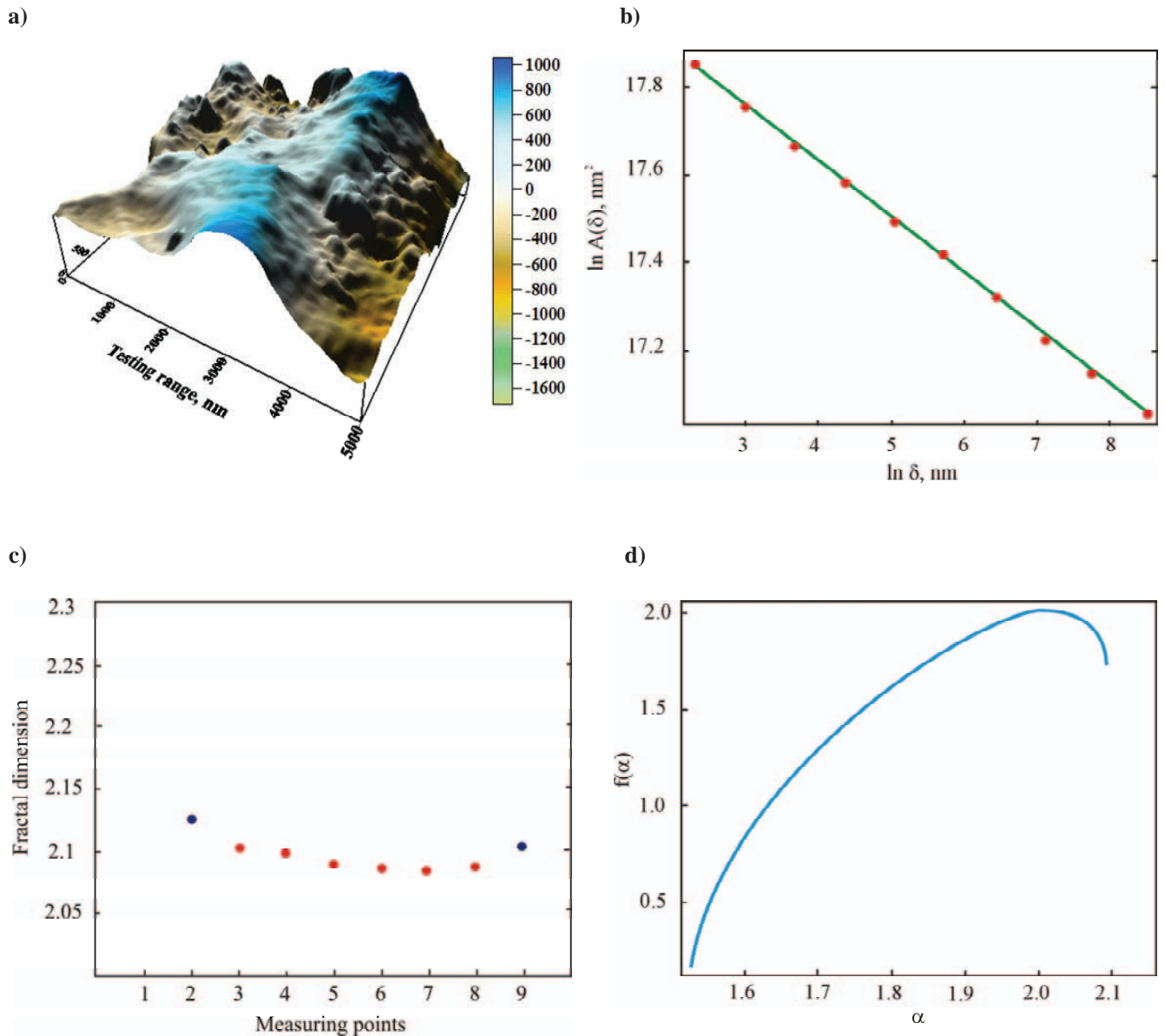
Fig. 69. a) Image of theTiN+multi(Ti,Al,Si)N+TiN coating surface obtained in the arc PVD process on the Al$_2$O$_3$+TiC (AFM, 5 μm) tool ceramics substrate b) bilogarithmic dependence of the approximated area size of the analysed surface on the mesh size used for its determination c) auxiliary diagram indicating the correct points selection on the bilogarithmic plot, and d) multi-fractal spectrum of the analysed coating surface

On figures 65-67 there are presented analogical images and diagrams obtained for the scanning range equal to 2 μm. Observations and outcomes got from a scanning range 5 μm remain true also in this case, what proves that in the scale of 2-5μm for the discussed coatings, a scanning range selection has no influence on the fractal and multi-fractal analysis results.

Analysing the received results for coatings acquired in the arc PVD process it was found that the fractal dimension value is situated within 2.006-2.252, whereas roughness is defined by R$_{2D}$ quantity within 0.037 to 0.564 μm (Table 9).

Surface topography images and results of the fractal and multi-fractal analysis for TiN+multi(Ti,Al,Si)N+TiN

a)

b)

c)

d)
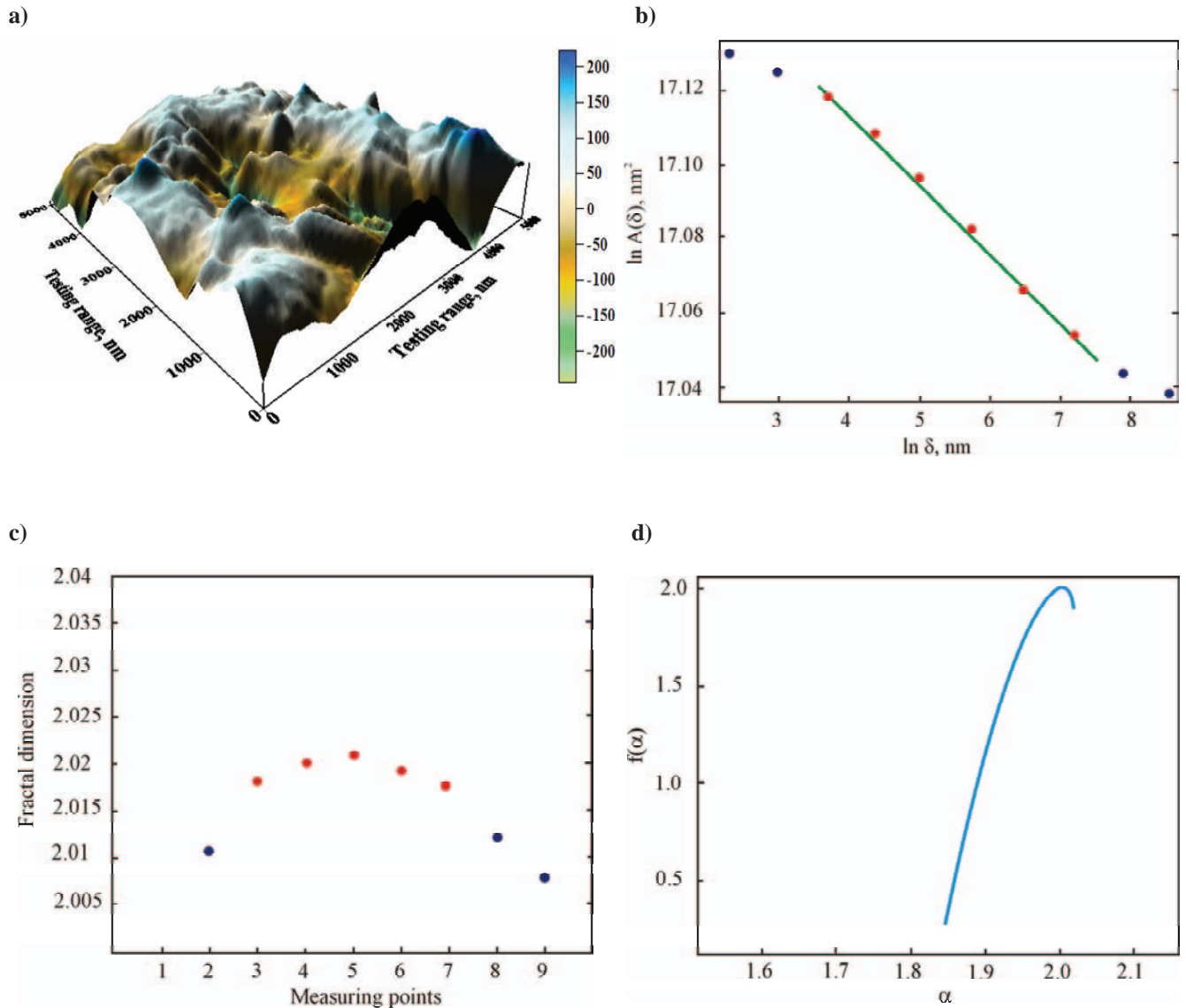
Fig. 70. a) Image of theTiN+multi(Ti,Al,Si)N+TiN coating surface obtained in the arc PVD process on the $Al_2O_3+ZrO_2$ (AFM, 5 μm) tool ceramics substrate b) bilogarithmic dependence of the approximated area size of the analysed surface on the mesh size used for its determination c) auxiliary diagram indicating the correct points selection on the bilogarithmic plot, and d) multi-fractal spectrum of the analysed coating surface

coatings obtained in the arc PVD process on a substrate made of tool ceramics Al_2O_3+SiC, Al_2O_3+TiC and $Al_2O_3+ZrO_2$. are presented in figures 68-70. Coatings received on a substrate made of ceramics Al_2O_3+SiC and Al_2O_3+TiC denote a close, high roughness ($R_{2D} \approx 0.4$ μm) in comparison with a coating, when the substrate is ZrO_2 ($R_{2D} \approx 0.09$ μm). Similar relations were obtained for the fractal dimension value (significantly lower the fractal

dimension value $D_s \approx 2.02$ of topography surface coating TiN+multi(Ti,Al,Si)N+TiN in comparison with a coating, when the substrate is ceramic whiteware ZrO_2). Analysing bilogarithmic graphs obtained for three presented sets of measuring data it can be found that $lnA(\delta)$ values increase systematically, already starting from the first steps of division (values acquired for $\delta = 5$ μm < values acquired for $\delta = 2.5$ μm < values acquired for

a)

b)

c)

d)
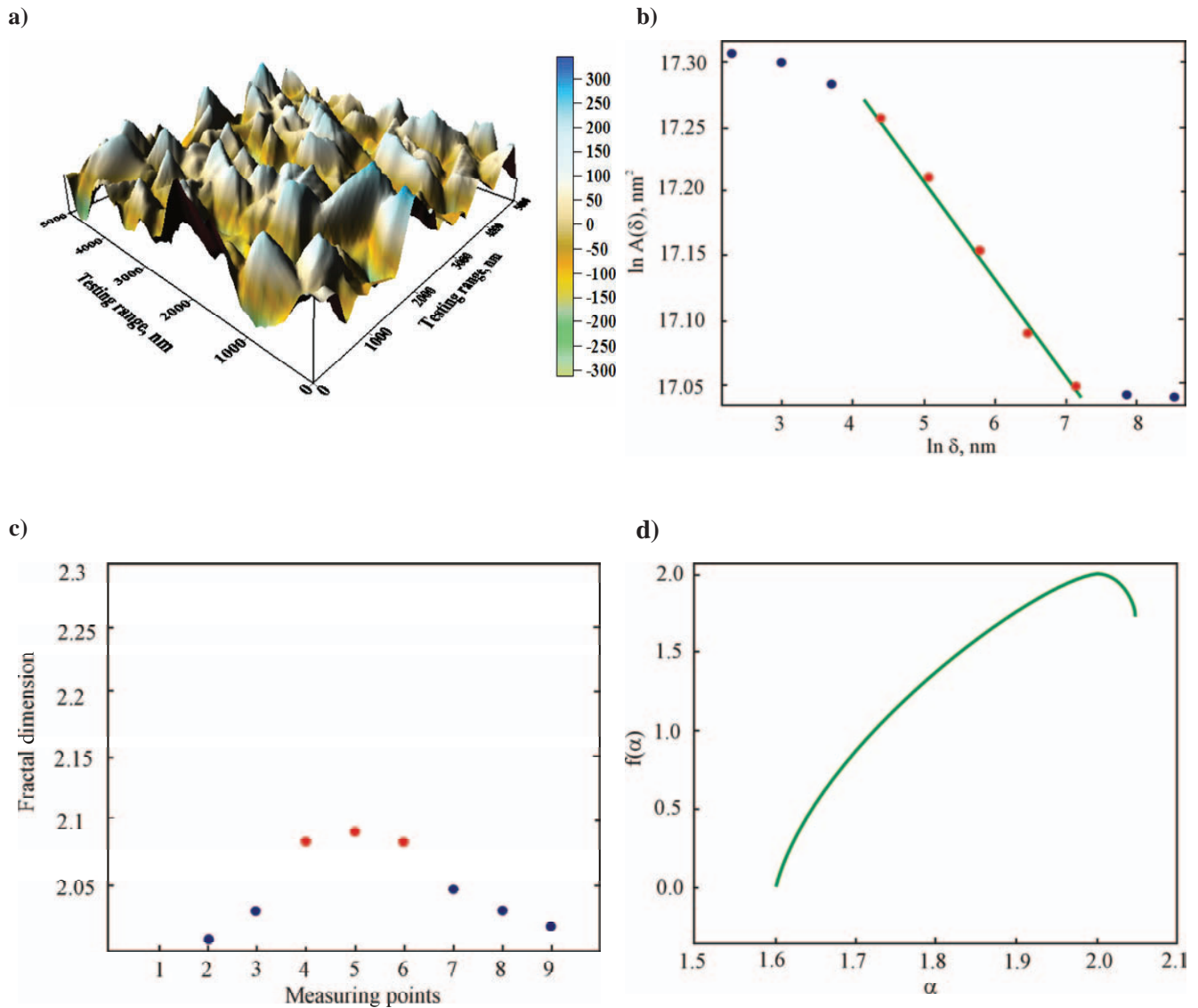
Fig. 71. a) Image of the Ti(C,N)+Al$_2$O$_3$ coating surface obtained in the high-temperature CVD process on the Si$_3$N$_4$ (AFM, 5 μm) tool ceramics substrate b) bilogarithmic dependence of the approximated area size of the analysed surface on the mesh size used for its determination c) auxiliary diagram indicating the correct points selection on the bilogarithmic plot, and d) multi-fractal spectrum of the analysed coating surface

δ = 1.25 μm < ... and so on), what denotes that the analysed surfaces also contain irregularities of high amplitude. Surface development (from the value of lnA(δ = 5 μm) = 17.03 nm^2 to lnA(δ = 9.8 nm) = 17.12 nm^2) for a coating obtained on a substrate made of tool ceramics Al$_2$O$_3$+ZrO$_2$, for over 17.8 nm^2 for substrate made of tool ceramics made of Al$_2$O$_3$+SiC and Al$_2$O$_3$+TiC is an effect of simultaneous occurrence upon the analysed surface of densely arranged irregularities with low and high amplitude, what is confirmed by the AFM images. The multi-fractal spectra comparison de notes that among three analysed surfaces, a coating acquired on a substrate of tool ceramics made of Al$_2$O$_3$+TiC is mostly homogenous (Δα = 0.167), as well as it contains the least unevennesses of high amplitude (α$_{max}$ = 2.013).

a)

b)

c)

d)
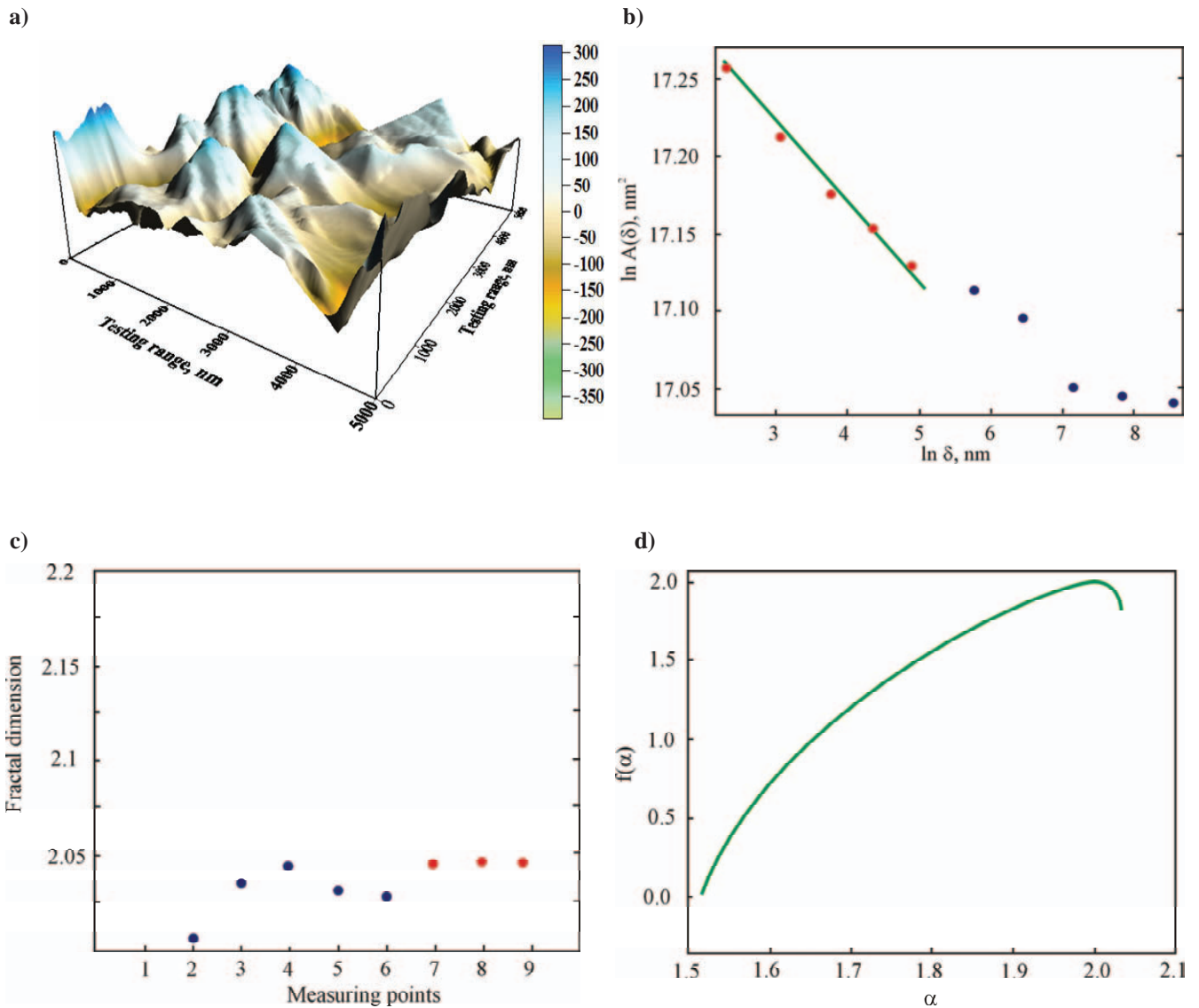
Fig. 72. a) Image of the TiN+Al$_2$O$_3$ coating surface obtained in the high-temperature CVD process on the Si$_3$N$_4$ (AFM, 5 µm) tool ceramics substrate b) bilogarithmic dependence of the approximated area size of the analysed surface on the mesh size used for its determination c) auxiliary diagram indicating the correct points selection on the bilogarithmic plot, and d) multi-fractal spectrum of the analysed coating surface

Coatings received on Al$_2$O$_3$+SiC and Al$_2$O$_3$+TiC are much more inhomogeneous ($\Delta\alpha > 0.5$) and they contain (particularly in case of a coating received on a substrate made of Al$_2$O$_3$+SiC) irregularities of high amplitude (adequately α_{max} = 2.09 & 2.15). Similarly as for coatings obtained in the magnetron PVD process, coatings obtained in the arc process are characterized by a positive difference of height of spectra arms $\Delta f > 0$. Comparing

shape of the multi-fractal spectra of coatings surface topography obtained in both processes, it was found that coatings received on ceramic materials in the arc PVD process are more inhomogeneous, and in some cases they contain bigger grains (surface development is related to surface waviness occurrence) than in case of coatings deposited on a substrate made of sintered high-speed steel in the magnetron process.

a)

b)

c)

d)
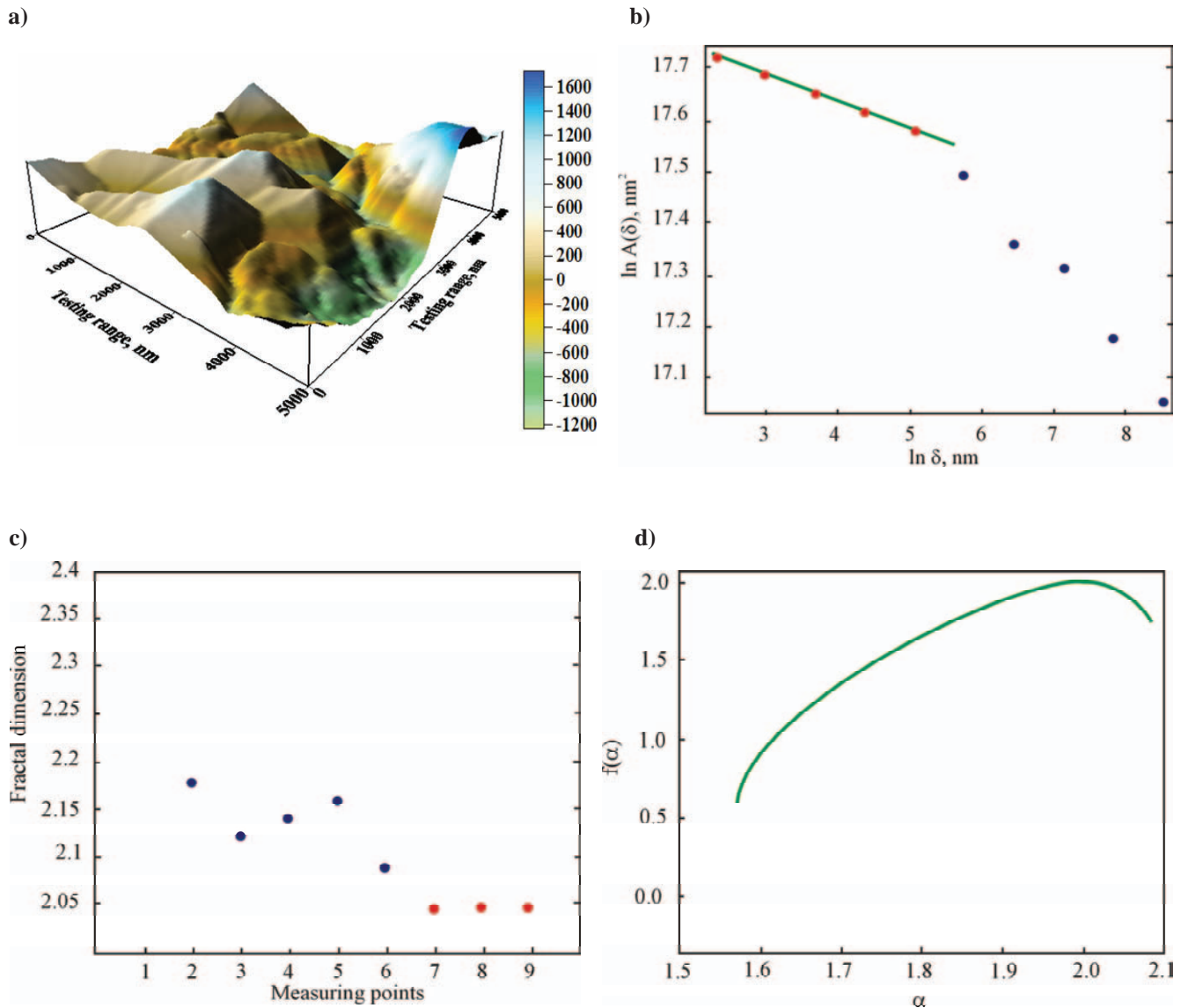
Fig. 73. a) Image of the TiN+Al$_2$O$_3$ coating surface obtained in the high-temperature CVD process on the Al$_2$O$_3$+ZrO$_2$ (AFM, 5 μm) tool ceramics substrate b) bilogarithmic dependence of the approximated area size of the analysed surface on the mesh size used for its determination c) auxiliary diagram indicating the correct points selection on the bilogarithmic plot, and d) multi-fractal spectrum of the analysed coating surface

Analysing the acquired results for coatings obtained in the high-temperature CVD process, it was found that their fractal dimension values are situated within 2.015-2.071, whereas roughness R$_{2D}$ within 0.079-0.531 μm.

On diagrams 71-75 there are presented surfaces topography images and results of the fractal and multi-fractal analysis for coatings obtained in high-temperature CVD process, for different

substrates, when the outer layer was Al$_2$O$_3$. Ti(C,N)+Al$_2$O$_3$ coatings and TiN+Al$_2$O$_3$ obtained on a substrate made of nitride ceramics Si$_3$N$_4$ are characterized by lower roughness (R$_{2D}$ <0,1 μm) in comparison with the other studies, whereas the fractal dimension values are close to them (D$_s$ = 2.03-2.07). Analyzing and comparing bilogarithmic diagrams acquired for coatings being characterized by high roughness defined by R$_{2D}$ quantity

a)

b)

c)

d)
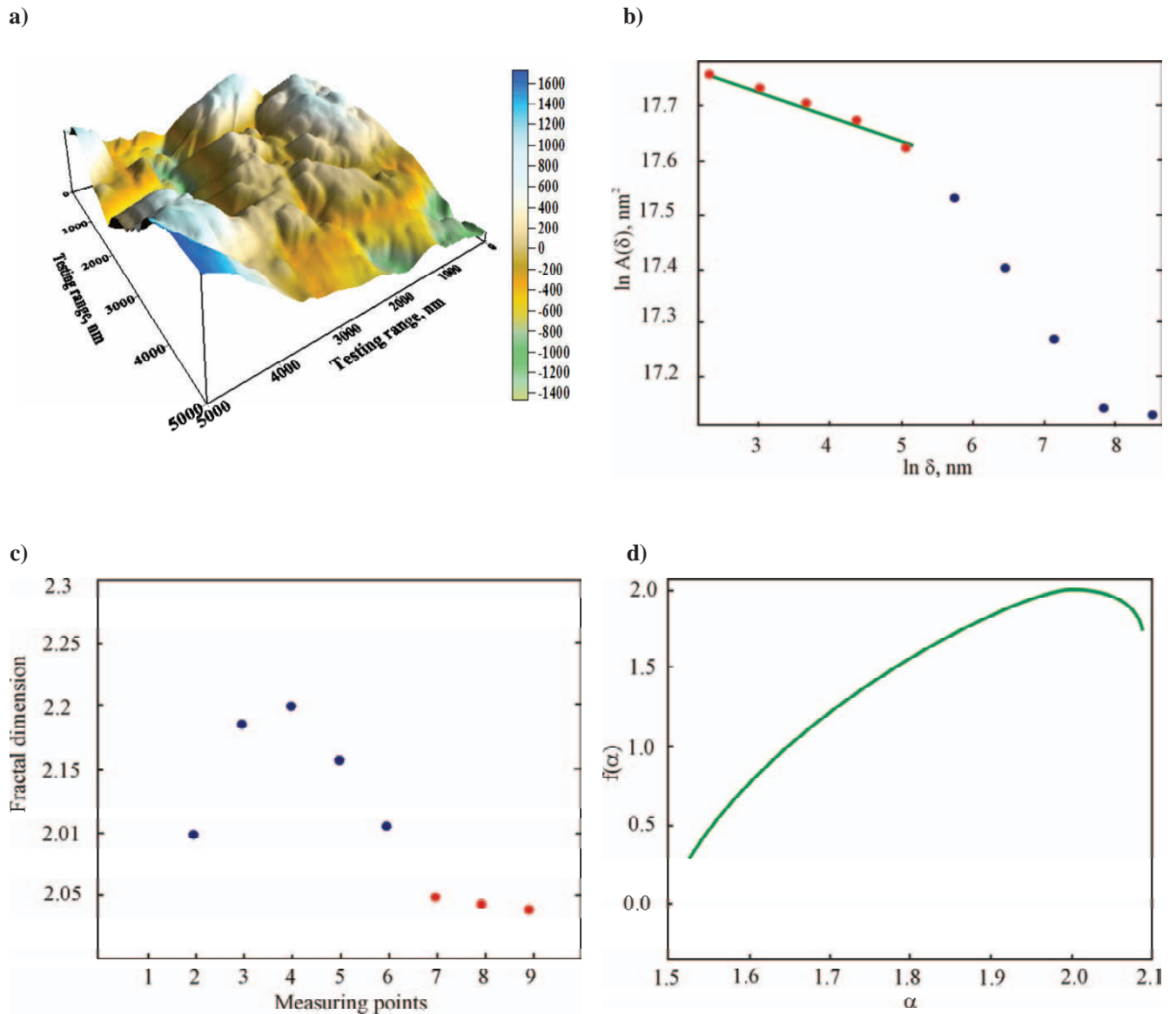
Fig. 74. a) Image of the TiN+Al$_2$O$_3$ coating surface obtained in the high-temperature CVD process on the Al$_2$O$_3$+TiC (AFM, 5 µm) tool ceramics substrate b) bilogarithmic dependence of the approximated area size of the analysed surface on the mesh size used for its determination c) auxiliary diagram indicating the correct points selection on the bilogarithmic plot, and d) multi-fractal spectrum of the analysed coating surface

(substrates made of tool ceramics made of Al$_2$O$_3$+SiC, Al$_2$O$_3$+TiC, Al$_2$O$_3$+ZrO$_2$) it was found that for the last steps of projective plane division, lnA(δ) values do not increase so significantly in relation to the first ones. This effect denotes irregularities occurrence of high amplitude in the form of big grains with smooth walls, what is confirmed by the AFM presented images (Fig. 71a-75a). In case of analyzed coatings received in the high-temperature CVD process, there is no dependence between roughness value R$_{2D}$ and the fractal dimension D$_s$, what results from the fact that high R$_{2D}$ value is connected with surface waviness (irregularity occurrence of high amplitude), and not with proper roughness.

a)

b)

c)

d)
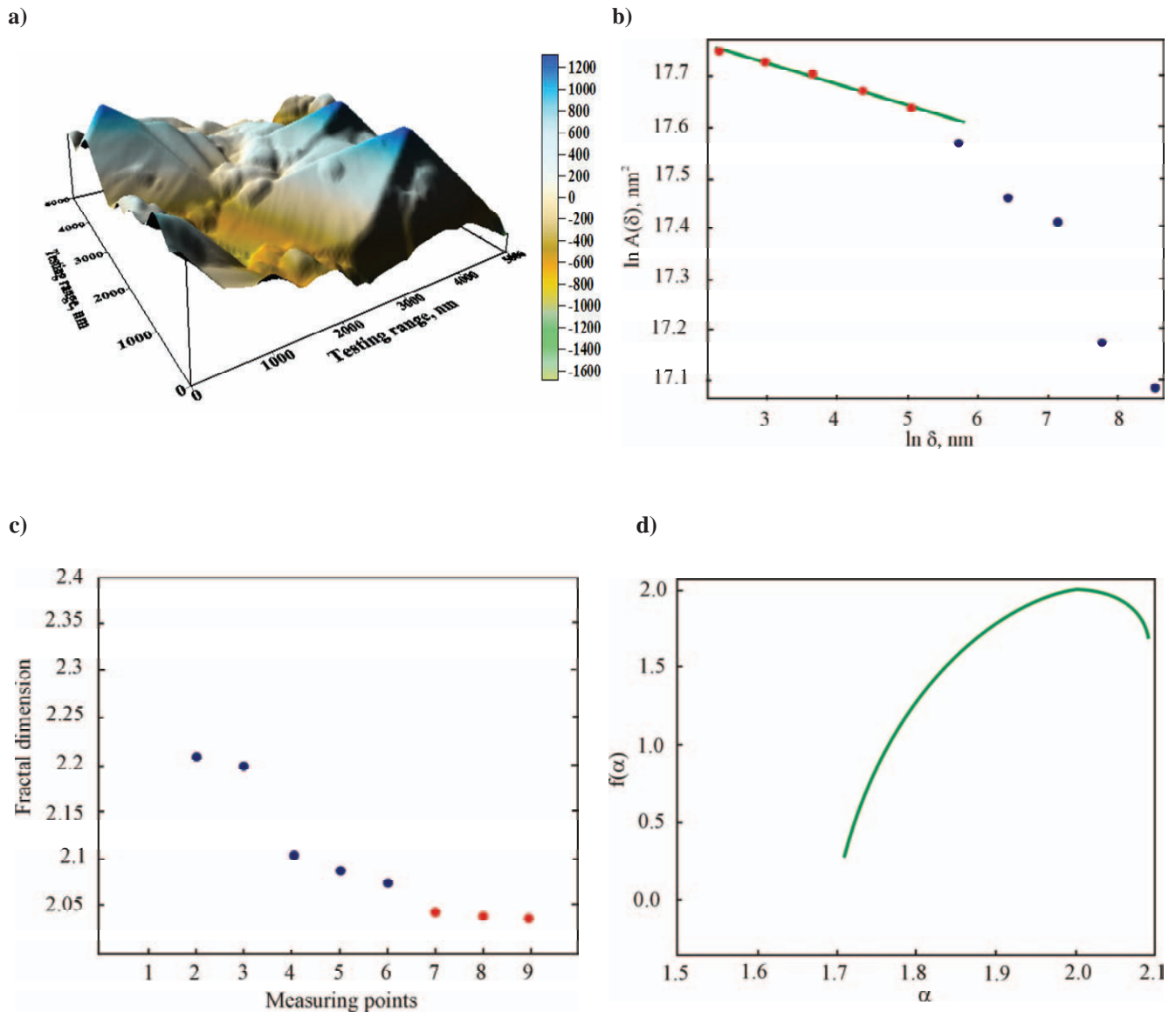
Fig. 75. a) Image of the $TiN+Al_2O_3$ coating surface obtained in the high-temperature CVD process on the Al_2O_3+SiC (AFM, 5 µm) tool ceramics substrate b) bilogarithmic dependence of the approximated area size of the analysed surface on the mesh size used for its determination c) auxiliary diagram indicating the correct points selection on the bilogarithmic plot, and d) multi-fractal spectrum of the analysed coating surface

Surface inhomogeneity is confirmed by the obtained multi-fractal spectrum bandwidth values ($\Delta\alpha = 0.29$-0.56), whereas unevenness occurrence of high amplitude – high α_{max} values. For all analyzed coatings obtained in the high-temperature CVD process, a positive difference is received for the height of the multi-fractal spectra arms $\Delta f > 0$, however, the difference is significantly lower than in the PVD processes. The right arm of the multi-fractal spectrum moves towards higher values α, but the left gets shorten (Fig. 71d-75d), what denotes an increasing role of high irregularities (large grains), defined by high values of probability.

Table 8.
The fractal and multi-fractal analysis results and R_{2D} values for coatings obtained in the high-temperature CVD & the magnetron PVD processes and substrate made of tool nitride ceramics Si_3N_4

Type and conditions of process	Substrate's material	Type of coating	R_{2D} [μm]	D_s	$α_{min}$	$α_{max}$	$Δα$	$f(α_{max})$	$f(α_{min})$
CVD (1000°C)	Si_3N_4	TiN+Al$_2$O$_3$	0.098±0.008	2.046±0.005	1.679±0.032	2.067±0.008	0.388±0.033	0.276±0.029	1.838±0.016
	Si_3N_4	TiN+Al$_2$O$_3$+TiN	0.170±0.021	2.034±0.005	1.697±0.054	2.021±0.002	0.325±0.054	0.005±0.002	1.865±0.022
	Si_3N_4	TiN+Al$_2$O$_3$+TiN+Al$_2$O$_3$+TiN	0.163±0.019	2.046±0.007	1.657±0.067	2.032±0.003	0.375±0.067	0.004±0.036	1.821±0.031
	Si_3N_4	Al$_2$O$_3$+TiN	0.166±0.022	2.030±0.004	1.550±0.048	2.032±0.006	0.481±0.048	0.016±0.003	1.830±0.033
	Si_3N_4	TiC+TiN	0.079±0.011	2.014±0.002	1.723±0.051	2.014±0.004	0.291±0.051	0.003±0.031	1.905±0.017
	Si_3N_4	Ti(C,N)+TiN	0.095±0.012	2.021±0.003	1.681±0.049	2.019±0.015	0.338±0.051	0.004±0.021	1.861±0.019
	Si_3N_4	Ti(C,N)+Al$_2$O$_3$+TiN	0.146±0.017	2.019±0.002	1.708±0.053	2.089±0.008	0.381±0.054	0.268±0.042	1.700±0.051
	Si_3N_4	Ti(C,N)+Al$_2$O$_3$	0.089±0.008	2.071±0.007	1.604±0.041	2.046±0.009	0.442±0.042	0.007±0.028	1.728±0.049
	Al$_2$O$_3$+ZrO$_2$	TiN+Al$_2$O$_3$	0.482±0.039	2.041±0.004	1.570±0.045	2.084±0.011	0.514±0.046	0.591±0.061	1.744±0.027
	Al$_2$O$_3$+TiC	TiN+Al$_2$O$_3$	0.531±0.043	2.039±0.005	1.524±0.052	2.087±0.014	0.563±0.054	0.278±0.028	1.751±0.023
	Al$_2$O$_3$+SiC$_{(w)}$	TiN+Al$_2$O$_3$	0.511±0.048	2.028±0.003	1.708±0.031	2.089±0.001	0.381±0.031	0.268±0.027	1.700±0.031
	Si_3N_4	-	0.031±0.003	2.008±0.001	1.832±0.022	2.005±0.002	0.172±0.022	0.009±0.009	1.955±0.005
PVD (100%N$_2$/460°C)	PM HS6-5-3-8	Ti+(Ti,Al)N	0.025±0.002	2.021±0.002	1.876±0.014	2.009±0.001	0.133±0.014	0.186±0.023	1.921±0.011
PVD (100%N$_2$/500°C)	PM HS6-5-3-8	Ti+(Ti,Al)N	0.040±0.004	2.018±0.001	1.787±0.043	2.016±0.001	0.229±0.043	0.005±0.019	1.915±0.014
PVD (100%N$_2$/540°C)	PM HS6-5-3-8	Ti+(Ti,Al)N	0.034±0.005	2.014±0.001	1.774±0.019	2.007±0.002	0.233±0.019	0.055±0.009	1.936±0.008
PVD (75%N$_2$;25%CH$_4$/460°C)	PM HS6-5-3-8	Ti+(Ti,Al)(C,N)	0.035±0.003	2.029±0.003	1.775±0.029	2.014±0.001	0.239±0.029	0.006±0.042	1.854±0.019
PVD (75%N$_2$;25%CH$_4$/500°C)	PM HS6-5-3-8	Ti+(Ti,Al)(C,N)	0.033±0.003	2.024±0.003	1.767±0.023	2.011±0.001	0.243±0.023	0.053±0.005	1.923±0.008
PVD (75%N$_2$;25%CH$_4$/540°C)	PM HS6-5-3-8	Ti+(Ti,Al)(C,N)	0.041±0.004	2.017±0.002	1.702±0.042	2.011±0.002	0.309±0.042	0.008±0.034	1.921±0.009
PVD (50%N$_2$;50%CH$_4$/460°C)	PM HS6-5-3-8	Ti+(Ti,Al)(C,N)	0.037±0.005	2.020±0.002	1.865±0.024	2.011±0.001	0.146±0.024	0.032±0.004	1.901±0.012
PVD (50%N$_2$;50%CH$_4$/500°C)	PM HS6-5-3-8	Ti+(Ti,Al)(C,N)	0.021±0.003	2.009±0.001	1.788±0.041	2.004±0.001	0.217±0.041	0.002±0.001	1.963±0.005
PVD (50%N$_2$;50%CH$_4$/540°C)	PM HS6-5-3-8	Ti+(Ti,Al)(C,N)	0.025±0.004	2.023±0.002	1.875±0.021	2.012±0.001	0.137±0.021	0.215±0.031	1.892±0.016
PVD (25%N$_2$;75%CH$_4$/460°C)	PM HS6-5-3-8	Ti+(Ti,Al)(C,N)	0.043±0.003	2.010±0.001	1.701±0.033	2.007±0.002	0.305±0.033	0.004±0.004	1.953±0.007
PVD (25%N$_2$;75%CH$_4$/500°C)	PM HS6-5-3-8	Ti+(Ti,Al)(C,N)	0.026±0.002	2.012±0.002	1.757±0.029	2.010±0.001	0.252±0.029	0.004±0.042	1.936±0.008
PVD (25%N$_2$;75%CH$_4$/540°C)	PM HS6-5-3-8	Ti+(Ti,Al)(C,N)	0.032±0.003	2.013±0.001	1.837±0.016	2.007±0.001	0.170±0.016	0.007±0.005	1.949±0.006
PVD (100%CH$_4$/460°C)	PM HS6-5-3-8	Ti+(Ti,Al)C	0.026±0.002	2.015±0.001	1.757±0.025	2.010±0.002	0.252±0.025	0.006±0.032	1.936±0.008
PVD (100%CH$_4$/500°C)	PM HS6-5-3-8	Ti+(Ti,Al)C	0.043±0.004	2.024±0.002	1.701±0.031	2.007±0.002	0.305±0.031	0.003±0.003	1.953±0.006
PVD (100%CH$_4$/540°C)	PM HS6-5-3-8	Ti+(Ti,Al)C	0.046±0.008	2.036±0.006	1.658±0.048	2.040±0.004	0.381±0.038	0.007±0.009	1.754±0.025

Table 9.
The fractal and multi-fractal analysis results and R_{2D} values for coatings obtained in the arc PVD process and a substrate made of tool oxide ceramics and cermets

Substrate's material	Type of coating	R_{2D} [μm]	D_s	α_{min}	α_{max}	$\Delta\alpha$	$f(\alpha_{max})$	$f(\alpha_{min})$
Al₂O₃+ZrO₂	TiN+(Ti,Al,Si)N	0.408±0.033	2.029±0.003	1.637±0.038	2.039±0.005	0.403±0.038	0.231±0.025	1.772±0.025
Al₂O₃+TiC	TiN+(Ti,Al,Si)N	0.095±0.012	2.027±0.003	1.740±0.026	2.008±0.001	0.268±0.026	0.004±0.031	1.947±0.009
Al₂O₃+SiC(w)	TiN+(Ti,Al,Si)N	0.184±0.023	2.016±0.002	1.651±0.067	2.025±0.003	0.375±0.067	0.216±0.029	1.875±0.014
Al₂O₃+ZrO₂	TiN	0.133±0.017	2.018±0.002	1.807±0.021	2.014±0.001	0.207±0.021	0.006±0.043	1.897±0.016
Al₂O₃+TiC	TiN	0.037±0.005	2.006±0.001	1.865±0.024	2.004±0.001	0.139±0.024	0.003±0.003	1.963±0.005
Al₂O₃+SiC(w)	TiN	0.564±0.054	2.122±0.018	1.532±0.057	2.118±0.019	0.586±0.060	0.216±0.033	1.764±0.033
Al₂O₃+ZrO₂	TiN+multi(Ti,Al,Si)N+TiN	0.087±0.009	2.019±0.005	1.846±0.016	2.013±0.003	0.167±0.016	0.284±0.051	1.897±0.019
Al₂O₃+TiC	TiN+multi(Ti,Al,Si)N+TiN	0.470±0.044	2.252±0.036	1.645±0.043	2.147±0.021	0.502±0.048	0.190±0.022	1.588±0.051
Al₂O₃+SiC(w)	TiN+multi(Ti,Al,Si)N+TiN	0.440±0.037	2.128±0.022	1.530±0.081	2.091±0.014	0.561±0.082	0.182±0.026	1.735±0.027
Al₂O₃+ZrO₂	(Ti,Al)N	0.260±0.029	2.032±0.004	1.788±0.022	2.026±0.004	0.238±0.022	0.280±0.031	1.862±0.015
Al₂O₃+TiC	(Ti,Al)N	0.082±0.007	2.014±0.002	1.779±0.029	2.014±0.002	0.236±0.029	0.003±0.042	1.900±0.018
Al₂O₃+SiC(w)	(Ti,Al)N	0.351±0.031	2.045±0.005	1.745±0.029	2.032±0.003	0.287±0.029	0.241±0.029	1.948±0.006
Al₂O₃+ZrO₂	TiN+(Ti,Al,Si)N+(Al,Si,Ti)N	0.261±0.025	2.034±0.004	1.612±0.054	2.0438±0.008	0.431±0.055	0.0113±0.002	1.800±0.034
Al₂O₃+TiC	TiN+(Ti,Al,Si)N+(Al,Si,Ti)N	0.236±0.019	2.060±0.008	1.642±0.061	2.038±0.004	0.396±0.061	0.092±0.011	1.823±0.019
Al₂O₃+SiC(w)	TiN+(Ti,Al,Si)N+(Al,Si,Ti)N	0.237±0.025	2.029±0.003	1.573±0.049	2.031±0.003	0.458±0.049	0.311±0.039	1.888±0.021
Cermetal T130A	TiN+(Ti,Al,Si)N	0.409±0.037	2.100±0.009	1.607±0.089	2.078±0.012	0.472±0.090	0.141±0.002	1.778±0.051
Cermetal CM	TiN+(Ti,Al,Si)N	0.306±0.041	2.101±0.007	1.541±0.099	2.074±0.011	0.532±0.103	0.228±0.012	1.744±0.031
Al₂O₃+ZrO₂	-	0.060±0.006	2.009±0.001	1.818±0.019	2.007±0.001	0.190±0.019	0.001±0.029	1.945±0.006
Al₂O₃+TiC	-	0.033±0.003	2.009±0.001	1.831±0.023	2.006±0.001	0.175±0.023	0.004±0.014	1.951±0.007
Al₂O₃+SiC(w)	-	0.043±0.004	2.008±0.001	1.828±0.021	2.006±0.001	0.178±0.021	0.002±0.039	1.960±0.008
Cermetal T130A	-	0.180±0.021	2.153±0.021	1.483±0.078	2.131±0.015	0.648±0.079	0.009±0.018	1.533±0.083
Cermetal CM	-	0.412±0.044	2.164±0.016	1.671±0.043	2.142±0.022	0.472±0.048	0.329±0.036	1.586±0.042

4.4. Setting a correlation between chosen properties of the investigated coatings and their fractal dimension

A complex method to affect phase composition, being a consequence of chemical composition, the adhesion of analyzed coatings to applied substrate's material correlating with a value of internal stresses, the applied combination of layers, and also a shape of surface decide about obtained mechanical and operational properties.

Measurements results for micro-hardness and the fractal dimension values of coatings received in the magnetron PVD process is shown on figure 76. The outcomes for investigated analyses point out at correlation between hardness and the fractal dimension value (Fig. 77) defined by the following analytical dependence $y=29210x-56263$. The carried out statistics analyses pointed out a strong, positive linear correlation (correlation coefficient $r=0.908$) between the fractal dimension value and hardness. In order to assess significance of a correlation coefficient, the value of empirical test statistics $t=7.807$ is compared afterwards to a critical value $t_{kryt} = 2.16$ (read out from the t-Student distribution table for the significance level $\alpha_{stat}=0.05$). As $t > t_{kryt}$, the correlation coefficient being assessed is considered as significant. The obtained results might be connected with the shape of the analysed coatings' surfaces. Columns width reduction is accompanied by both the fractal dimension value

increase and hardness growth. Higher values for the fractal dimension can certify of more irregular, developed surface. Surface development increase, which is accompanied by increase of the fractal dimension value, can be interpreted by occurrence of higher number of columns, densely packed, therefore narrower. In case of surface containing wider columns, surface development and the fractal dimension value are lower.

$$y=29210x - 56263$$
$$R^2=0.82420$$
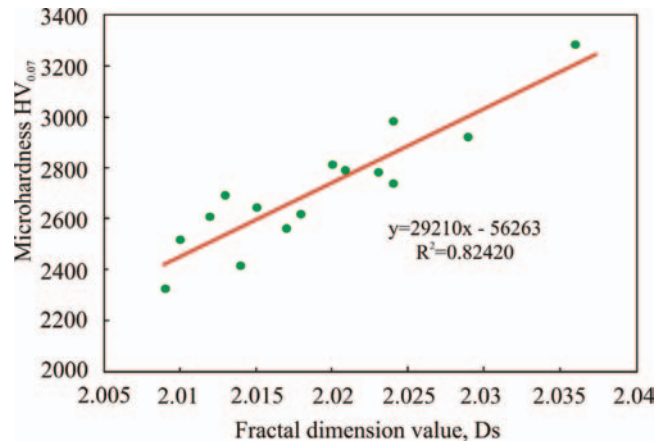
Fig. 77. The correlation between hardness and the fractal dimension value for coatings received in the magnetron PVD process
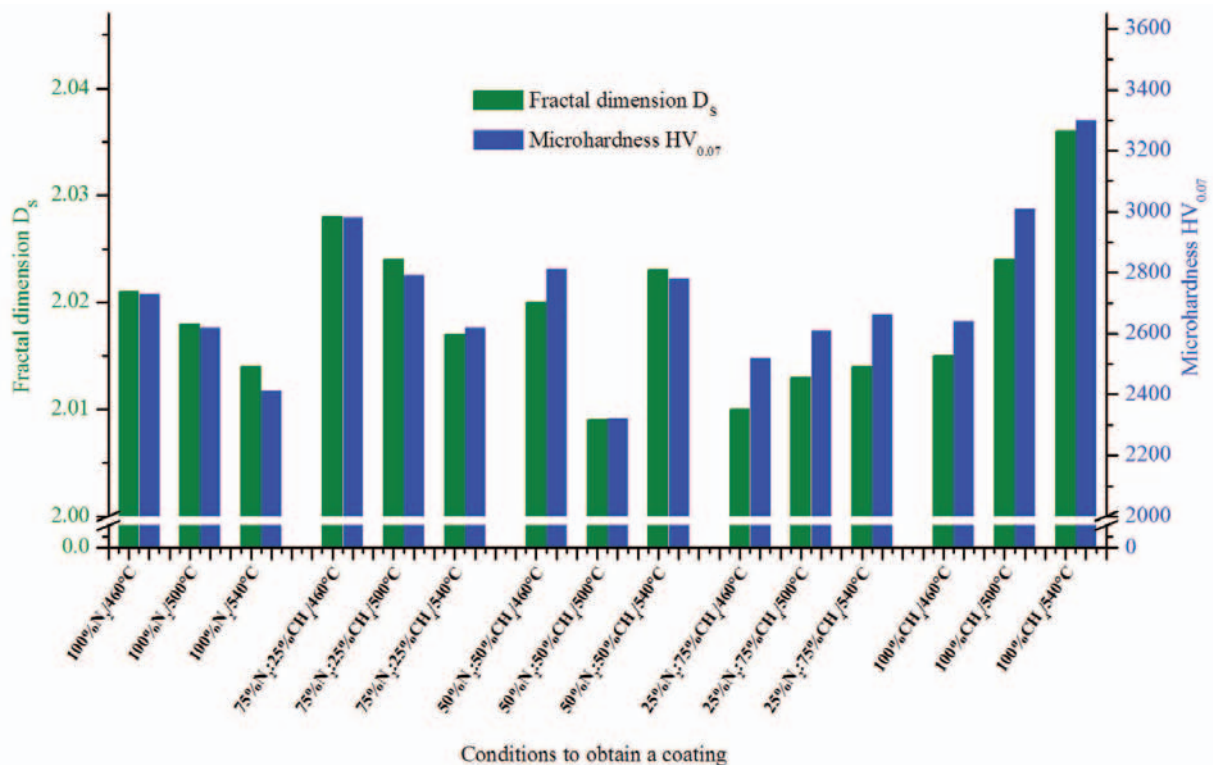
Fig. 76. Matching of obtained results of the fractal dimension values D_s and measurement of coatings hardness acquired in the magnetron PVD process

On figure 78 the obtained results of the fractal dimension values and coatings erosion resistance are presented depending on the magnetron PVD process conditions, including $\Delta\alpha$ values defining a degree of the analyzed surface irregularities. Correlation between erosion resistance for the discussed coatings and the fractal dimension value was found which is defined by the following analytical dependence y=298x-596 (Fig. 79), acquiring the correlation coefficient r=0.929. Since the empirical test statistics value t=9.012 is higher than the critical value t_{kryt} = 2.16, it allows finding significance of the assessed coefficient.

For the analyzed coatings it was found that out of fractal quantities, defining analyzed coatings surface topography, the most essential is the fractal dimension value D_s and the multi-fractal spectrum bandwidth $\Delta\alpha$. Coatings denoting higher values of the fractal dimension are characterized by higher erosion resistance, and comparing coatings of its closer value, better operational properties are denoted by coatings of lower value $\Delta\alpha$, and so more homogenous. In case of an erosion test, carried out for coatings obtained in the magnetron PVD process, a powdery erodent comes out of a nozzle at set pressure and hits against investigated sample surface canted at the fixed angle. One may judge that in case of this test employed for coatings with the similar D_s fractal dimension value, coatings with the higher $\Delta\alpha$ parameter value (fig. 78) demonstrate a lower erosion resistance, where the bigger and wider columns' tops protrude to the surface. These locations, regardless of the coatings deposition parameters, are probably responsible for initiating their failure process. This process is connected with the proceeding deepening and damaging in these locations until the substrate material is completely stripped and coating material is removed.
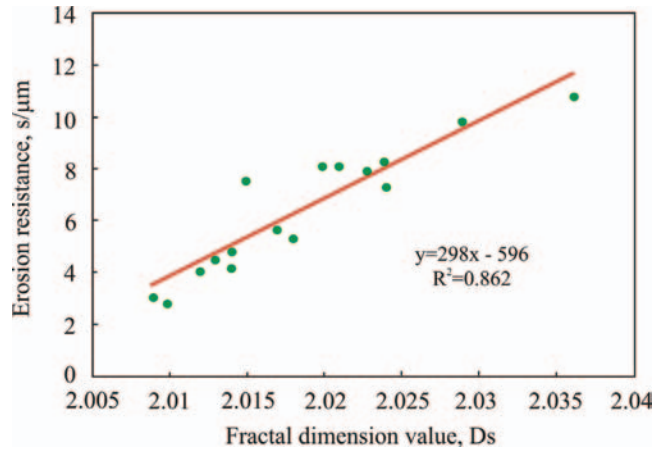
Fig. 79. The correlation between erosion resistance and the fractal dimension value for coatings received in the magnetron PVD process
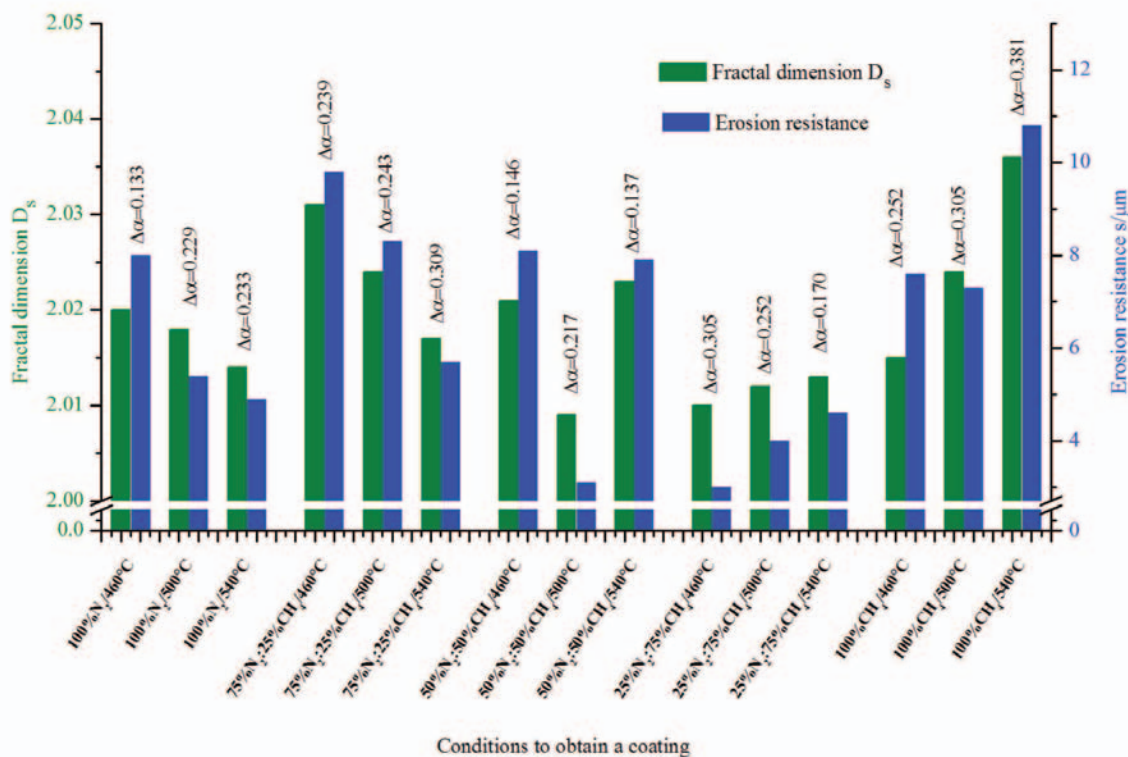
Fig. 78. Matching of obtained results of the fractal dimension values D_s, for quantities $\Delta\alpha$ and erosion resistance of coatings obtained in the magnetron PVD process

On figure 80 results of the fractal dimension values and intensity of distinguished orientation for increase of analyzed PVD coatings are matched up, depending on conditions to get them. Between the fractal dimension value and the component fraction <110> a significant positive correlation was found (Fig. 81), defined by the function: $y=0.0005x+1.9942$ (correlation coefficient $r=0.819$, the empirical test statistics value $t=5.146$, critical value $t_{kryt}=2.160$).

The component fraction analysis <110> in the investigated coatings, from the temperature level to obtain them, showed strong negative correlations for the coatings received in atmosphere containing high nitrogen concentration ($100\%N_2$ and $75\%N_2$ & $25\%CH_4$) as well as strong positive correlations in case of atmosphere contacting high carbon concentration ($25\%N_2$ & $75\%CH_4$ and $100\%CH_4$), whose significance is confirmed by comparing the empirical test statistics value t with the critical value $t_{kryt}=12.706$. Analogical relations were found for the fractal dimension dependence on coatings deposition temperature, however in this particular case, the conducted statistic analyses did not confirmed their significance (table 10). For the coatings received in the arc PVD and the high-temperature CVD processes, significantly higher fractal dimension values and higher $\Delta\alpha$ values were found.

On figure 82 the obtained results are presented for the fractal dimension values and operational properties depending on substrates' materials, including a value of the quantity $\Delta\alpha$. In the event of coatings obtained in the arc PVD process it was observed a positive correlation between the fractal dimension value and tool life increase (correlation coefficient $r=0.601$, the empirical test statistics value $t=2.914$, critical value $t_{kryt}=2.131$) (Fig. 82).
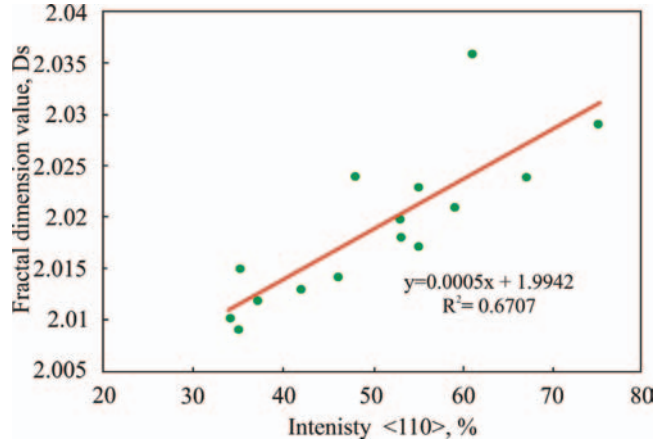
Fig. 81. The correlation between the fractal dimension value and orientation intensity <110> for coatings received in the magnetron PVD process
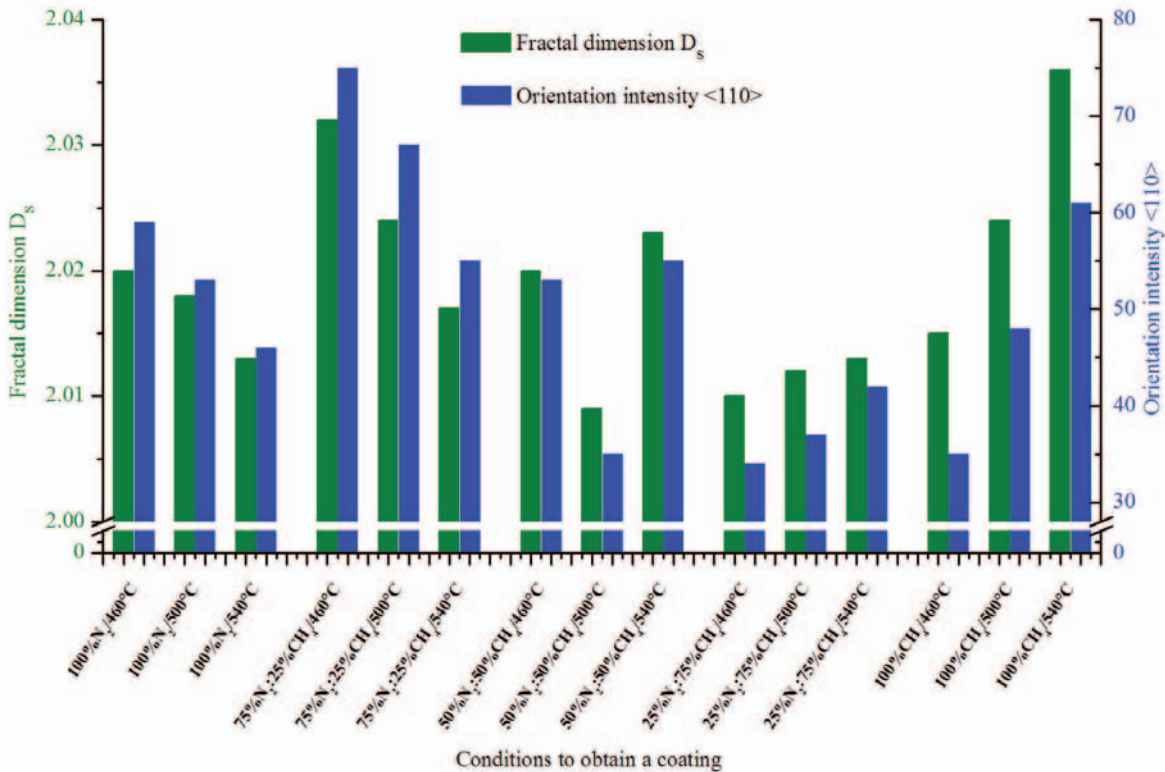
Fig. 80. Matching of obtained results of the fractal dimension values D_s, and orientation intensity <110> of coatings obtained in the magnetron PVD process

Low values of correlation coefficient of operational properties and fractal quantities (r=0,6011) reflects inhomogeneity of coatings on the basis of titanium nitride, obtained in the arc PVD process, defined by high quantity of $\Delta\alpha$. Coatings obtained in the arc PVD process are characterized by significantly wider range of the fractal dimension values than the other coatings obtained in the other processes. Considering results of measurements corresponding to coatings defined by low fractal dimension value (Ds<2.1), high value of correlation coefficient between the fractal dimension value and operational properties is obtained (correlation coefficient r=0.7599, t=3.6977, t_{kryt}=2.2281) (Fig. 83).

In case of coatings received in the high-temperature CVD process, for options when outer coating is made of Al_2O_3, and on its surface there are characteristic cubes, which can be referred to observed cones / columns in the event of coatings obtained on a substrate made of sintered high-speed steel (Fig. 84) as well as when substrate's material is nitride ceramics Si_3N_4 (Fig. 86) it was found that similar dependence of operational properties defined in a cutting ability test and fractal quantities, and in case of coatings obtained in the magnetron and the arc PVD process. In the first case correlation coefficients between the fractal dimension values and tool life increase are obtained r=0.9747 (analytical dependence y=2022x-4042, Fig. 85), whereas for coatings obtained on a substrate made of Si_3N_4 r = 0.9575 (analytical dependence y=2619x-0,5272, Fig. 87). Detailed results of

statistic analyses, considering critical values of the analyzed coatings obtained in the magnetron and the arc PVD as well as the high-temperature CVD process for discussed options are presented in table 11.
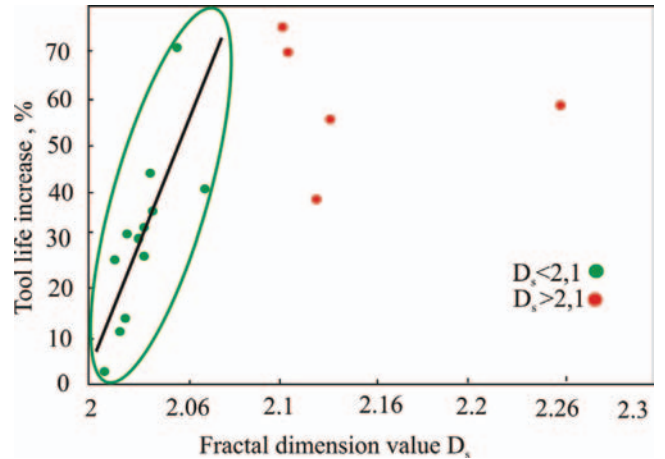
Fig. 83. Dependence of the obtained fractal dimension value and operational properties defined in cutting ability test of coatings obtained in the arc PVD process
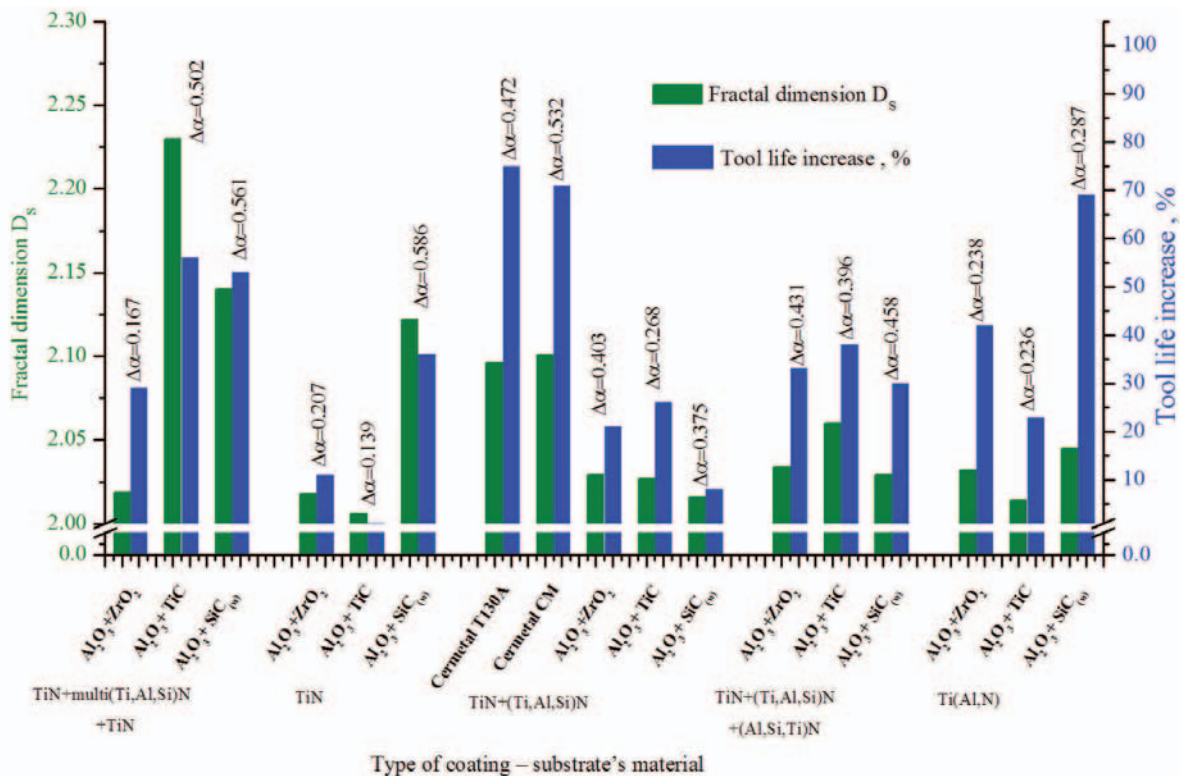
Fig. 82. Comparison of received results for the fractal dimension values D_s, $\Delta\alpha$ and operational properties of coatings obtained in the arc PVD process
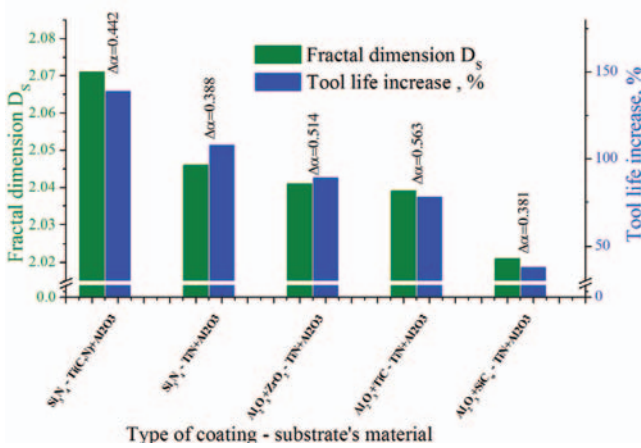
Fig. 84. Comparison of obtained results for the fractal dimension values D_s, $\Delta\alpha$ and operational properties of coatings obtained in the high-temperature CVD process (external layer made of Al_2O_3)
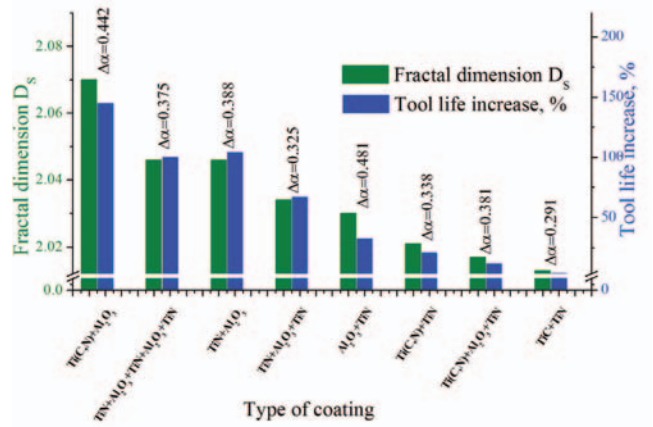
Fig. 86. Comparison of obtained results for the fractal dimension values D_s, $\Delta\alpha$ and operational properties of coatings obtained in the high-temperature CVD process (substrate made of nitride ceramics Si_3N_4)
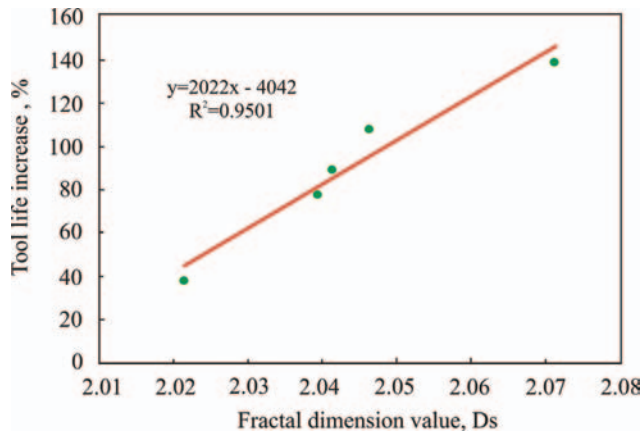
Fig. 85. Correlation between tool life increasion and the fractal dimension value for coatings received in the in the high-temperature CVD process (external layer made of Al_2O_3)
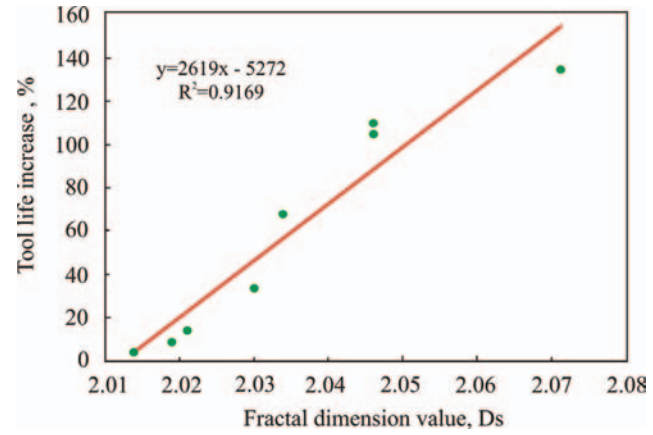
Fig. 87. Correlation between tool life increasion and the fractal dimension value for coatings received in the in the high-temperature CVD process (substrate made of nitride ceramics Si_3N_4)

Table 10.
Comparison of obtained statistic values determined at significance level $\alpha_{stat}=0,05$ of dependence of the fractal dimension including texture on temperature of coatings obtained in the magnetron PVD process (critical value is $t_{kryt}=12,706$)

Type of coating	Furnace atmosphere	The correlation between <110> orientation intensity and temperature		The correlation between the fractal dimension and temperature	
		Correlation coefficient r	Statistics value	Correlation coefficient r	Statistics value
Ti+(Ti,Al)N	100%N_2	-0.999	16.455> t_{kryt}	- 0.997	12.124< t_{kryt}
Ti+(Ti,Al)(C,N)	75%N_2:25%CH_4	-0.993	31.176> t_{kryt}	- 0.995	10.392< t_{kryt}
Ti+(Ti,Al)(C,N)	50%N_2:50%CH_4	0.091	0.055< t_{kryt}	0.203	0.209< t_{kryt}
Ti+(Ti,Al)(C,N)	25%N_2:75%CH_4	0.990	29.445> t_{kryt}	0.982	5.196< t_{kryt}
Ti+(Ti,Al)C	100%CH_4	0.999	37.278> t_{kryt}	0.997	12.124< t_{kryt}

Table 11.
Comparison of obtained results for correlation statistic values between selected coatings properties obtained in the magnetron and arc PVD process and the high-temperature CVD process

Type of process	Substrate's material	Type of coating	Correlated quantities		Correlation coefficient r	Statistics value t	Critical value t_{kryt}
Magnetron PVD	PM HS6-5-3-8	Ti+(Ti,Al)N, Ti+(Ti,Al)($C_x N_{1-x}$), Ti+(Ti,Al)C	⋏ adhesion	⋏ stresses	0.679	3.333	2.160
			⋏ hardness	⋏ fractal dimension	0.908	7.807	2.160
			⋏ erosion resistance	⋏ fractal dimension	0.929	9.012	2.160
			⋏ texture	⋏ fractal dimension	0.819	5.146	2.160
Arc PVD	1) $Al_2O_3+ZrO_2$, 2) Al_2O_3+TiC, 3) $Al_2O_3+SiC_{(w)}$, 4) cermet CM, 5) cermet T130A	TiN*, TiN+multi(Ti,Al,Si)N+TiN*, (Ti,Al)N*, TiN+(Ti,Al,Si)N+(Al,Si,Ti)N*, TiN+(Ti,Al,Si)N**, (* - coatings obtained on substrates 1-3, **- coating obtained on a substrate 1-5)	⋏ adhesion	⋏ stresses	0.913	8.683	2.131
			⋏ tool life increase	⋏ fractal dimension	0.601	2.914	2.131
High-temperature CVD	1) Si_3N_4 2) $Al_2O_3+ZrO_2$ 3) Al_2O_3+TiC 4) $Al_2O_3+SiC_{(w)}$	$Ti,N+Al_2O_3*$ $Ti(C,N)+Al_2O_3**$ (* - coatings obtained on substrates 1-4, **- coating obtained on a substrate 1)	⋏ tool life increase	⋏ fractal dimension	0.975	7.557	3.182
	Si_3N_4	$TiN+Al_2O_3$, $TiN+Al_2O_3+TiN$, $TiN+Al_2O_3+TiN+Al_2O_3+TiN$, Al_2O_3+TiN, $TiC+TiN$, $Ti(C,N)+TiN$, $Ti(C,N)+Al_2O_3+TiN$, $Ti(C,N)+Al_2O_3$	⋏ tool life increase	⋏ fractal dimension	0.958	8.136	2.447

5. Summary and conclusions

Works [36-38], presenting structural zones models of coatings point out a fact that structure and topography of coating surface decide their mechanical properties, and consequently, their wear resistance. Employment of the contemporary examination techniques, especially of the scanning electron microscopy [130-132] and the atomic force microscopy [107, 108, 134], makes observation of coating surface possible, obtained on tool materials with atomic resolution, however, the results are still used only in a limited range. Fractal geometry is a valuable complement to analysis methods for results obtained using the atomic force microscopy [79, 126, 135-137], rendering it possible to obtain quantitative information characterizing topography of the investigated relationships are mentioned in literature between fractal quantities and roughness [138-140], as well as about fabrication conditions [127, 141, 142] of many engineering materials, which was a premise to undertake the research whose goal was employment of the quantitative analysis of surface topography of coatings obtained in the PVD & CVD processes on tool materials to predict their properties.

The first step to solve that problem was a complex characterisation of coatings' topography and structure which have an impact on a shape of analysed objects' surface. The materials used for investigations were the single- and multi-layer coatings, obtained in the magnetron- and arc PVD process as well as in the high temperature CVD process based on tool materials. The coatings selection, representative in terms of types and conditions proceeding in deposition processes, types of substrate material, as well as chemical and phase compositions, and also a combination of applied layers provided diversity of their surface topography as well as mechanical and functional properties.

Surface topography for the analysed coatings was investigated using the scanning electron microscopy SEM as well as the atomic force microscopy AFM. Furthermore, chemical and phase compositions investigations, as well as texture examinations were performed, confirming that these factors have an effect on topography of coatings obtained in the PVD & CVD processes. Also, measurements for mechanical and service properties were made to define their relationship with coatings' topography.

Roughness measurements results of the analysed coatings being defined by R_a differed substantially depending on the applied deposition process. Coatings obtained in the magnetron PVD process are characterized by a lower roughness value than coatings obtained in the CVD technique and in the arc PVD process. The low roughness value of coatings obtained in the magnetron PVD process can be related to their surface topography containing homogenous, in terms of size, tiny irregularities that was confirmed by observations done with the SEM technique. Roughness increase is affected in case of other deposition processes, also by occurrences of much higher irregularities, apart from the tiny ones. Coatings obtained in the high temperature CVD process, when the outer layer is made of Al_2O_3 feature an exception in the high roughness coatings

group. Mainly big polyhedron shaped grains are observed on their surface, which was noted also in other papers [130-133].

As regards texture analysis many studies [23, 24, 98, 133, 143-145] present the effect of deposition conditions on the privileged growth direction of the coatings obtained in the PVD & CVD processes and their relationship to mechanical properties. However, these papers were limited to a qualitative assessment of texture without quantitative analyses rendering it possible to define the effect of the distinguished component on mechanical properties. Thorough analysis was made in the presented paper of the Orientation Distribution Function (ODF) for coatings obtained in the magnetron PVD process by carrying out the qualitative- and quantitative texture analyses. The X-ray examinations revealed that in case of coatings obtained in the magnetron PVD process, that orientation <110> was privileged one differentiated in terms of volume fractions for identified texture components. Analysis of the pole figures for coatings obtained in the high-temperature CVD- and of the Ti(Al,N) in the arc PVD process revealed that their texture is very weak. The other coatings received in the arc process, independently on the substrate material, were characteristic of the growth plane from the {111} family.

Measurements of internal stresses for the analysed PVD & CVD wear resistant coatings were made with the commonly used X-ray method $\sin^2\psi$ [23, 95, 99, 100] and multi-reflection method g- $\sin^2\psi$ [33, 91, 103, 104] developed lastly. Comparison of both methods and the obtained results indicates, in the author's opinion, that the correct choice of stress measuring technique for thin layers deposited on tool materials, making it possible to obtain results encumbered with smaller error, is dependent mainly on crystal structure of coatings and their texture as well as on combinations of applied layers and used substrate's material. In all analysed samples compressive stresses appeared. The highest values of internal stresses were found for coatings obtained in the magnetron PVD process, whereas, the lowest ones for coatings obtained in the high-temperature CVD process. Obtained values of stress measurements for the investigated coatings, depending on applied type of deposition process, do not differ from data quoted in literature [22, 91, 132-134] and they exhibit a strict relation to their adhesion to substrates' materials. Moreover, analytical relationships are presented in this paper defining these correlations.

Presented literature study shows a number of fractal geometry applications in the area of the material engineering [59, 63, 66, 74, 75, 114, 115]. One of more important problems within this sphere is to develop effective and reliable algorithms determining fractal quantities [146-150], adequate to different types of investigated material and their application. The author of this paper used the Projective Covering Method (PCM), originally developed for determining the fractal dimension of rocks surface [60], to determine the fractal dimension of coatings' surface, and then applied in investigations and analyses of various engineering materials [52, 112, 113, 116-120, 129], whereas, this method had not been used so far to define and characterise the coatings received in PVD & CVD processes. One of advantages of the PCM method is its

capability to analyse results obtained by nano-metric resolution when using the Atomic Force Microscope - AFM and also the fact that all dimensions used in calculations are expressed in the same units and they do not require additional scaling, what, for instance, is a serious disadvantage of time analyses [151-153].

In this paper a modified methodology to determine fractal quantities of surface by means of the PCM method was presented in details. To analyse, and then to modify the applied method for determining the fractal dimension, the author was inclined by appearing incorrect, overestimated values of the fractal dimension (D_s>3), obtained while conducting test analyses. Correctness of a corrected method to determine the fractal dimension was then confirmed using sets of data modelling surfaces with a set value of the fractal dimension which utilize midpoint distribution algorithms and Falconer's algorithm [55]. In order to broaden the area of the fractal geometry applications, also in cases of surface whose particular fragments are differentiated by a possibility to assess homogeneity of surface topography received in the PVD & CVD processes on tool materials in particular, the analysis of the multi-fractal spectrum shape was applied. It was found that all examined coatings, independently on a type of process of their production and the applied substrate's material, exhibit fractal nature of surface being different by a range of fractality and quantities which define the multi-fractal spectrum.

The obtained results determining influence of deposition conditions of coatings upon the fractal quantities value of surface are compatible to the earlier literature reports [127, 141, 142, 154]. Particularly, a relation between the fractal dimension and roughness [139, 140, 142] was confirmed. In the following papers [126, 127, 130, 141, 155, 156] it was revealed that to define roughness of the analysed surfaces one can utilize the multi-fractal spectrum bandwidth $\Delta\alpha$. The analyses carried out and results revealed in this paper have not confirmed these reports. For the investigated PVD & CVD coatings obtained on tool materials, $\Delta\alpha$ value neither correlated with the fractal dimension value D_s, nor with the R_{2D} roughness value. It was also found that homogeneity of analysed objects influences significantly on $\Delta\alpha$ spectrum bandwidth. Performed analyses (both for model and experimental data) revealed that the multi-fractal spectrum of the homogenous surfaces of a high fractal dimension value can be narrower from a surface spectrum of a low dimension value, but less homogenous. An extreme case is mono-fractal surface whose spectrum is reduced to a single point. Therefore, in the author's opinion, the multi-fractal spectrum bandwidth cannot be used to characterise surface roughness. However, it is substantiated to compare bandwidth and other values defining the shape of the multi-fractal spectra of coatings being differentiated by single, selected parameter of their reception (e.g.: by a type of coatings, temperature or process duration, chemical composition or substrate's material which they were produced upon) to define its influence on homogeneity of analysed surface.

Topography pictures presented in this paper showing coatings surface were obtained with the Atomic Force Microscope – AFM, as well as examples of the fractal- and multi-fractal analysis application to assess:

- Effect of deposition conditions on topography of coatings' surface (Ti,Al)(C,N) acquired in the magnetron PVD process on a substrate made of sintered high-speed steel PM HS6-5-3-8,
- Influence of a type of substrate on topography of coatings' surface TiN+multi(Ti,Al,Si)N+TiN acquired in the arc PVD process,
- Influence of the substrate type and combination of applied layers on topography of coatings surface obtained in the high-temperature CVD process, when outer layer was made of Al_2O_3.

Values of the fractal dimension for coatings' topography obtained in the magnetron PVD process were correlated with micro-hardness and erosion resistance, whereas the fractal dimension values of coatings' topography obtained in the high-temperature CVD process (on a substrate made of Si_3N_4 ceramics and when the outer layer was made of Al_2O_3) and in the arc PVD process was correlated with tool life increase specified in the cutting ability test. It was shown that the presented interdependencies give a possibility to predict coatings' properties received in the PVD & CVD processes on tool materials based on fractal quantities defining their surface demonstrating significant correlations between the fractal dimensions defining the coatings' surface and their mechanical and/or operational properties is a confirmation of this paper's thesis.

Based on the obtained experimental studies results the of analyses performed, the following conclusions were formulated:

1. Prediction of hardness and erosion resistance of coatings obtained in the magnetron PVD process on a substrate made of sintered high-speed steel PM HS6-5-3-8 based on a value of the surface fractal dimension D_s for topography of their surface is possible.
2. In case of coatings obtained in the arc PVD process, prediction of the operational properties defined in the cutting ability test is possible, when the value of their surface fractal dimension D_s<2.1. For coatings showing higher D_s values, predicting the consumer properties on the basis of analysis of the fractal surface topography is encumbered with serious error because of their heterogeneity defined by a high $\Delta\alpha$>0.47 value.
3. For coatings obtained in the high-temperature CVD process prediction of their operational properties based on values of the surface fractal dimension D_s is possible when the external value was made of Al_2O_3 as well as for coatings produced on a substrate made from the Si_3N_4 nitride ceramics .
4. Growth of the compression stresses values results in the increased coatings' adhesion substrate material (independent from deposition process type).
5. It was indicated in this paper that texture is the crucial factor, deciding not only the mechanical and service properties, but also influencing the surface topography of coatings obtained in the PVD & CVD processes. This aspect requires further investigations for coatings showing distinct differences in terms of their privileged growth orientation type.

Acknowledgements

References

[1]   J. Pacyna, Metal science: chosen problems, AGH, Scientifically Didactic College Publishing House, Cracow 2005.

[2]   M. Soković, J. Mikuła, L.A. Dobrzański, J. Kopać, L. Koseć, P. Panjan, J. Madejski, A. Piech, Cutting properties of the Al$_2$O$_3$+SiC(w) based tool ceramic reinforced with the PVD and CVD wear resistant coatings, Journal of Materials Processing Technology 164-165 (2005) 924-929.

[3]   S.J. Bull, D.G. Bhat, M.H. Staia, Properties and performance of commercial TiCN coatings, Surface and Coatings Technology 163-164 (2003) 507-514.

[4]   W. Grzesik, Fundamentals of tool materials cutting, WNT, Warsaw 1998.

[5]   M. Wysiecki, Contemporary tool materials, WNT, Warsaw 1997.

[6]   J. Sieniawski, A. Cyunczyk, Solid state structure, Technical University Press, Rzeszow 2008.

[7]   J.I. Goldstein, D.E. Newburry, P. Echlin, D.C. Joy, A.D. Romig Jr., C.E. Lyman, C. Fiori, E. Lifshin, Scanning Electron Microscopy and X-ray Microanalysis. A Text for Biologists, Materials Scientists, and Geologists, Plenum Press, New York 1992.

[8]   R. Howland, L. Benatar, STM/AFM: microscopes with scanning probe – theory and practice, WIM PW, Warsaw 2002.

[9]   M. Hebda, A. Wachal, Tribology, WNT, Warsaw 1980.

[10]   PN EN ISO 4287: (1997) Geometrical Product Specifications (GPS), Surface texture: Profile Method - Terms, definitions and surface texture parameters.

[11]   B. Nowicki, Multiparameter representation of surface roughness, Wear 102 (1985) 161-176.

[12]   D.J. Whitehouse, P. Vanherck, W. De Bruin, C.A. van Luttervelt, Assessment of surface typology analysis techniques in turning, Annals of the CIRP 23/2 (1974) 265-282.

[13]   G.P. Petropoulos, Multi-parameter analysis and modeling of engineering surface texture, Journal of Achievements in Materials and Manufacturing Engineering 24/2 (2007) 91-100.

[14]   J.H. Hsieh, C. Liang, C.H. Tu, W. Wu, Deposition and characterization of TiAlN and multi-layered TiN/TiAlN

[15]   coatings unbalanced magnetron sputtering, Surface and Coatings Technology 108-109 (1998) 132-137.

[15]   A. Michalski, S. Sobczak, M. Kupczyk, BN coatings obtained by the pulse plasma method, Materials Engineering 6 (2000) 349-353.

[16]   T. Burakowski, A. Mazurkiewicz, K. Miernik, J. Smolik, J. Walkowicz, Current state and directions of developments of anti-wear technologies, Tribology 5 (2000) 877-899.

[17]   L.A. Dobrzański, The design and manufacture of functional gradient materials, PAN, Cracow, 2007, 130-150.

[18]   S. Mitura, A. Mitura, P. Niedzielski, P. Couvart, Nanocrystalline Diamond Coatings, Chaos, Solitions and Fractals 10/12 (1999) 2165-2176.

[19]   Y. Sahin, G. Sur, The effect of Al O, TiN and Ti (C,N) based CVD coatings on tool wearn machining metal matrix composites, Surface and Coatings Technology 179 (2004) 349-355.

[20]   M.K. Kazmanli, M. Urgen, A.F. Cakir, Effect of nitrogen pressure, bias voltage and substrate temperature on the phase structure of Mo–N coatings produced by cathodic arc PVD, Surface and Coatings Technology 167 (2003) 77-82.

[21]   M. Kupczyk, Technological and functional quality of cutting tool flanks with the anti wear coatings, Technical University Press, Poznan, 1997 (in Polish)

[22]   D. Sheeja, B.K. Tay, K.W. Leong, C.H. Lee, Effect of film thickness on the stress and adhesion of diamond-like carbon coatings, Diamond and Related Materials 11 (2002) 1643-1647.

[23]   M. Leoni, P. Scardi, S. Rossi, L. Fedrizzi, Y. Massiani, (Ti,Cr)N and Ti/TiN PVD coatings on 304 stainless steel substrates: Texture and residual stress, Thin Solid Films 345 (1999) 263-269.

[24]   W. J. Chou, G. P. Yu, J.H. Huang, Mechanical properties thin films coatings on 304 stainless steel substrate, Surface Coatings Technology 149 (2002) 7-13.

[25]   L. Chen, S.Q. Wang, S.Z. Zhou, J. Li, Y.Z. Zhang, Microstructure and mechanical properties of Ti(C,N) and TiN/Ti(C,N) multilayer PVD coatings, International Journal of Refractory Metals & Hard Materials 26 (2008) 456-460.

[26]   L. Chen, Y. Du, S.Q. Wang, J. Li, A comparative research on physical and mechanical properties of (Ti,Al)N and (Cr,Al)N PVD coatings with high Al content, International Journal of Refractory Metals & Hard Materials 25 (2007) 400-404.

[27]   M. Dubar, A. Dubois, L. Dubar, Wear analysis of tools in cold forging, PVD versus CVD TiN coatings, Wear 259 (2005) 1109-1116.

[28]   S. Santos, W. Sales, F. Jose da Silva, S. Franco, M. Bacci da Silva, Tribological characterisation of PVD coatings for cutting tools, Surface and Coatings Technology 184 (2004) 141-148.

[29]   H. K. Tonshoff, C. Blawit, Development and evaluation of PACVD coated cermets tools, Surface and Coatings Technology 93 (1997) 88-92.

[30]   L. Cunha; M. Andritschky, L. Rebouta; R. Silva, Corrosion of TiN, (TiAl)N and CrN hard coatings

produced by magnetron sputtering, Thin Solid Films 317/1 (1998) 351-355.

[31] O. Takai; Y. Taki; T. Titagawa, Deposition of carbon nitride thin films by arc ion plating 317/1 (1998) 380-383.

[32] U. Krueger, H. Brändle, Enabling High Technology, Barclays Capital Global Technology Conference, 2008.

[33] A. Baczmanski, C. Braham, W. Seiler, N. Shiraki, Multi-reflection method and grazing incidence geometry used for stress measurement by X-ray diffraction, Surface and Coatings Technology 182 (2004) 43-54.

[34] C. Friedrich, G. Berg, E. Broszeit, C. Berger, Measurement of the hardness of hard coatings using a force indentation function, Thin Solid Films 290-291 (1996) 216-220.

[35] G. Berg, C. Friedrich, E. Broszeit, C. Berger, Scratch test measurment of tribological haed coatings in practice, Journal of Analitical Chemistry 358 (1997) 281-285.

[36] J.A. Thornton, The microstructure of sputter-deposited coatings, Journal of Vacuum Science Technology A 4 (1986) 3059-3065.

[37] A.P. Messier, A.P. Giri, R.A. Roy, Revised structure zone model for thin film physical structure, Journal of Vacuum Science and Technology 2 (1984) 500-5003.

[38] B.A. Movchan, A.V. Demchishin, Fizika Metallov i Metallovedenie 28 (1969) 653-656.

[39] K. Pawlik, Determination of the Orientation Distribution Function from Pole Figures In Arbitrarily Defined Cells, Physica Status Solidi (b) 134 (1986) 477-483.

[40] A. Śliwa, L.A. Dobrzański, W. Kwaśny, W. Sitek, Finite element method application for modeling of PVD coatings properties, Journal of Achievements in Materials and Manufacturing Engineering 27/2 (2008) 171-174.

[41] L.A. Dobrzański, A. Śliwa, W. Kwaśny, The computer simulation of internal stresses in coatings obtained by the PVD process, CAMS, Journal of Achievements in Materials and Manufacturing Engineering 20 (2007) 355-358.

[42] B.B. Mandelbrot, How long is the coast of Britain? Statistical self-similarity and fractional dimension, Science 156 (1967) 636-638.

[43] B.B. Mandelbrot, The Fractal Geometry of Nature, W.H. Freeman, New York 1983.

[44] N.A. Smirnova, M. Hayakawa, Fractal characteristics of the ground-observed ULF emission in relation to geomagnetic and seismic activities, Journal of Atmospheric and Solar-Terrestrial Physics 69 (2007) 1883-1841.

[45] K. Oleschko, Fractal Analysis of Teotihuacan, Journal of Archaeological Science 27 (2000) 1007-1016.

[46] T. Stojic, I. Reljin, B. Reljin, Adaptation of multifractal analysis to segmentation of microcalcifications in digital mammograms-Physica A 367 (2006) 494-508.

[47] J. Robbins, Fractals, Wibet 2, Warsaw 1994.

[48] W. Kwaśny, J. Mikuła, L.A. Dobrzański, Fractal and multifractal characteristics of coatings deposited on pure oxide ceramics, Journal of Achievements in Materials and Manufacturing Engineering 17 (2006) 257-260.

[49] L. Wojnar, K.J. Kurzydłowski, J. Szala, Practice of image analysis, Polish Society for Stereology, Cracow 2002.

[50] W. Kwaśny, K. Gołombek, L.A. Dobrzański, Multifractal character of surface topography of the coatings on cemented carbides, Proceedings of the 15th IFHTSE Congress, Vienna-Austria, (2006) 532-537.

[51] W. Kwaśny, M. Woźniak, J. Mikuła, L.A. Dobrzański, Structure, physical properties and multifractal characteristics of the PVD and CVD coatings deposition onto the Al_2O_3+TiC ceramics, Journal of Computional Materials Sciences and Surface Enginering 1 (2007) 97-113.

[52] W. Kwaśny, L.A. Dobrzański, Structure, physical properties and fractal character of surface topography of the Ti+TiC coatings on sintered high speed steel, Journal of Materials Processing Technology 164-165 (2005) 1519-1523.

[53] W. Kwaśny, L.A. Dobrzański, M. Pawlyta, W. Gulbiński, Fractal nature of surface topography and physical properties of the coatings obtained using magnetron sputtering, Journal of Materials Processing Technology 157-158 (2004) 183-187.

[54] K. Falconer, Fractal Geometry. Mathematical Foundations and Applications, Wiley, Chichester, 2003.

[55] W. Kwaśny, A modification of the method for determination of the surface fractal dimension and multifractal analysis, Journal of Achievements in Materials and Manufacturing Engineering 33 (2009) 115-125.

[56] T. Martyn, Fractal and algorithm object, Nakom, Poznań 1996 (in Polish).

[57] H.O. Peitgen, D. Saupe, The Sciences of Fractal Images, Springer-Verlag, New York 1988.

[58] B.B. Mandelbrot, Multifractal measures, especially for the geophysicist, Pure and Applied Geophysics 131 (1989) 5-42.

[59] J. C. Russ: Fractal dimension measurement of engineering surfaces, International Journal of Machine Tools and Manufacture 38/5-6 (1998) 567-571.

[60] H. Xie, J.A. Wang, E. Stein, Direct fractal measurement and multifractal properties of fracture surfaces, Physics Letters A 242 (1998) 41-50.

[61] B.B. Mandelbrot, D.E. Passoja, A.J. Paullay, Fractal character of fracture surfaces of metals, Nature 308 (1984) 721-722.

[62] U. Wendt, K. Stiebe-Lange, M. Smid, On the influence of imaging conditions and algorithms on the quantification of surface topography, Journal of Microscopy 207 (2002) 169-179.

[63] X. Wang, H. Zhou, Z. Wang, M. Tian, Y. Liu and Q. Kong, Fractal analysis of cyclic creep fractured surfaces of two high temperature alloys, Materials Science and Engineering A 266 (1999) 250-254.

[64] V.I. Betekhtin, P.N. Butenko, V.L. Gilyarov, V.E. Korsukov, A.S. Luk'yanenko, B.A. Obidov, V.E. Khartsiev, The effect of uniaxial tension on the relief geometry of the surface of an Fe77Ni1Si9B13 amorphous alloy, Technical Physics Letters 28 (2002) 26-29.

[65] F. Paun, E. Bouchaud, Morphology of damage cavities in aluminium alloys, International Journal Fracture 121 (2003) 43-54.

[66] A. Eftekhari, Fractal study of Ni-Cr-Mo alloy for dental applications: effect of beryllium, Applied Surface Science 220 (2003) 343-348.

[67] J.J. Mecholsky, D.E. Passoja, K.S. Feinberg-Ringel, Quantitative analysis of brittle fracture surfaces using

fractal geometry, Journal of the American Ceramic Society 72 (1989) 60-65.

[68] J.Y. Thompson, K.J. Anusavice, B. Balasubramaniam, J.J.J. Mecholsky, Effect of microcracking on the fracture roughness and fracture surface fractal dimension of lithia-based glass-ceramics, Journal of the American Ceramic Society 78 (1995) 3045-3049.

[69] A. Celli, A. Tucci, L. Esposito, P. Carlo, Fractal analysis of cracks in alumina–zirconia composites, Journal of the American Ceramic Society 23 (2003) 469-479.

[70] C.T. Chen, J. Runt, Fractal analysis of polystyrene fracture surfaces, Polymer communications 30 (1989) 334-335.

[71] L. Czarnecki, A. Garbacz, J. Kurach, On the characterization of polymer concrete fracture surface-Cement & Concrete Composites 23 (2001) 399-409.

[72] F. Lapique, P. Meakin, J. Feder, T. Jossang, Self-affine fractal scaling in fracture surfaces generated in ethylene and propylene polymers and copolymers, Journal of the American Ceramic Society 86 (2002) 973-983.

[73] S. Stach, J. Cybo, J. Cwajna, S. Rozkosz, Multifractal description of fracture morphology. Full 3D analysis of a fracture surface, Materials Science-Poland 23/2 (2005) 577-584.

[74] C.H. Shek, G. M. Lin, K.L. Lee, J. K. L. Lai, Fractal fracture of amorphous Fe Ni V Si B alloy, Journal of Non-Crystalline Solids 224 (1998) 244-248.

[75] A. Provata, P. Falaras, A. Xagas, Fractal features of titanium oxide surfaces, Chemical Physics Letter 297 (1998) 484-490.

[76] S.L. Mills, G.C. Lees, C.M. Liauw, S. Lynch, Dispersion assessment of flame retardant filler/polymer systems using a combination of X-ray mapping and multifractal analysis, Polymer Testing 21 (2002) 941-948.

[77] M.A. Lebyodkin, Y. Estrin, Multifractal analysis of the Portevin-Le Chatelier effect: General approach and application to AlMg and AlMg /Al$_2$O$_3$ alloys, Acta Materialia 53 (2005) 3403-3413.

[78] C.R. Neto, K. Bube, A. Cser, A. Otto, U. Feudel, Multifractal spectrum of a laser beam melt ablation process, Physica A 344 (2004) 580-586.

[79] Y. Hui-Shehg, S. Xia, L. Shou-Fu, W. Young-Rui, W. Zi-Qin, Multifractal spectra of atomic force microscope images of amorphous electroless NiCuP alloy, Applied Surface Science 191 (2002) 123-127.

[80] W. Muller, A. Boreiko, U. SchloXmacher, X. Wang, M.N. Tahir, W. Tremel, D. Brandt, J.A. Kaandorp, H.C. Schroder, Fractal-related assembly of the axial filament in the demosponge Suberites domuncula: Relevance to biomineralization and the formation of biogenic silica, Biomaterials 28 (2007) 4501-4511.

[81] I.V. Shishkovsky, Y.G. Morozov, I. Smurov, Nanofractal surface structure under laser sintering of titanium and nitinol for bone tissue engineering, Applied Surface Science 254 (2007) 1145-1149.

[82] C.J. Buchko, K.M. Kozloff, D.C. Martin, Surface characterization of porous, biocompatible protein polymer thin films, Biomaterials 22 (2001) 1289-1300.

[83] S. Blacher, V. Maquet, F.Schils, D. Martin, J. Schoenen, G. Moonen, R. Jerome, J.P. Pirard, Image analysis of the axonal ingrowth into poly(d,l-lactide) porous scaffolds in relation to the 3-D porous structure, Biomaterials 24 (2003) 1033-1040.

[84] K. Anselme, M. Bigerelle, B. Noel, E. Dufresne, D. Judas, A. Iost, P. Hardouin, Qualitative and quantitative study of human osteoblast adhesion on materials with various surface roughnesses, Journal of Biomedical Materials Research 49 (2000) 155-166.

[85] D. Chapard, I. Degasne, G. Hure, E. Legrand, M. Audran, M.F. Basle, Image analysis measurements of roughness by texture and fractal analysis correlate with contact profilometry, Biomaterials 24 (2003) 1399-1407.

[86] J.L. Drummond, M. Thompson, B.J. Super, Fracture surface examination of dental ceramics using fractal analysis, Dental Materials 21 (2005) 586-589.

[87] R.J. Wilding, J.C. Slabbert, H. Kathree, C.P. Owen, K. Crombie, P. Delport, The use of fractal analysis to reveal remodelling in human alveolar bone following the placement of dental implants, Archives of Oral Biology 40 (1995) 61-72.

[88] R. Lopes, N. Betrouni, Fractal and multifractal analysis, Medical Image Analysis 13 (2009) 634-649.

[89] B. Świdzińska, Fractals in Computer Graphics, Press office PW, Warsaw 2000.

[90] http//www.fractalus.com

[91] S.J. Skrzypek, New Approach to Measuring Residual Macro-Stresses with the Application of the Grazing Angle X-Ray Diffraction Geometry, Scientifically Didactic College Publishing House, Cracow, 2002.

[92] A.C. Varmeulen, An elastic constants database and XEC calculator for use in XRD residual stress analysis, Advances of X-ray Analysis 44 (2001) 128-133.

[93] J. Dudognon, M. Vayer, A. Pineau, R. Erre, Grazing incidence X-ray diffraction spectra analysis of expanded austenite for implanted stainless steel, Surface & Coatings Technology 202 (2008) 5048-5054.

[94] D. Bobrowski, Probability in technical applications, WNT, Warsaw 1986.

[95] S. Chowdhury, M.T. Laugier, J. Henry, XRD stress analysis of CVD diamond coatings on SiC substrates, International Journal of Refractory Metals & Hard Materials 25 (2007) 39-45.

[96] E. Łągiewka, The design and manufacture of functional gradient materials, PAN, Cracow, (2007) 151-176.

[97] J. Bonarski, X-ray texture tomography, PAN, Cracow 2001.

[98] M. Ahlgren, H. Blomqvist, Influence of bias variation on residua stress and texture In TiAlN PVD coatings, Surface Coatings Technology 200 (2005) 157-160.

[99] U. Welzel, J. Ligot, P. Lampartem, A.C. Vermeulen, J. Mittemeijer, Stress analysis of polycrystalline thin films and surface regions by X-ray diffraction, Journal pf Applied Crystalography 38 (2005) 1-29.

[100] D. Senczyk, Fundamentals of X-ray tensometry, Technical University Press, Poznan 2005.

[101] K. Van Hacker, L. De Buyser, J.P. Celis, P. Van Houtte, Charackterization of thin nickiel electrocoatings by the low-incident-beam-angle diffraction method, Journal of Applied Crystallography 27 (1994) 56-66.

[102] C. Quaeyhaegens, G. Knuyt, L.M. Stals, Study of the residual macroscopic stress in TiN coatings deposited on various steel type, Surface and Coatings Technology 74-75 (1995) 104-109.

[103] S. Wroński, K. Wierzbanowski, A. Baczmański, Ch. Braham, A. Lodini, Corrections for residua stress in X-Ray grazing incidence technique, Archives of Metallurgy and Materials 53 (2008) 225-281.

[104] C.-H. Ma, J.-H. Huang, H. Chen, Residual stress measurement in textured thin film by grazing-incidence X-ray diffraction, Thin Solid Films 418 (2002) 73-78.

[105] J.A. Thornton, D.W. Hoffman, Stress-related effects in thin films, Thin Solid Films 171 (1986) 5-31.

[106] J.-H. Huang, C.-H. Ma, H. Chen, Effect of Ti interlayer on the residual stress and texture development of TiN thin films deposited by unbalanced magnetron sputtering, Surface & Coatings Technology 201 (2006) 3199-3204.

[107] P.W. Shum, K.Y. Li, Z.F. Zhou, Y.G. Shen, Structural and mechanical properties of titanium-aluminium-nitride films deposited by reactive close-field unbalanced magnetron sputtering, Surface & Coatings Technology 185 (2004) 245-253.

[108] Z.-J. Liu, P.W. Shum, Y.G. Shen, Surface growth of (Ti,Al)N thin films on smooth and rough substrates, Thin Solid Films 496 (2006) 326-332.

[109] P. Cichosz, Narzędzia skrawające, Wydawnictwo Naukowo-Techniczne, Warszawa 2006.

[110] S. Hogmark, S. Jacobson, M. Larsson, Design and evaluation of tribological coatings, Wear 246 (2000) 20-33.

[111] M. Fallqvist, M. Olsson, S. Rupii, Abrasive wear of multilayer Al_2O_3-Ti(C,N) CVD coatings on cemented carbide, Wear 263 (2007) 74-80.

[112] H. Xie, J.-A. Wang, M. A. Kwasniewski, Multifractal characterization of rock fracture surfaces, International Journal of Rock Mechanics and Mining Sciences (1999) 19-27.

[113] H.W. Zhou, H. Xie, Anisotropic characterization of rock fracture surfaces subjected to profile analysis, Physics Letters A (2004) 355-362.

[114] B. Liang Y. Shi R.-W. Hartel, Correlation of Rheological and Microstructural Properties in a Model Lipid System, Journal of the American Oil Chemists' Society 85 (2008) 397-404.

[115] Z. Zhou, S. Liu , L. Chu, L. Gu, Fractal analysis of worn surfaces of ZnO whisker/natural rubber-styrene butadiene rubber-butyl rubber composites, Journal of Applied Polymer 90 (2003) 667-670.

[116] H. Xie, F. Gao, The mechanics of cracks and a statistical strength theory for rocks, International Journal of Rock Mechanics and Mining Sciences 37 (2000) 477-488.

[117] S. Stach, S. Roskosz, J. Cybo, J. Cwajna, Multifractal description of fracture morphology: investigation of the fractures of sintered carbides, Materials Characterization 51 (2003) 87-93.

[118] Y. Ju, L Sudak, H. Xie, Study on stress wave propagation in fractured rocks with fractal joint surfaces, International Journal of Solids and Structures 44 (2007) 4256-4271.

[119] Y. Wang, B. Du, J. Liu, J. Lu, B. Shi, H Tang, Surface analysis of cryofixation-vacuum-freeze-dried polyaluminum

[120] chloride–humic acid (PACl–HA) flocs, Journal of Colloid and Interface Science 316 (2007) 457-466.

[120] S.G. Wang, The dependence of the fractal dimension of fractured surface on material in three dimensions, Physica B: Physics of Condensed Matter 348 (2004) 183-189.

[121] M.F. Barnsley, Fractals Everywhere, AP Professional Boston, 1988.

[122] E. Ott, Chaos w układach dynamicznych, WNT, Warsaw 1997.

[123] A.B. Chhabra, R.V. Jensen, Direct determination of the f(α) singularity spectrum, Physical Review Letters 62 (1989) 1327-1330.

[124] A.B. Chhabra, C. Meneveau, R.V. Jensen, K.R. Sreenivasan, Direct determination of the f(α) singularity spectrum and its application to fully developed turbulence, Physical Review A 40 (1989) 5284-5294.

[125] H.-O. Peitgen, H. Jurgens, D. Saupe, Chaos and Fractals. New Frontiers of Science, Springer-Verlag, New York, 1992.

[126] X. Sun, Z. Fu, Z. Wu, Multifractal analysis and scaling range of ZnO AFM images, Physica A 311 (2002) 327-338.

[127] C. Liu, X.L. Jiang, T. Liu, L. Zhao, W.X. Zhou, W.K. Yuan, Multifractal analysis of the fracture surfaces of foamed polypropylene/polyethylene blends, Applied Surface Science 255 (2009) 4239-4245.

[128] W. Kwaśny, K. Gołombek, L. A. Dobrzański, M. Pawlyta, Modeling of surface with require geometrical features and their fractal and multifractal characteristic, Materials Engineering 5/153 (2006) 1101-1106.

[129] W. Kwaśny, L.A. Dobrzański, Fractal nature of surface topography and physical properties of the TiN coatings obtained in the PVD process, Proceedings of the 12th Scientific International Conference „Achievements in Mechanical and Materials Engineering AMME'2003", Zakopane, (2003) 551-556.

[130] D. Pakuła, L.A. Dobrzański, K. Gołombeka, M. Pancielejko, A. Kriz, Structure and properties of the Si_3N_4 nitride ceramics with hard wear resistant coatings, Journal of Materials Processing Technology 157-158 (2004) 388-393.

[131] L.A. Dobrzański, D. Pakuła, Comparison of the structure and properties of the PVD and CVD coatings deposited on nitride tool ceramics, Journal of Materials Processing Technology 164-165 (2005) 832-842.

[132] L.A. Dobrzański, J. Mikuła, The structure and functional properties of PVD and CVD coated Al_2O_3 + ZrO_2 oxide tool ceramics, Journal of Materials Processing Technology 167 (2005) 438-446.

[133] L.A. Dobrzański, J. Mikuła, Structure and properties of PVD and CVD coated Al2O3 + TiC mixed, oxide tool ceramics for dry on high speed cutting processes, Journal of Materials Processing Technology 164-165 (2005) 822-831.

[134] Y. Fu, H. Du, S. Zhang, Y.W. Gu, Stress and surface morphology of TiNiCu thin films: effect of annealing temperature, Surface and Coatings Technology 198 (2005) 389-394.

[135] Y. Jin, W. Wu, L. Li, J. Chen, J. Zhang, Y. Zuo, J. Fu, Effect of sputtering power on surface topography of dc magnetron sputtered Ti thin films observed by AFM, Applied Surface Science 255 (2009) 4673-4679.

[136] A. P. Xagas, E. Androulaki, A. Hiskia, P. Falaras, Preparation, fractal surface morphology and photocatalytic properties of TiO2 films. Thin Solid FilmsVolume 357/2 15 (1999) 173-178.

[137] T. Silk, Qi Hong, Jüri Tamm and Richard G. Compton, AFM studies of polypyrrole film surface morphology II. Roughness characterization by the fractal dimension analysis, Synthetic Metals 93/1, (1998) 65-71.

[138] X. Sun, Z. Fu, Z. Wu, Fractal processing of AFM images of rough ZnO films. Materials Characterization 48 (2002) 169-175.

[139] G. Reisel, R.B. Heimann, Correlation between surface roughness of plasma-sprayed chromium oxide coatings and powder grain size distribution: a fractal approach. Surface & Coatings Technology 185 (2004) 215-221.

[140] D. Risovic, S. Mahovic, M. Gojo, On correlation between fractal dimension and profilometric parameters in characterization of surface topographies, Applied Surface Science 255 (2009) 4283-4288.

[141] Z.W. Chen, J.K.L. Lai, C.H. Shek, Multifractal spectra of scanning electron microscope images of SnO_2 thin films prepared by pulsed laser deposition, Physics Letters A 345 (2005) 218-223.

[142] K.T. Lam, L.W. Ji, Fractal analysis of InGaN self-assemble quantum dots grown by MOCVD. Microelectronics Journal 38/8-9 (2007) 905-909.

[143] S. Yang, Z. He, Q. Li, D. Zhu, J. Gong, Diamond films with preferred <110> texture by hot filament CVD at low pressure, Diamond and Related Materials 17 (2008) 2075-2079

[144] R. Shishkov, G. Kirilova, D. Dochev, M. Balcheva, Obtaining of (Ti,Me)N films by magnetron sputtering in a vacuum furnace, Proceedings of the 8th Scientific International Conference „Achievements in Mechanical and Materials Engineering AMME'1999", Rydzyna, (1999) 531-534.

[145] C. Blawert, D. Manova, M. Störmer, J.W. Gerlach, W. Dietzel, S. Mändl, Correlation between texture and corrosion properties of magnesium coatings produced by PVD, Surface & Coatings Technology 202 (2008) 2236-2240

[146] P.I. Oden, A. Majumdar, B. Bhushan, A. Padmanabhan, J.J. Graham, AFM Imaging, Roughness Analysis and Contact Mechanics of Magnetic Tape and Head Surfaces, Journal of Tribology 114 (1992) 666-674.

[147] J. Krim, I. Heyvaert, C. Van Haesendonck, Y. Bruynseraede, Scanning tunneling microscopy observation of self-affine fractal roughness in ion-bombarded film surfaces, Physical Reviev Archive 70 (1993) 57 60.

[148] J.M. Gómez-Rodríguez, A. Asenjo, R.C. Salvarezza, A.M. Baró, Measuring the fractal dimension with STM: application to vacuum-evaporated gold, Journal Physical Chemistry 96/1 (1992) 347-350.

[149] J.M. Williams, T.P. Beebe, Analysis of fractal surfaces using scanning probe microscopy and multiple-image variography. 1. Some general considerations, Journal Physical Chemistry 97/23 (1993) 6249-6254.

[150] N. Almqvist, Fractal analysis of scanning probe microscopy images, Surface Science 355 (1996) 221-228.

[151] J. Barkoulas, N. Travlos, Chaos in an emerging capital market? The case of the Athens Stock Exchange.Applied Financial Economics 8 (1998) 231-243.

[152] V. K. Yeragani, K. Srinivasan, S. Vempati, R. Pohl, R. Balon, Fractal dimension of heart rate time series: an effective measure of autonomic function. Journal Applied Physiology 75 (1993) 2429-2438.

[153] J. B. Bassingthwaighte, G. M. Raymond, Evaluation of the dispersional analysis method for fractal time series. Annals of Biomedical Engineering 23 (1995) 491-505.

[154] D. Raoufi, H. Reza Fallah, A. Kiasatpour, A. Rozatian, Multifractal analysis of ITO thin films prepared by electron beam deposition method, Applied Surface Science 254/7 (2008) 2168-2173.

[155] S. Gan, Q. Zhou, X. Xu, Y. Hong, Y. Liu, S. Fu, Study on the surface roughness of substrate with multi-fractal spectrum. Microelectronic Engineering 84/5-8 (2007) 1806-1809.

[156] A. Chaudhari, Y. Sanders Ch-Ch,S. Lee, Multifractal analysis of growing surface, Applied Surface Science 238 (2004) 513-517.